Progress in Polymer Science 129 (2022) 101548

Contents lists available at ScienceDirect

Progress in Polymer Science

journal homepage: www.elsevier.com/locate/progpolymsci

Progress of Conjugated Polymers as Emerging Thermoelectric Materials

Suhao Wang[a,*], Guangzheng Zuo[b], Jongho Kim[a], Henning Sirringhaus[c]

[a] Laboratoire de Physicochimie des Polymères et des Interfaces, CY Cergy Paris Université, 5 Mail Gay Lussac, 95000 Neuville-sur-Oise, France
[b] Institute of Physics and Astronomy, University of Potsdam, 14476 Potsdam, Germany
[c] Optoelectronics Group, Cavendish Laboratory, JJ Thomson Avenue, Cambridge CB3 0HE, UK

ARTICLE INFO

Article history:
Received 1 November 2021
Revised 28 March 2022
Accepted 8 April 2022
Available online 13 April 2022

Keywords:
Organic thermoelectrics
Seebeck coefficient
Doping
Polaron
Conducting polymers
Structure- performance relationship

ABSTRACT

Thanks to the combined efforts of scientists in several research fields, the preceding decade has witnessed considerable progress in the use of conjugated polymers as emerging thermoelectric materials leading to significant improvements in performance and demonstration of a number of diverse applications. Despite these recent advances, systematic assessments of the impact of molecular design on thermoelectric properties are scarce. Although several reviews marginally highlight the role of chemical structure, the understanding of structure-performance relationships is still fragmented. An in-depth understanding of the relationship between molecular structure and thermoelectric properties will enable the rational design of next-generation thermoelectric polymers. To this end, this review showcases the state-of-the-art thermoelectric polymers, discusses structure-performance relationships, suggests strategies for improving thermoelectric performance that go beyond molecular design, and highlights some of the most impressive applications of thermoelectric polymers.

Table of content

* Corresponding Author.
E-mail address: suhao.wang1@cyu.fr (S. Wang).

1. Introduction

Owing to scarcity of resources and the continuous exploitation of fossil fuels, energy and environmental issues have become a global challenge and burden. The low energy utilization rate, which results in more than 60% of world energy being wasted as waste heat [1], deserves extraordinary attention and consideration. Coupled with the world's ever-growing population, there has been a tremendous increase in energy demand and interest in renewable energy. Correspondingly, thermoelectric (TE) technology, which converts waste heat into electrical energy in a quiet and environmentally benign manner, is attracting unprecedented interest [2]. Thermoelectric generators (TEGs) are being widely studied as renewable heat energy conversion devices as they do not have any mechanical components that can break down. During the past two decades, inorganic semiconductors based on metal alloys have been studied as effective TE materials [3,4]. The constituent atomic elements of these alloys, on the other hand, have a low natural abundance and are hence exceedingly expensive [2]. Moreover, these materials often have a certain level of toxicity that is harmful to the environment. Also, metal alloy processing requires high temperatures, thus increasing manufacturing costs. Further-

https://doi.org/10.1016/j.progpolymsci.2022.101548

more, because inorganic materials are often rigid, capturing waste heat from irregularly shaped objects is thus problematic. All of the aforementioned drawbacks make it difficult for inorganic semiconductors to be widely used for waste heat recovery.

Conjugated polymers are currently being hailed as promising organic thermoelectric (OTE) materials [5–10], owing to the fact that (i) their constituent atomic elements are a lot more abundant than their inorganic counterparts, (ii) using room-temperature and solution-based manufacturing methods, conjugated polymers can be scaled up for mass production of thermoelectric devices at a much lower cost [11–13], (iii) since conjugated polymers are flexible and lightweight, it is possible to harvest wasted heat from a variety of shapes [14–20], (iv) their adaptable structure allows for reasonable design to tune their TE properties [21–23], (v) their low toxicity makes conjugated polymers favourable as environmentally friendly energy materials. Consequently, during the preceding decade, a great deal of effort has been made to develop thermoelectric polymers, as indicated by the surge of publications over the years (Fig. 1A) Nevertheless, having only begun in recent years, the research of thermoelectric polymers is still in its infancy. Firstly, performance of thermoelectric polymers is often substantially inferior to that of their inorganic counterparts. Moreover, the understanding of structure-performance relationship is still fragmented, and unlike inorganic TE materials, there is still a lack of well-established structure-functional properties paradigm.

The TE figure of merit is conveyed as: $ZT = \sigma S^2 T/\kappa$, σ being electrical conductivity, S being the Seebeck coefficient, κ being thermal conductivity and T being temperature. Because the κ in a great majority of conducting polymers is innately low, the TE properties of polymers are usually evaluated in terms of power factor (PF): $PF = \sigma S^2$. For a significant number of OTE materials, especially those based on conjugated polymers, S and σ follow the empirical relationship $S \propto \sigma^{-1/4}$ [8,24]. Hence, the PF and σ typically follow the empirical relationship: $PF \propto \sigma^{1/2}$. Thus, to increase σ is of vital importance for TE polymers. Also, since getting a large power output necessitates excellent σ for practical application, a majority of research effort is therefore being made to increase the σ of conjugated polymers, as a prerequisite and principal strategy to improve the PFs. Currently, p-type (hole-transporting) conjugated polymers are well developed, reaching decent electrical conductivity values up to >4000 S cm^{-1} [25–35], with a record-high σ value of ~9000 S cm^{-1} [34]. Nonetheless, the advancement of n-type (electron-transporting) polymers is considerably slower. Most n-doped polymers exhibit limited electrical conductivity (typically <1 S cm^{-1}), with only a few exceptions exceeding 20 S cm^{-1} [36–40], with the current record σ value of ~90 S cm^{-1} [40]. As shown in Fig. 1B, the overall electrical conductivity of n-doped conjugated polymers is much lower than that of p-doped conjugated polymers.

The logical design of next-generation thermoelectric polymers will be enabled by a thorough understanding of their performance limitations. Firstly, the intrinsic properties of conjugated polymers are dictated by their chemical and electronic structure. Thus, an in-depth understanding of structure-property relationship is essential to guiding the design of next-generation high-performance OTEs. On the other hand, due to the nature of disorder in conjugated polymers, their intrinsic σ is typically very low. The TE properties of pristine polymers can thus only be tuned to a very limited extent. Already being proven to be an important enabler via reducing ohmic losses in organic semiconductor (OSC) devices including organic field-effect transistors (OFETs) [41–43] and organic solar cells (OSCs) [44,45], doping is also nowadays widely utilized to delicately tune the TE properties of conjugated polymers [9]. Hereby, the redox doping happens either through the transfer of an electron from dopant molecules to the Lowest Unoccupied Molecular Orbital (LUMO) of polymer (reducing, n-doping), or through from the Highest Occupied Molecular Orbital (HOMO) of polymer to dopant molecules (oxidizing, p-doping) (Fig. 2, upper). Efficient doping relies on both a good match of the energy levels for sufficient thermodynamic driving force and good miscibility between dopant molecules and polymers. Besides, different from redox doping, acid-base doping involves the transfer of hydride ions/cations from dopant molecules to OSCs (Fig. 2, lower), such as proton acid-base, Lewis acids and bases. Other recently developed doping methods include ion-exchange doping in which a molecular dopant ion after inducing the initial charge transfer is exchanged by a stable electrolyte/ionic liquid ion [46,47].

There has been a long-lasting challenge in the development of OTEs and more generally in the whole field of thermoelectrics: S and σ are inversely interrelated as a function of charge density (n), such that achieving high power factor suffers from the trade-off between σ and S. According to the equation $\sigma = n\mu q$, σ depends on both n and charge carrier mobility(μ). Typically, when tuning the doping levels of conjugated polymers, a certain amount

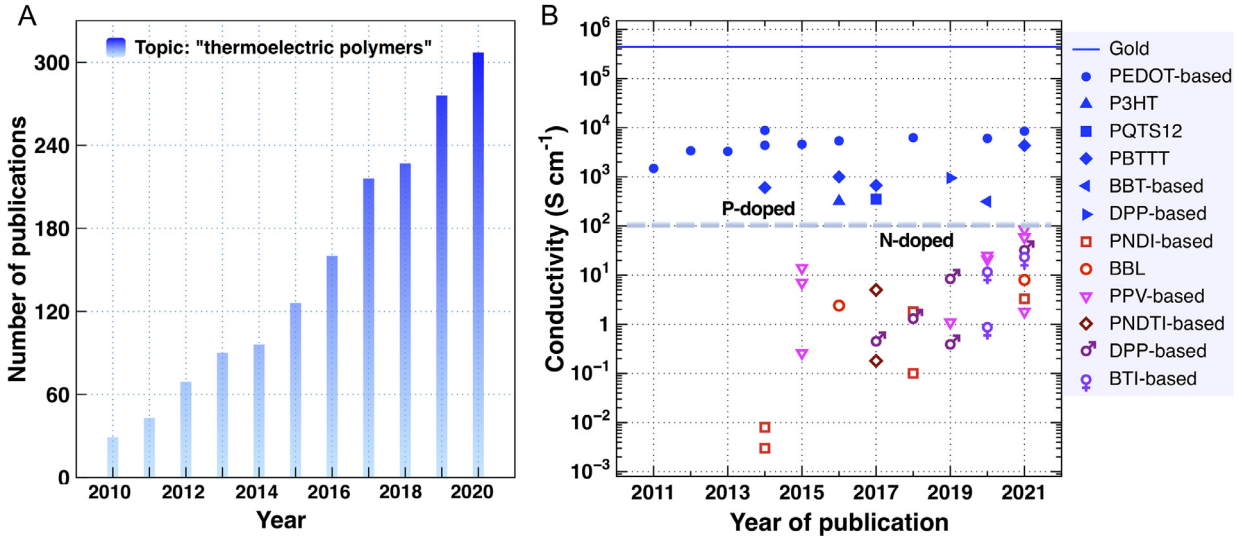

Fig. 1. (A) Number of publications on the topic "thermoelectric polymer" during the past decade, according to Web of Science. (B) State-of-the-art electrical conductivities (those <10^{-3} S cm^{-1} are not shown) for typical solution-processed p-doped polymers (PEDOT-based, PBTTT-based, shown in blue, filled) and n-doped polymers (shown in other colors, open), plotted as a function of the year in the past decade.

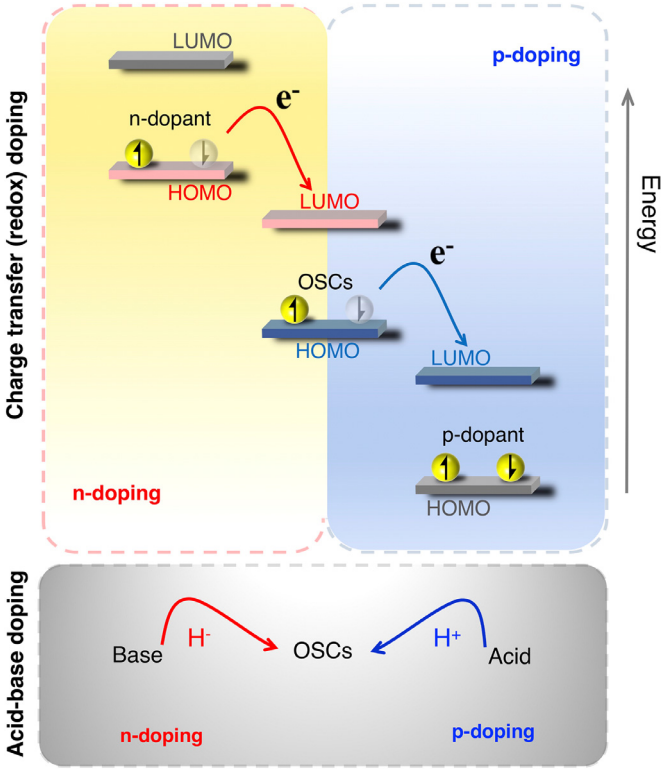

Fig. 2. Schematic illustration of redox doping (upper) which involves the transfer of an electron to the LUMO (n-doping) or from the HOMO of the OSCs (p-doping), and acid-base doping which takes place through the transfer of hydride ions (n-doping) or hydride cations (p-doping) to the OSCs.

of dopant needs to be blended with polymers in order to ensure a large n and thus a good σ. The large n, on the other hand, inevitably decreases S. Moreover, the massive fraction of dopants may disturb the film morphology and decrease μ, thus resulting in an undesired reduction in σ. Thus, decoupling S and σ would allow for further improving the PFs.

In the preceding decade, several remarkable reviews have been published in the field of OTEs, including the topics of fundamentals of TE materials, flexible TE materials, TE composites, doping, and various applications. Herein, we will systematically discuss the structure-functional relationships and molecular design guidelines through reviewing the state-of-the-art TE polymers and recent development of dopants. Furthermore, we will highlight key strategies for overcoming the trade-off between S and σ, and underline some most striking applications of TE polymers.

2. Advances in p-type thermoelectric conjugated polymers and p-dopants

The development of p-type TE polymers could be traced back to last century since the discovery of conducting polymers based on Polyacetylene (PA) [48]. When doped with iodine, PA exhibits excellent σ of $>10^4$ S cm^{-1} [49] and ultra-high σ even exceeding 10^5 S cm^{-1} [50]. Although the TE properties PA doped with iodine [51,52] and metal halide [53] were investigated, due to its poor ambient stability [54] and marginal solubility in organic solvents, further investigation of PA as TE candidates was hampered.

Later, several classes of p-type conjugated polymers emerged as promising candidates for OTEs, including the most widely investigated poly(3,4-ethylenedioxythiophene)(PEDOT)-based polymers, polythiophene-based classic semicrystalline polymers, namely poly(3-heylthiophene) (P3HT), poly(3,3′-dialkylquaterthiophene) (PQT), and poly(2,5-bis(thiophen-2-yl)thieno-[3,2-b]thiophene)(PBTTT), as well as donor-acceptor (D-A) copolymers such as benzothiadiazole(BT)-based copolymers, diketopyrrolopyrrole(DPP)-based copolymers, etc.(Fig. 3)

2.1. PEDOT:PSS as an example of PEDOT family

When initially using 3,4-ethylenedioxythiophene (EDOT) as monomer in the late 1980s, PEDOT was successfully synthesized, but it was both insoluble and infusible [55]. The highest σ value of 31 S cm^{-1} was reported by measuring its pressed pellets. To solve the processability issue, EDOT was oxidized with persulfates and polymerized in aqueous poly(styrenesulfonate) (PSS) solution, forming aqueous dispersion of PEDOT:PSS with high stability where PSS help both disperse and dope PEDOT [56]. While the introduction of PSS greatly enhanced the processability of the PEDOT, the excess of insulating PSS in the solid-state films limits the achievable σ, and adversely disrupts the molecular packing of PEDOT. As a consequence, the as-deposited PEDOT:PSS films exhibit low σ of between $10^{-1}$and 1 S cm^{-1} and modest S of less than 20 μV K^{-1}, leading to inefficient TE properties with modest PF in the range of 10^{-2} μW m^{-1} K^{-2} [57,58]. To address this issue, the introduction of secondary dopants has been proven to be valid in enhancing the TE performance of PEDOT:PSS, such as polar solvent treatment [59,60], acids treatment [25,28,61], and surfactant treatment [62]. Accordingly, the σ and PF of PEDOT:PSS were greatly enhanced.

For instance, adding a polar solvent of dimethyl sulfoxide (DMSO) to PEDOT:PSS solution induced morphological improvement and lead to a much higher maximum σ of ≈930 S cm^{-1} together with a highest PF of ≈30 μW m^{-1} K^{-2}, whereas post-treating PEDOT:PSS with ionic liquid (IL) 1-ethyl-3-methylimidazolium tetrafluoroborate (EMIMBF$_4$) further promoted better microstructure with enhanced polaron density, improving S and leading to a higher maximum PF of ≈39 μW m^{-1} K^{-2} [59]. Hereby, the task of secondary dopant is to improve the charge transport properties through the improvement of its morphology, whereas it has negligible impact on the doping extent of PEDOT:PSS thus hardly affecting S. For instance, it was observed that the crystallinity and the ordering along the through-plane were both enhanced after the addition of ethylene glycol (EG) to the solution of PEDOT:PSS(Fig. 4A), leading to a tremendous enhancement of the charge carrier mobility of PEDOT:PSS, from 0.045 to 1.7 cm^2 V^{-1} s^{-1} [60]. Consequently, the σ of PEDOT:PSS increased to 830 S cm^{-1} when the EG concentration reached 3%, over 2 orders of magnitude higher that (1.2 S cm^{-1}) for the pristine PEDOT:PSS [60].

Interestingly, when treating PEDOT:PSS with binary secondary dopants, namely DMSO and poly(ethylene oxide) (PEO), both refinement of microstructure and transition of polarons to bipolarons were identified, and as a result, σ and S were concurrently enhanced, reaching 1300 S cm^{-1} and 40 μV K^{-1} and resulting in a large PF of 157.4 μW m^{-1} K^{-2}. [64]. Previously, vacuum-assisted filtration was employed to fabricate free-standing flexible PEDOT:PSS papers. When these papers were treated by formic acid (FA), a large σ of 1900 S cm^{-1} was achieved and a decent S of 20.6 μV K^{-1} was recorded, yielding an optimal PF of 80.6 μW m^{-1} K^{-2} [65]. Remarkably, post-treating PEDOT: PSS films using Sulfuric acid (H_2SO_4) induced structural reorganization and lead to the origination of highly ordered polymer nanofibrils (Fig. 4B), resulting in an extraordinary increase in σ from 1 S cm^{-1} to 4380 S cm^{-1} [25].

On the other hand, since a pristine PEDOT: PSS has a relatively high doping level of over 30%, which is not the optimal doping level for reaching the best PF of the material. Hence, chemical dedoping has been extensively used to tune the doping level of PEDOT:PSS, allowing for the manipulation of band structure

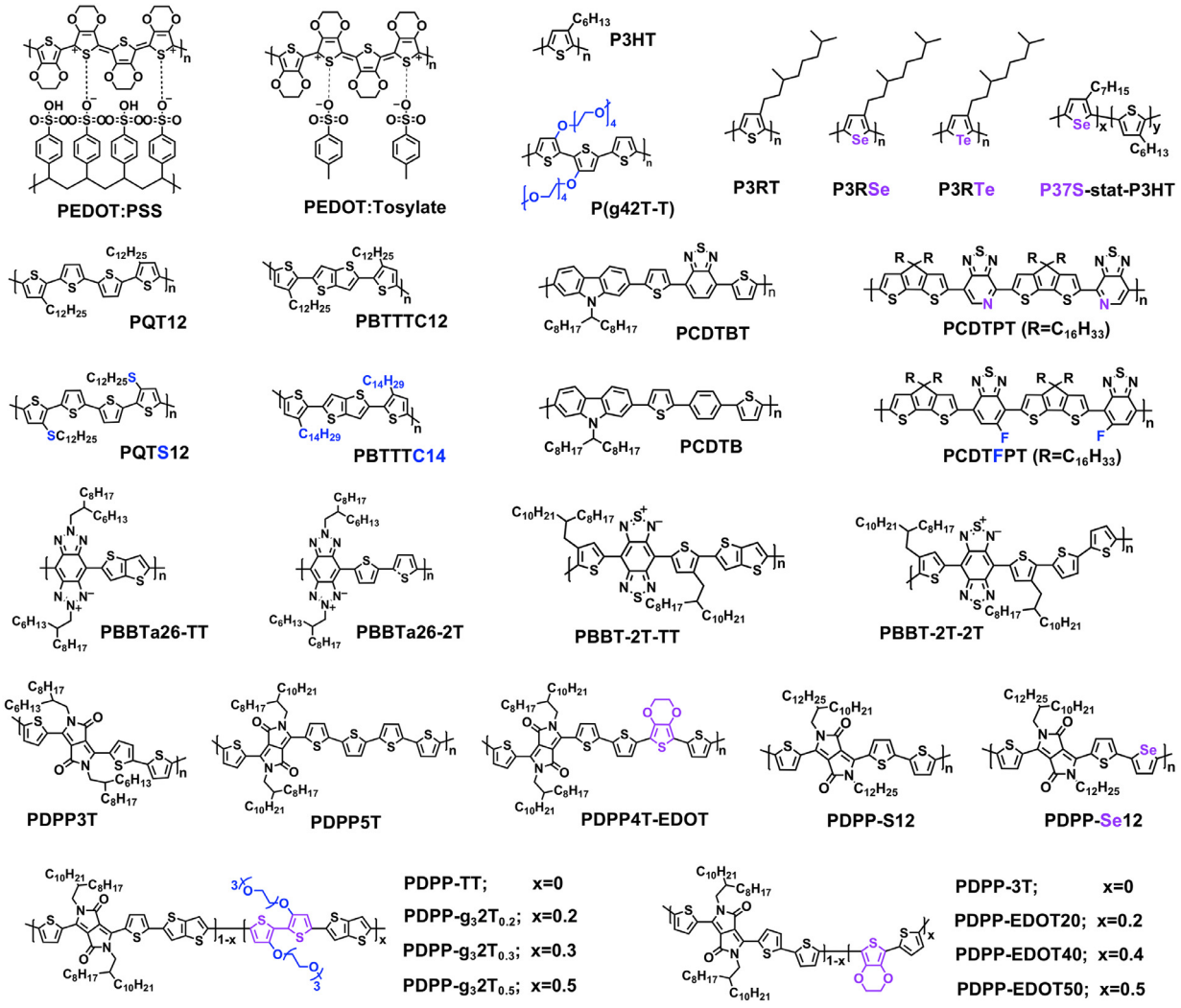

Fig. 3. Chemical structures of p-type conjugated polymers.

as well as density of states (DOS) of the conjugated polymers. Hereby, the shape of DOS directly determines the S of conjugated polymers [66,67]. The reducing agents that are used for dedoping PEDOT:PSS films include tetrakis(dimethylamino)ethylene (TDAE) [68], hydrazine [63,68,69], sodium sulfite (Na_2SO_3) [68,70], and sodium borohydride ($NaBH_4$) [68,70], etc. For instance, after adding 5% DMSO to PEDOT:PSS solution, PEDOT:PSS films were obtained via spin coating (Fig. 4C). After that, these films were dedoped by covering a blend of DMSO and hydrazine, the so called overcoating (Fig. 4C). As a consequence, the excess PSS was eliminated and neutral states of PEDOT chains were formed, thus leading to an enhancement of S and a decrease of σ. Through carefully tuning the content of hydrazine in DMSO, the doping level could be optimized and finally an optimal PF as large as 142 μW m^{-1} K^{-2} was recorded, with corresponding S and σ being 67 μV K^{-1} and 578 S cm^{-1}, respectively [63]. In a similar fashion, when PEDOT:PSS was treated by p-toluenesulfonic acid monohydrate (TSA), a highest σ of 1260 S cm^{-1} and a best PF of 70.7 μW m^{-1} K^{-2} were achieved, at which the S was 24.1 μV K^{-1}. Remarkably, when post-treating the corresponding films with hydrazine/DMSO mixtures, the optimal PF was enhanced to a very high value of 318.4 μW m^{-1} K^{-2} when the S was 49.3 μV K^{-1} [69]. It is worth mentioning that the efficient thermopower of PEDOT: PSS originates from the sum of electronic Seebeck coefficient and ionic Seebeck coefficient [71]. The ionic Seebeck contribution can lead to a transient behavior and an initial enhancement of the Seebeck coefficient, which can however not be maintained in steady state. If not taken into account, this can result in an overestimation of the achievable power factor in steady state.

Besides, smaller anions were often used to substitute PSS in order to minimize the insulating phase, among which tosylate (Tos) represents a most promising milestone as it allows for enhancing the PF of PEDOT up to 324 μW m^{-1} K^{-2} at room temperature [5] and demonstrates semi-metallic behavior which is highly desired for OTEs [72]. Similar to the case of PEDOT:PSS, both secondary dopant and dedoping effect help improve the σ of the PEDOT-Tos films [5,73-76]. As this review is not intended to be a comprehensive report of the literature, we refer the readers to several excellent recent review papers systematically summarizing chemical synthesis, structure as well as transport and TE properties of PEDOT-based polymers [77–80]. Generally speaking, remarkable progress has been realized in developing PEDOT-based polymers as efficient TE materials during the past two decades, with a wealth of knowledge being yielded.

2.2. Classic semicrystalline polymers as promising thermoelectric materials

2.2.1. Poly(3-heylthiophene) and its inspired research

The successful synthesis of regioregular P3HT in late 1990s represents an important milestone in the development of organic electronics [81]. As a solution-processable benchmark p-type poly-

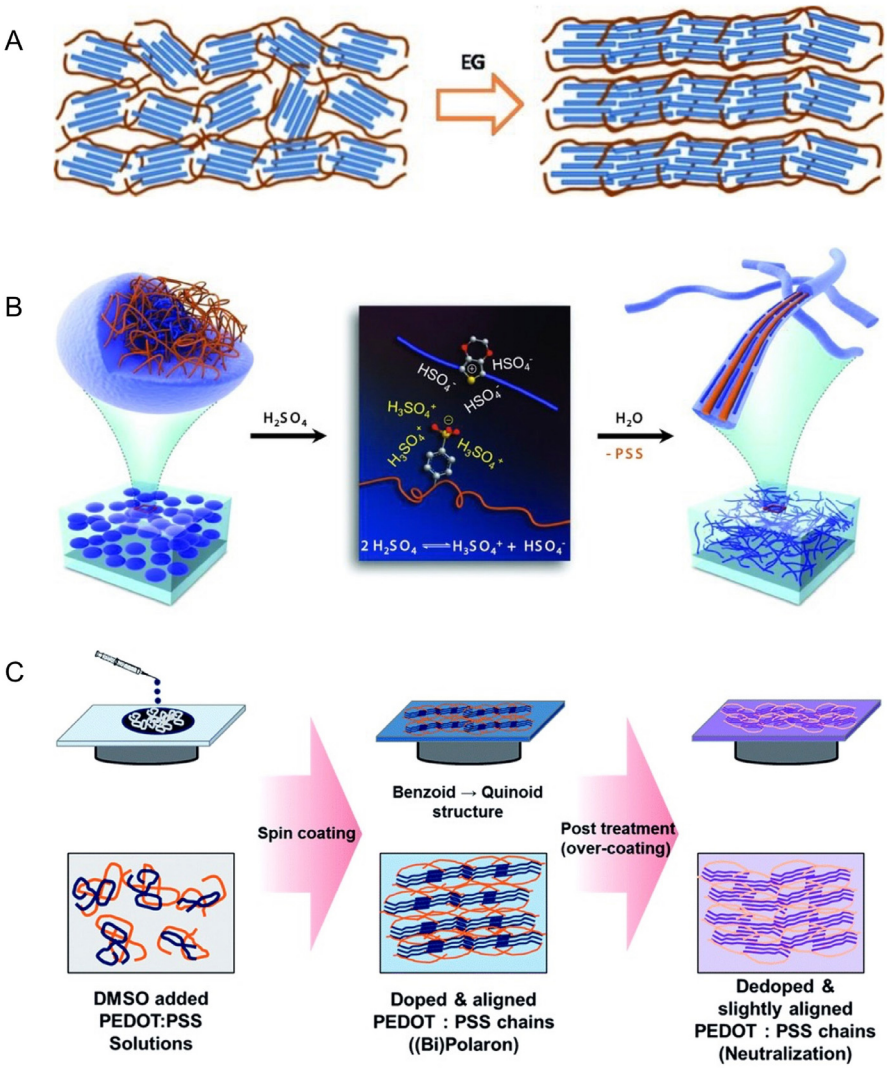

Fig. 4. (A) Illustration of morphological change in the PEDOT:PSS films upon the addition of EG. [60], Copyright 2013. Reproduced with permission from John Wiley & Sons Inc. (B) Diagram showing that he amorphous PEDOT: PSS grains (left) are reformed into crystalline PEDOT:PSS nanofibrils (right) via a charge-separated transition mechanism (middle) induced by a concentrated H_2SO_4 treatment. [25], Copyright 2014. Reproduced with permission from John Wiley & Sons Inc. (C) Schematic diagram of the dedoping procedure of PEDOT: PSS nanofilms by using over-coating and dedoping methods. [63], Copyright 2016. Reproduced with permission from The Royal Society of Chemistry.

mer, P3HT is semicrystalline in thin films and exhibits decent hole mobility of ≈0.1 $cm^2\ V^{-1}\ s^{-1}$ [82,83]. According to the well-established paradigms during the past two decades, the charge transport properties of semicrystalline polymers are sensitive to regioregularity [82], molecular weight (Mw) [84], and polydispersity (PDI) [85]. When doped with nitrosonium hexafluorophosphate (NOPF6) by immersing the polymer film in the dopant solution, P3HT exhibit a maximal σ of 1 S cm^{-1} and a highest PF of 0.14 μW $m^{-1}\ K^{-2}$ [86]. It was observed that the PF_6^- disrupted the molecular packing of P3HT, thus affecting the overall TE properties. Later, when immersed in the solution of ferric salt with triflimide anion $Fe(TFSI)_3$, the mechanically flexible P3HT films thus obtained exhibited a much larger maximum σ of ≈87 S cm^{-1} and a highest PF exceeding 20 μW $m^{-1}\ K^{-2}$ at room temperature [87].

The molecular dopant 2,3,5,6-Tetrafluoro-7,7,8,8-tetracyanoquinodimethane (F4TCNQ) (Fig. 5) was employed to dope P3HT through ground-state charge transfer forming polarons/bipolarons [88], where the integer charge transfer happens from P3HT's HOMO to F4TCNQ's LUMO [89]. Thin films of F4TCNQ-doped P3HT via mixed-solution doping typically shows a maximum σ of ca. 1-2 S cm^{-1} [90,91]. Hereby, the mixed-solution doping tends to form aggregates even at low doing levels, affecting the film morphology/charge carrier mobility and limiting the maximum σ [92]. To address this issue, sequential doping (i.e., spin coating layers of F4TCNQ on top of P3HT films, Fig. 6) produces substantially more homogeneous nanoscale films, where dopant molecules does not disrupt P3HT crystallites, leading to a better maximum σ of ca. 3-9 S cm^{-1} [93–96]. As a further step, F4TCNQ was sublimated to diffuse into the pristine P3HT film, resulting in efficient doping and to a greater extent maintaining the crystalline structure of neat P3HT [97,98], with consequently maximum σ values of 12.7 S cm^{-1} and 48 S cm^{-1} being achieved. In another approach, to solve the inadequate miscibility of polymer/dopant in common organic solvents, oligo ethylene glycol side chains were introduced to the P3HT backbone, yielding the analogous p(g42T-T). Such a modification greatly improves the compatibility of F4TCNQ and p(g42T-T), resulting in a maximum σ of ≈100 S cm^{-1} together with a much higher degree of thermal stability for the doped solid-state thin films [99].

As aforementioned, regioregularity has a huge impact on the electronic and electrical properties of P3HT such that the doped regioregular P3HT gives σ values that are ca. 3 orders of magnitudes higher than that of the regiorandom version [98,100]. The effect of Mw on the TE properties was revealed by comparing various

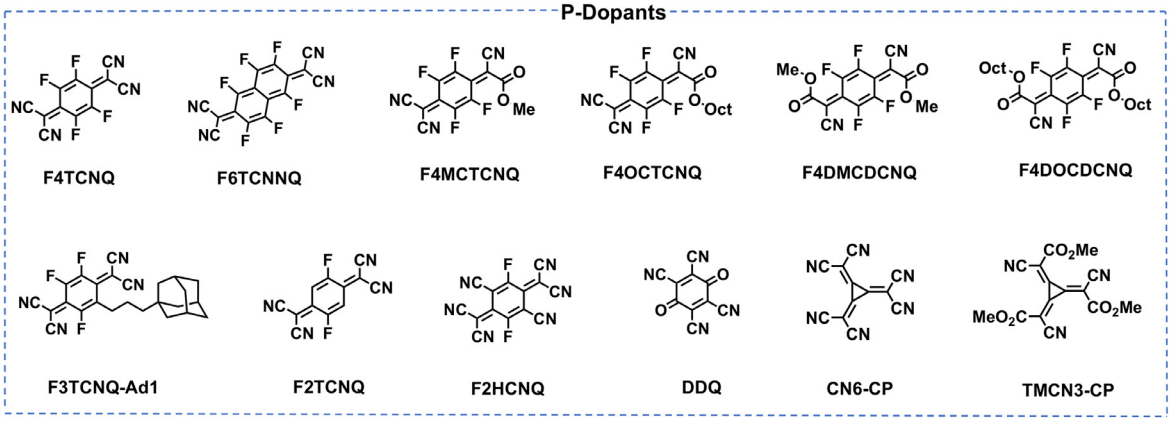

Fig. 5. Chemical structures of p-dopants.

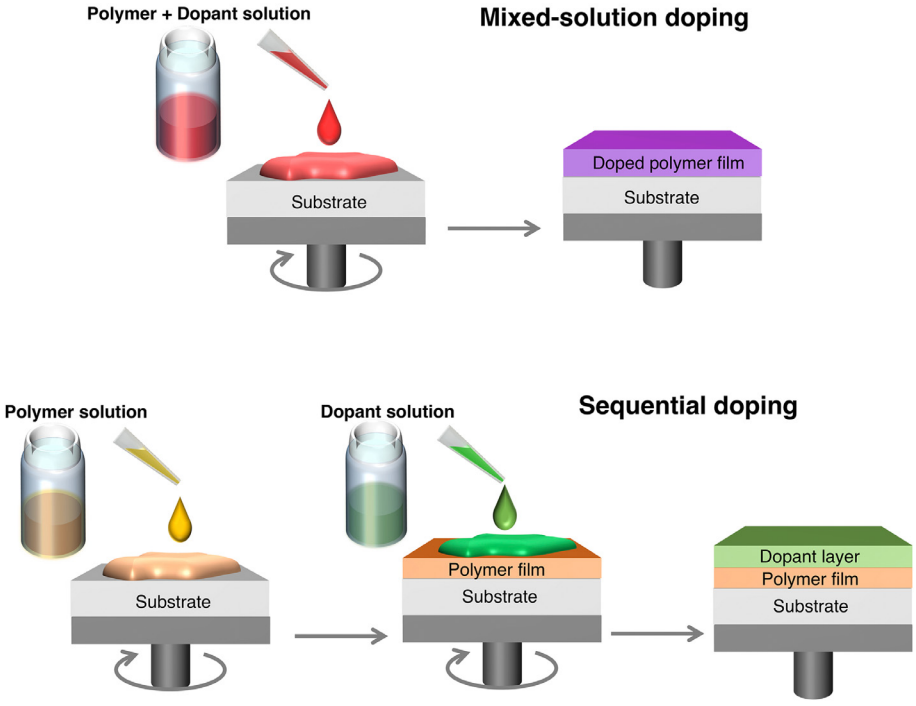

Fig. 6. Schematic illustration of mixed-solution doping and sequential doping.

doped P3HT layers, where the σ increases from 21kDa to 44kDa and to 77kDa, and subsequently drops from 77kDa to 94kDa, implying a trade-off between Mw and TE performance [101]. Besides, the effect of heteroatom on the TE characteristic of poly(3-alkylchalcogenophenes) was recently investigated by comparing poly(3- alkylthiophene) (P3RT), poly(3-alkylselenophene) (P3RSe) and Poly(3-alkyltellurophene) (P3RTe) [102]. Interestingly, P3RTe with heaviest tellurium is the easiest to dope and reaches highest PF of 10 μW m^{-1} K^{-2} at low dopant concentrations, whereas at greater dopant concentrations, P3RSe gives the maximum PF of 13 μW m^{-1} K^{-2}. More recently, poly(3-heptylselenophene) (P37S) and P3HT were statistically copolymerized to yield P37S-stat-P3HT with controllable bandgap and valence band location through tuning the contents of P37S. Generally, when sequentially doped with F4TCNQ, the higher the P37S content contained in the P37S-stat-P3HT, the higher the σ, with the highest σ of $>$ 20 S cm^{-1}achieved for 100% pure P3ST, whereas exceptions happened for P37S-stat-P3HT when P37S content are larger than 50% due to decreased crystallinity in the doped state and thus lower Hall mobility [103]. Hence, it is critical to take both the crystallinity of the polymers in their pristine state and their swellability during doping into consideration when designing novel polymers.

2.3.2. Poly(3,3′-dialkyl-quaterthiophene) and analogous polymer

Poly(3,3′-dialkyl-quaterthiophene) (PQT) is another semicrystalline p-type polymer showing lamellar structures in the solid-state films and a decent hole mobility of ≈0.2 cm^2 V^{-1} s^{-1} [104]. When doped with NOBF4, PQT exhibit an optimal σ of ≈ 35 S cm^{-1} [105]. Strikingly, when sulfur atom is incorporated between the dodecyl side chains and the thiophene rings, the yielded analogous PQTS12 could be doped to a much greater of ca. 350 S cm^{-1}, ca.10 times higher than that of PQT12. Hereby, the enhanced electrical performance could be attributed to both a greater doping extent and a larger charge carrier mobility of the doped film. Firstly, the incorporation of sulfur atoms boosts the HOMO level of the PQTS12, creating a stronger driving power for the charge transfer between the PQTS12 and NOBF4. Secondly, PQTS12 exhibits tighter π–π stacking in the pristine state, leading to stronger intermolecular coupling and efficient charge transport. Thirdly, NOPF4 tends to interact with the sulfur atom in the side chains such that the

stacking of polymer backbones is undisturbed, facilitating efficient charge transport even in the doped state [105].

2.3.3. Poly(2,5-bis(thiophen-2-yl)thieno- [3,2-b]thiophene)

Poly(2,5-bis(thiophen-2-yl)thieno- [3,2-b]thiophene) (PBTTT) is an intensively investigated liquid-crystalline polymer showing pronounced long-range crystallinity in the solid-state thin films [106] and excellent charge carrier mobility up to ≈1 cm^2 V^{-1} s^{-1} [107]. The high crystallinity is ascribed to both its rigid backbone and the advantageous side-chain interdigitation [108]. When initially doped with NOPF6, the as-cast PBTTT exhibited a σ of ≈ 33 S cm^{-1} and after thermal annealing, the NOPF6-doped film gave an enhanced σ of ≈ 55 S cm^{-1} [109]. The PF was improved by three times owing to the enhanced structural order induced by thermal annealing [109]. When immersed in the solution of $Fe(TFSI)_3$, PBTTT exhibited a large maximum σ of ≈220 S cm^{-1} and a highest PF exceeding 14 μW m^{-1} K^{-2} [110].

When doped with F4TCNQ by mixed-solution doping, PBTTT-C14 exhibited an optimal σ of 2-3.5 S cm^{-1} [112,113]. Similar to the case of P3HT, doping methods play crucial roles in determining the molecular stacking and σ of the doped PBTTT films. When F4TCNQ was evaporated on top of PBTTT films, the dopants selectively diffuse into the electrically inert domain where the insulating alkyl chains reside (Fig. 7A) [111]. Thus, both charge carrier mobility and charge density could be well manipulated by controlling the F4TCNQ diffusion, leaving the molecular packing undisrupted even at high doping levels (Fig. 7B) [111]. Unexpectedly, the interplay between the PBTTT side chains and F4TCNQ even promote a stronger chain alignment/crystallites orientation, as evidenced by the X-ray rocking scan shown in Fig. 7C where complete-width at half-maximum values are much smaller for doped PBTTT. As a result, a substantial Hall mobility of approx. 1.8 cm^2 V^{-1} s^{-1} was attained, with a maximum of σ of 250 S cm^{-1} as well as signatures of metallic transport, such as observation of weak localization phenomena [111]. The solid-state diffusion method also leads to a higher TE power factor which has been ascribed to a resulting higher intrinsic mobility as well as higher free carrier concentrations [114]. Later, a comparative study was performed for PBTTT doped by vapor and mixed solution, where resonant soft x-ray scattering (RSoXs) was employed to measure the exact extent of polymer backbone alignment [115]. It is noteworthy that the vapor-doped samples have an apparently larger orientation correlation length (OCL), which corresponds to noticeable higher charge carrier mobility, leading to a remarkable highest σ of 670 S cm^{-1} [115]. Besides, when alky silane (tride-cafluoro-1,1,2,2,-tetrahydrooctyl)-trichlorosilane (FTS) was employed to vapor-dope PBTTT, the films exhibited high σ values of ≈ 466 S cm^{-1} [112] and ≈ 1000 S cm^{-1} [116], respectively. Although the exact doping mechanism is not clear yet, it is assumed that FTS acts as an interfacial dopant and the charge carrier are either induced by electrostatic doping from the perpetual dipole or protonic doping from the extremely acidic silanol groups [116].

2.3. Donor-acceptor copolymers as emerging efficient thermoelectric materials

2.3.1. Benzothiadiazole(BT)- and pyridinethiadiazole(PT)-based copolymers

The first copolymers of cyclopentadithiophene(CDT) and benzothiadiazole(BT) (PCDTBT) was reported almost simultaneously by two independent research groups with different focuses, one on organic solar cells [117,118] and the other on organic field-effect transistors [119,120], both showing high performance. Later, PCDTBT was doped with $FeCl_3$, reaching a remarkably high σ of 500 S cm^{-1} and a decent PF of 19 μW m^{-1} K^{-2} [121]. In comparison, the analogous polymer with benzene moiety PCDTB could only be doped to a maximum σ of 130 S cm^{-1} and a highest PF of 14 μW m^{-1} K^{-2} under the same doping conditions [121]. Recently, pyridinethiadiazole (PT)-based PCDTPT and fluorinated benzothiadiazole (FBT)-based PCDTFBT were synthesized to have shallow LUMO values and their TE properties were investigated. When efficiently doped with F4TCNQ, both polymers retained good solubility and decent molecular packing even at high load of dopants, and thus preserved good charge carrier mobility and reached good σ, finally resulting in highest PF values of 21.8 μW m^{-1} K^{-2} PCDTPT and 31.5 μW m^{-1} K^{-2} for PCDTFBT [122]. Later, PCDTPT was doped with trityl tetrakis(pentafluorophenyl) borate (TrTPFB), reaching σ of ≈4 S cm^{-1} and a maximum PF of 7 μW m^{-1} K^{-2} [123].

2.3.2. Benzo [1,2-c;4,5-c′]bisthiadiazole(BBT)-based copolymers

Recently, several BBT-based proquinoidal polymers such as PBBTa26-2T and PBBTa26-TT were synthesized to show highly coplanar D-A character with a minimum dihedral angle [124].When doped with F4TCNQ, both polymers exhibited high σ values, 43.1 S cm^{-1} for PBBTa26-2T and 102.1 S cm^{-1} PBBTa26-TT. The stronger quinoidal character of PBBTa26-TT allows for better polaron delocalization along the backbone, resulting in a superior σ value. However, owing to its significantly higher charge density in the doped state, the S of PBBTa26-TT is obviously smaller than that of PBBTa26-2T. Hence, the optimized

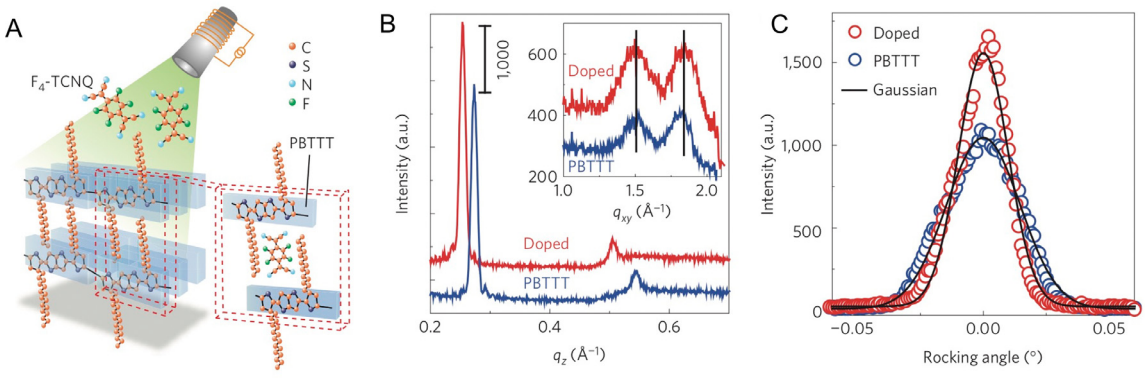

Fig. 7. (A) Schematic diagram of the doping method showing the evaporation procedure of F4TCNQ and resulting edge-on stacking of PBTTT with F4TCNQ molecules diffusing into the interdigitated side-chain region. The molecular structures of PBTTT and F4TCNQ are presented as circles of different colours representing different atoms as described in the legend. (B) Specular scans from X-ray diffraction (XRD) measurements for the out-of-plane scattering profile along q_z for doped and pristine PBTTT. The inset shows the in-plane diffraction spectra along q_{xy} from Grazing-Incidence Wide-Angle X-ray Scattering (GIWAXS). q_{xy} and q_z are the in-plane and the normal components of the scattering vector, respectively. (C) Rocking scans for the (100) diffraction peaks. Black curves denote Gaussian fits, where the full-width at half-maximum values are measured to be 0.023° for doped PBTTT and 0.032° for pristine PBTTT. [111], Copyright 2016. Reproduced with permission from Macmillan Publishers Ltd.

maximum PF of PBBTa26-TT(6.8 $\mu W\,m^{-1}K^{-2}$) is also smaller than that of PBBTa26-2T(11.8 $\mu W\,m^{-1}K^{-2}$) [124]. Previously, proquinoid BBT polymers PBBT-2T-TT and PBBT-2T-2T were reported to be highly planar and have large carrier mobilities [125,126]. Very recently, the aforementioned two polymers were sequentially doped by $FeCl_3$ to investigate their TE properties. Strikingly, their strong quinoid structure enables favorable intramolecular polaron/bipolaron delocalization and high intermolecular order over a long range. As a result, both polymers exhibited very high maximum σ values, 287 S cm^{-1} for PBBT-2T-TT 313.9 S cm^{-1} for PBBT-2T-2T [127]. Furthermore, the substantial intra- and intermolecular polaron/bipolaron delocalization also gave rise to a favorable increase in their S as a result of carrier-induced softening. Consequently, high maximum PFs of 65.2 $\mu W\,m^{-1}K^{-2}$ for PBBT-2T-TT and 43.5 $\mu W\,m^{-1}K^{-2}$ for PBBT-2T-2T were achieved [127].

2.3.3. Diketopyrrolopyrrole (DPP)-based copolymers

Due to their planar skeleton and narrow band-gap, DPP-based D-A copolymers have attracted lots of attention and have been intensively investigated in the field of OFETs and OPVs during the past decade [128,129]. As a high-performance polymer, the DPP-based copolymer PDPP3T exhibits a decent hole mobility of ca. 0.6 $cm^2\ V^{-1}\ s^{-1}$ [129]. When doped with $FeCl_3$ by carefully controlling the dopant concentration, PDPP3T reaches outstanding optimal PF of 276 $\mu W\,m^{-1}K^{-2}$ when its S is 226 $\mu V\ K^{-1}$ and its σ is ca. 55 S cm^{-1} [130]. Besides, a DPP-based copolymer PDPP5T was doped with FeCl3/nitromethane solutions to reach a maximum σ of ≈120 S cm^{-1} and a highest PF of 11.1 $\mu W\ m^{-1}\ K^{-2}$. Interestingly, when one thiophene unit of PDPP5T was replaced by EDOT, a new polymer PDPP-4T-EDOT was yielded with improved HOMO level and better planarity of backbones, leading to more efficient p-doping and far superior TE performance (maximum σ of ≈270 S cm^{-1} and an optimal PF as high as 298.2 $\mu W\ m^{-1}\ K^{-2}$ [131].

Recently, when doped with $FeCl_3$, PDPPS-12 gives a strikingly highest σ of ca. 318 S cm^{-1} [132]. Previously, selenophene substitution was proven to be a useful strategy for enhancing the intermolecular interactions as well as achieving high charge carrier mobility [133,134]. For instance, DPP-selenophene copolymer PDPPSe-12 was reported to show a very large hole mobility of over 7 $cm^2\ V^{-1}\ s^{-1}$ [135]. In comparison, when doped with $FeCl_3$, PDPPSe-12 gives a much larger maximum σ of ca. 997 S cm^{-1}, over 3 times higher than that of doped PDPPS-12. Since the atom radius of selenium is obviously larger as compared to that of sulfur, the intermolecular interaction is stronger for PDPPSe-12. As a result, when dopant molecules are incorporated into the polymer films, the molecular packing of PDPPSe-12 remains nearly unchanged before and after doping, whereas it becomes less ordered for PDPPS-12 under the same doping treatment (Fig. 8A, B).

Remarkably, at a low doping level, PDPPSe-12 exhibits a very large Hall mobility of ca. 1.9 $cm^2\ V^{-1}\ s^{-1}$, the record value for conducting polymers, whereas PDPPS-12 shows a lower Hall mobility of 0.92 $cm^2\ V^{-1}\ s^{-1}$ (Fig. 8D). Interestingly, both PDPPSe-12 and PDPPS-12 have comparable S values at low doping levels and ex-

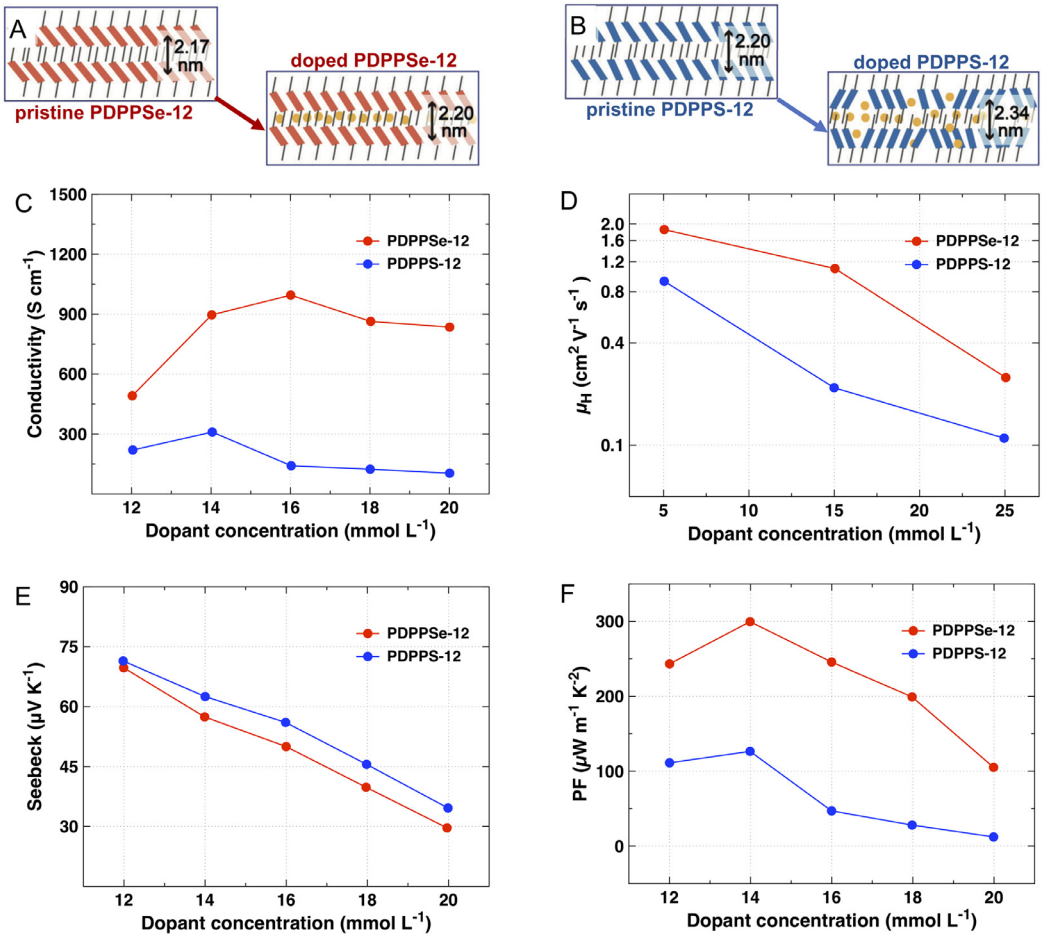

Fig. 8. Illustration of molecular packing of films before and after doping for (A) PDPPS-12 and (B) PDPPSe-12. (The yellow dots represent the dopant molecules, [132], Copyright 2019. Adapted with permission from John Wiley & Sons). (C) Electrical conductivity, (D)Hall mobility, (E) Seebeck coefficient, and (F) Power factor of PDPPS-12 and PDPPSe-12 films with different doping conditions. [132], Copyright 2019. Reproduced with permission from John Wiley & Sons Inc.

hibit almost identical trend with increasing doping levels (Fig. 8E). Finally, the maximum PF of PDPPSe-12 reached > 300 $\mu W\,m^{-1}K^{-2}$, over two times larger than that of PDPPS-12(Fig. 8F).

Recently, random copolymerization has been demonstrated as an effective approach toward efficient DPP-based TE polymers [136]. (Fig. 9A) When doped with $FeCl_3$, PDPP-TT exhibits a highest σ of ≈45 S cm^{-1}, and an optimal PF of 43 $\mu W\,m^{-1}K^{-2}$ when its S is ca. 94 $\mu V\ K^{-1}$. Interestingly, by random copolymerization of DPP with donor units thienothiophene (TT) and oligo ethylene glycol substituted bithiophene (g_32T), the TE performance of the copolymers consisting DPP-TT and g_32T-TT building blocks firstly increased and then decreased with the increasing amount of g_32T (Fig. 9B, C). Consequently, at a g_32T-TT content of 30%, the corresponding copolymer PDPP-$g_32T_{0.3}$ exhibited the best optimized TE performance, reaching a significantly higher σ of 360 S cm^{-1} and an optimal PF of 110 $\mu W\,m^{-1}K^{-2}$ when its S is ca. 56 $\mu V\ K^{-1}$. The remarkably improved TE performance is ascribed to the introduction of additional donor g_32T-TT which on one hand enhanced the HOMO level of the polymer allowing for better charge transfer upon doping and on the other hand facilitated a higher doping efficiency thanks to the polar side chains. Note that Hall effect measurement indicated a simultaneous improvement of both carrier concentration and carrier mobility for PDPP-$g_32T_{0.3}$, well explaining the significantly higher σ observed. More recently, EDOT was employed to copolymerize randomly with DPP-3T, yielding a series of random copolymers (PDPP-$EDOT_{0.2}$, PDPP-$EDOT_{0.4}$, and PDPP-$EDOT_{0.5}$) with enhanced electrical conductivity compared to the reference D-A copolymer PDPP-3T (Fig. 9D, E) [137]. When doped with $FeCl_3$, PDPP-3T exhibited a highest σ of only ≈0.28 S cm^{-1}, and an optimal PF of ca. 1.6 $\mu W\,m^{-1}K^{-2}$ when its S is ca. 242 $\mu V\ K^{-1}$. After doping with $FeCl_3$, their σ increased to 0.76, 2.8, and 4.1 S cm^{-1} for PDPP-$EDOT_{0.2}$, PDPP-$EDOT_{0.4}$, and PDPP-$EDOT_{0.5}$, respectively, and their S decreased to 177, 152, and 105 $\mu V\ K^{-1}$, respectively. At the EDOT content of 40%, the best optimized TE performance was achieved, with PF of 6.4 $\mu W\,m^{-1}K^{-2}$ being achieved for PDPP-$EDOT_{0.4}$, four times higher than that of the reference copolymer PDPP-3T. Table 1 summerizes the electrical and TE properties of p-type conjugated polymers.

2.4. The development of p-dopants

2.4.1. F4TCNQ and its derivatives

Considering that small dopants have a strong tendency to diffuse rendering the doped layers unstable under operating condi-

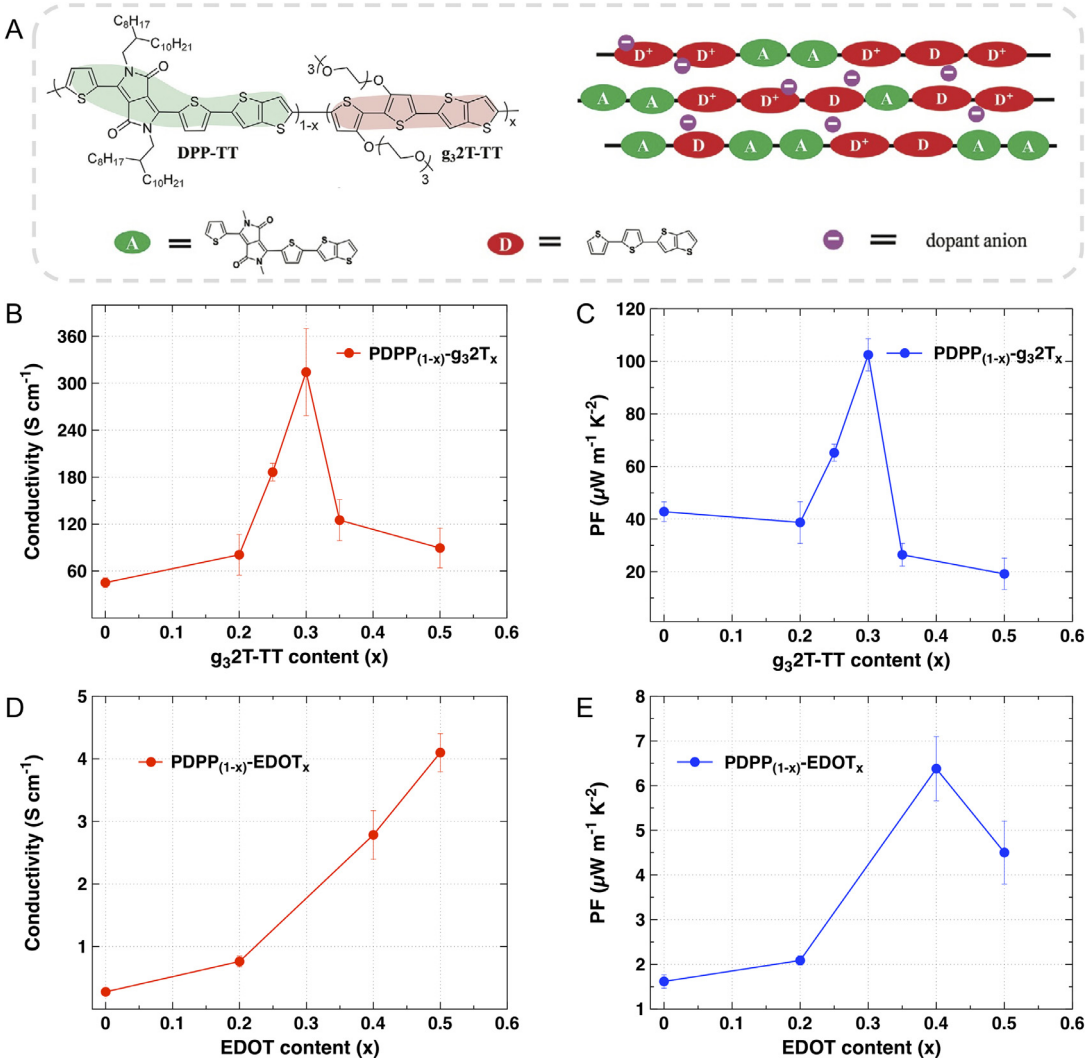

Fig. 9. (A) Illustration of the random copolymerization strategy for PDPP$_{(1-x)}$-g_32T_x. [136], Copyright 2020. Adapted with permission from John Wiley & Sons Inc. (B) Electrical conductivity and (C) Power factor of doped films for PDPP$_{(1-x)}$-g_32T_x with different content of g_32T. [136], Copyright 2020. Reproduced with permission from John Wiley & Sons Inc. (D) Electrical conductivity and (E) Power factor of doped films for PDPP$_{(1-x)}$-EDOT$_x$ with different EDOT content. [137], Copyright 2021. Reproduced with permission from John Wiley & Sons Inc.

Table 1
A summary of Conductivity, Seebeck coefficient and Power factor of state-of-the-art p-type conjugated polymers.

Polymer	Dopant (Method) [a]	σ_{max} [S cm^{-1}]	S [μV K^{-1}] [b]	PF_{max} [μW m^{-1}K^{-2}]	Ref.
PEDOT: PSS	_ (S)	~0.1-1	20	~10^{-2}	[57]
	EG (S)	830	_	_	[60]
	DMSO(S)	_	_	18.2	[59]
	DMSO-PEO(S)	1300	40	157.4	[64]
	DMSO(P-T)	~930.4	~18	30.1	[59]
	EMIMBF4–DMSO(P-T)	~930	~24	38.5	[59]
	FA(P-T)	1900	20.6	80.6	[65]
	H_2SO_4(P-T)	4830	_	_	[25]
	H_2SO_4(P-T)	~4840	10.4	51.9	[28]
	DMSO-Hydrazine(P-T)	578	67	142	[63]
	TSA(S)	1260	_	70.7	[69]
	TSA(S)-Hydrazine(P-T)	1647	49.3	318.4	[69]
	MeOH (S) //	4600	_	_	[27]
	MeOH(S) // -EtOH (P-T) //	~8800	_	~800	[34]
PEDOT: Tos	TDAE(P-T)	~300	~220	324	[5]
	DMF(S)	1500	55	453.8	[72]
	DMF(S)	640	~34	78.5	[74]
	Pyridine-DMF(S)	~1225	~44	~237	[76]
P3HT	NOPF6 (Immerse)	1	_	0.14	[86]
	F4TCNQ(M-S)	1/1.8	_	_	[91]/[90]
	F4TCNQ(Sq.)	3/5.5/9.1	_	_	[94]/[93]/[95]
	F4TCNQ(Sq.) //	22	60	8	[138]
	F4TCNQ(Vapor)	5/12.7	_	_	[96]/[98]
	F4TCNQ(Vapor)	48	85	27	[97]
	$Fe(TFSI)_3$ (Immerse)	87	_	20	[87]
	$Fe(TFSI)_3$ (Immerse) //	320	39	62.4	[139]
P(g42T-T)	F4TCNQ(M-S)	100	_	_	[99]
PQT12	NOBF4(Immerse)	35	20.1	1.4	[105]
PQTS12	NOBF4(Immerse)	350	16.2	7.9	[105]
PBTTT	NOPF6 (Immerse)	55	13.5	0.98	[109]
	F4TCNQ(M-S)	3.51	60	1.3	[112]
	F4TCNQ(Immerse) //	190	77	100	[140]
	F4TCNQ(Vapor)	250	_	_	[111]
	F4TCNQ(Vapor)	670	42	120	[115]
	$Fe(TFSI)_3$ (Immerse)	220	13	14	[110]
	FTS(Vapor)	~466	23	~25	[112]
	FTS(Vapor)	~1000	33	~110	[116]
	EBSA(Immerse)	1300	14	25	[116]
	$FeCl_3$-BMP TFSI(P-T)	~1100	_	_	[47]
	$FeCl_3$-BMP TFSI(P-T) //	4345	_	137	[35]
PCDTB	$FeCl_3$(Immerse)	130	_	14	[121]
PCDTBT	$FeCl_3$(Immerse)	500	_	19	[121]
PCDTPT	F4TCNQ(M-S)	5.13	211	21.8	[122]
	TrTPFB(M-S)	~4	_	~7	[123]
PCDTFBT	F4TCNQ(M-S)	8.73	213	31.5	[122]
PBBTa26-2T	F4TCNQ(M-S)	43.1	_	11.8	[124]
PBBTa26-TT	F4TCNQ(M-S)	102.1	_	6.8	[124]
PBBT-2T-2T	$FeCl_3$(Sq.)	313.9	_	43.5	[127]
PBBT-2T-TT	$FeCl_3$(Sq.)	287	49.4	65.2	[127]
PDPP-3T	$FeCl_3$(Sq.)	~85	226	276	[130]
PDPP-5T	$FeCl_3$(Drop)	120	42.2	11.1	[131]
PDPP-4T-EDOT	$FeCl_3$(Drop)	272	174.2	298.2	[131]
PDPPS-12	$FeCl_3$(Immerse)	318	80	178	[132]
PDPPSe-12	$FeCl_3$(Immerse)	997	62	364	[132]
PDPP-TT	$FeCl_3$(Immerse)	45	94	43	[136]
PDPP-$g_32T_{0.2}$	$FeCl_3$(Immerse)	~81	63	~39	[136]
PDPP-$g_32T_{0.3}$	$FeCl_3$(Immerse)	360	56	110	[136]
PDPP-$g_32T_{0.5}$	$FeCl_3$(Immerse)	~89	38	~19	[136]
PDPP-3T	$FeCl_3$(Immerse)	0.28	242	1.6	[137]
PDPP-$EDOT_{0.2}$	$FeCl_3$(Immerse)	0.76	177	2.1	[137]
PDPP-$EDOT_{0.4}$	$FeCl_3$(Immerse)	2.8	152	6.4	[137]
PDPP-$EDOT_{0.5}$	$FeCl_3$(Immerse)	4.12	105	4.5	[137]

[a] (S) via solution processing, (P-T) via post treatment, (Sq.) via sequential doping
[b] S values corresponding to the PF_{max}.

tions and leading to undesired dedoping [141], a variety of molecular dopants have been developed and employed for doping of conjugated polymers (Fig. 5). Nowadays, electron deficient dopants such as F4TCNQ and its derivatives are most widely investigated for doping TE polymers, as discussed in the preceding sections. Nevertheless, the thermal stability of F4TCNQ is poor as it typically sublimates at roughly 140°C under vacuum conditions. This may result in a fall of doping level when the doped films get in contact with heat sources in practical applications. Increasing the size of the dopants can enhance the thermal stability. The F6TCNNQ with larger molecular size, for example, exhibits much higher sublimation points over 200°C allowing for better control of vacuum deposition and resulting in reduced diffusion [142]. On the other hand, doping polymers with F4TCNQ often causes a reduction in the

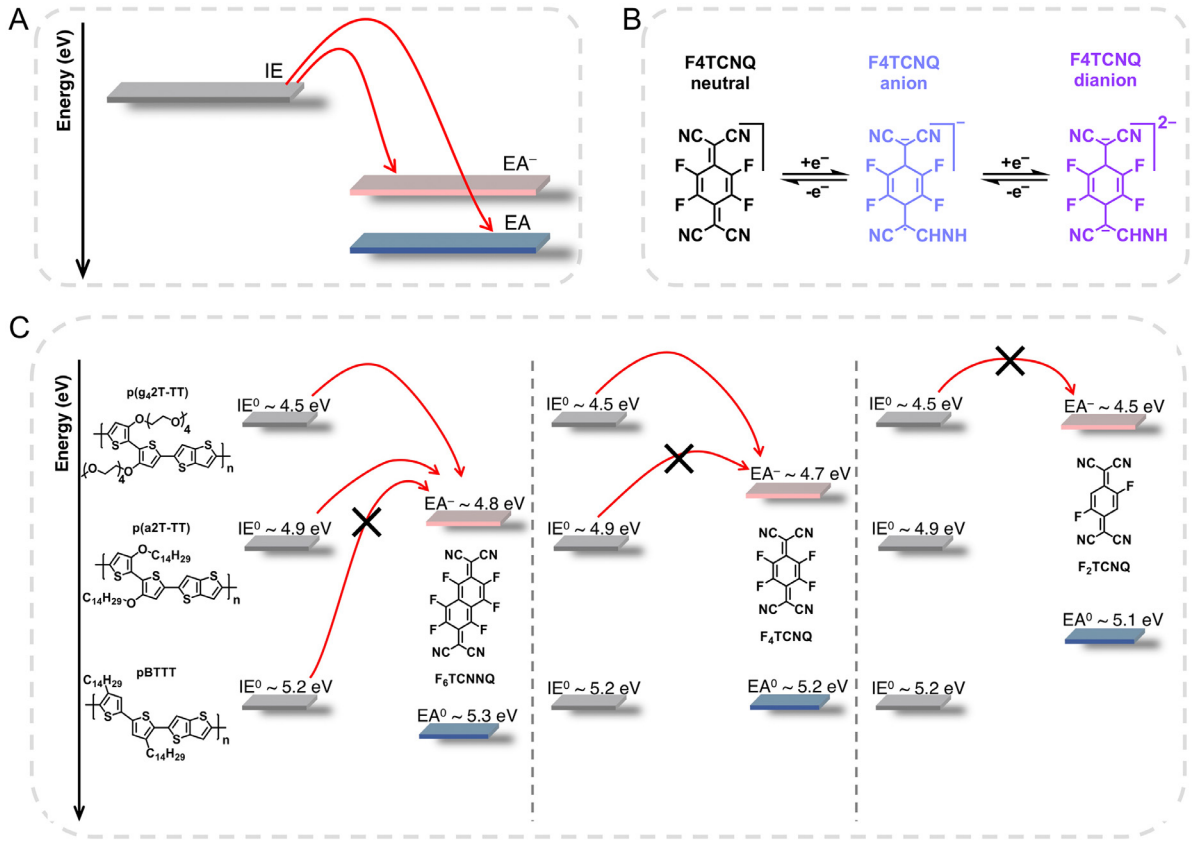

Fig. 10. (A) Energy diagram showing that as long as the IE of the host polymer is lower than the electron affinity of the negatively charged dopant (EA^-), double doping can happen. (B) Illustration of F4TCNQ in the format of neutral, anion and dianion. [145], Copyright 2019. Reproduced with permission from Macmillan Publishers Ltd.(C) Energy diagram summarizing the formation of dopant dianions. Green (red) arrows indicate where electron transfer from the polymer to the dopant anion is observed (absent). [145], Copyright 2019. Reproduced with permission from Macmillan Publishers Ltd.

solubility of polymers, making it difficult to process doped films [94,113]. To solve the solubility issue, alky esters were utilized to substitute the nitrile groups of F4TCNQ, resulting in a series of highly soluble derivatives, F4MCTCNQ, F4OCTCNQ, F4DMCDCNQ, and F4DOCDCNQ with minor changes in acceptor strength [143]. Besides, replacing one single fluorine atom of F4TCNQ with a bulky adamantanyl propyl chain yielded the analogous F3TCNQ-Ad1 with comparable electronic properties but far superior solubility, allowing for easy solution processing [144].

It was previously assumed that every dopant could contribute only a single charge carrier to its host polymer forming only one polaron. This assumption is often based on the behavior of inorganic semiconductors in which Coulomb repulsion between two equal charges localized on the same dopant often causes an obvious increase in activation energy of doping, preventing double ionization of the dopant. However, a recent study showed that dianions formation — that is, double doping —can be achieved when the ionization energy (IE) of the host polymer is lower than the electron affinity (EA) of the negatively charged dopant (Fig. 10A, B) [145]. In such instances, in addition to the double ionization of the dopants, a majority of generated charge carriers take part in charge transport, resulting in a doping efficiency as high as 170% at relatively low dopant concentrations. As shown in Fig. 10C, a variety of dopant-host combinations were investigated. The authors discovered that the EA^- of both F4TCNQ and F6TCNNQ is large enough to accept a second electron from P($g_4$2T-TT), whereas the EA^- of F2TCNQ is substantially smaller, not allowing for double doping of P($g_4$2T-TT). This work paved a new path for doping of conjugated polymers, making it possible for efficient doping with significantly lower dopant concentrations. This not only saves materials, but it also reduces the disruption of polymer film microstructure caused by the introduction of large amounts of dopants.

2.4.2. Other representative p-type dopants

Besides F4TCNQ, 2,3-Dichloro-5,6-dicyano-1,4-benzoquinone (DDQ) is another common p-type dopant for hole-transporting polymers in organic semiconducting devices. When P($g_4$2T-T) was doped with DDQ, it exhibited similar electrical property as F4TCNQ-doped P($g_4$2T-T) [99]. Note that DDQ is remarkably cheaper than F4TCNQ by over a hundred of times. Nevertheless, due to its low EA (ca. 4.6 eV), DDQ is not an efficient dopant for most of the semicrystalline polythiophenes such as P3HT, PQT and PBTTT. Recently, radialenes such as hexacyanotrimethylenecyclopropane (CN6-CP) have been developed for efficient p-doping [146]. Thanks to it large EA of ≈5.9 eV, CN6-CP is able to efficiently dope polymers with high-lying IE such as DPP-based copolymers. For instance, when doped with F4TCNQ and F6TCNNQ, the DPP-based copolymer exhibited a low maximum σ of below 10^{-2} S cm^{-1}. By contrast, when doped with CN6-CP, the same polymer gave a significantly enhanced σ of over 30 S cm^{-1} [146]. Nevertheless, the marginal solubility of CN6-CP in common organic solvents severely hampers it wide applicability for mix-solution doping. To overcome the solubility issue, methyl esters were employed to replace three of the nitrile groups of CN6-CP, yielding the analogous TMCN3-CP with significantly improved solubility [147]. Note that the introduction of methyl esters resulted in a decreased EA of 5.5 eV, yet it is still high enough to effectively dope DPP-based polymers as well as P3HT. The future success of p-dopant design relies on the development of strong dopants with sufficiently high electron affinity and good solubility.

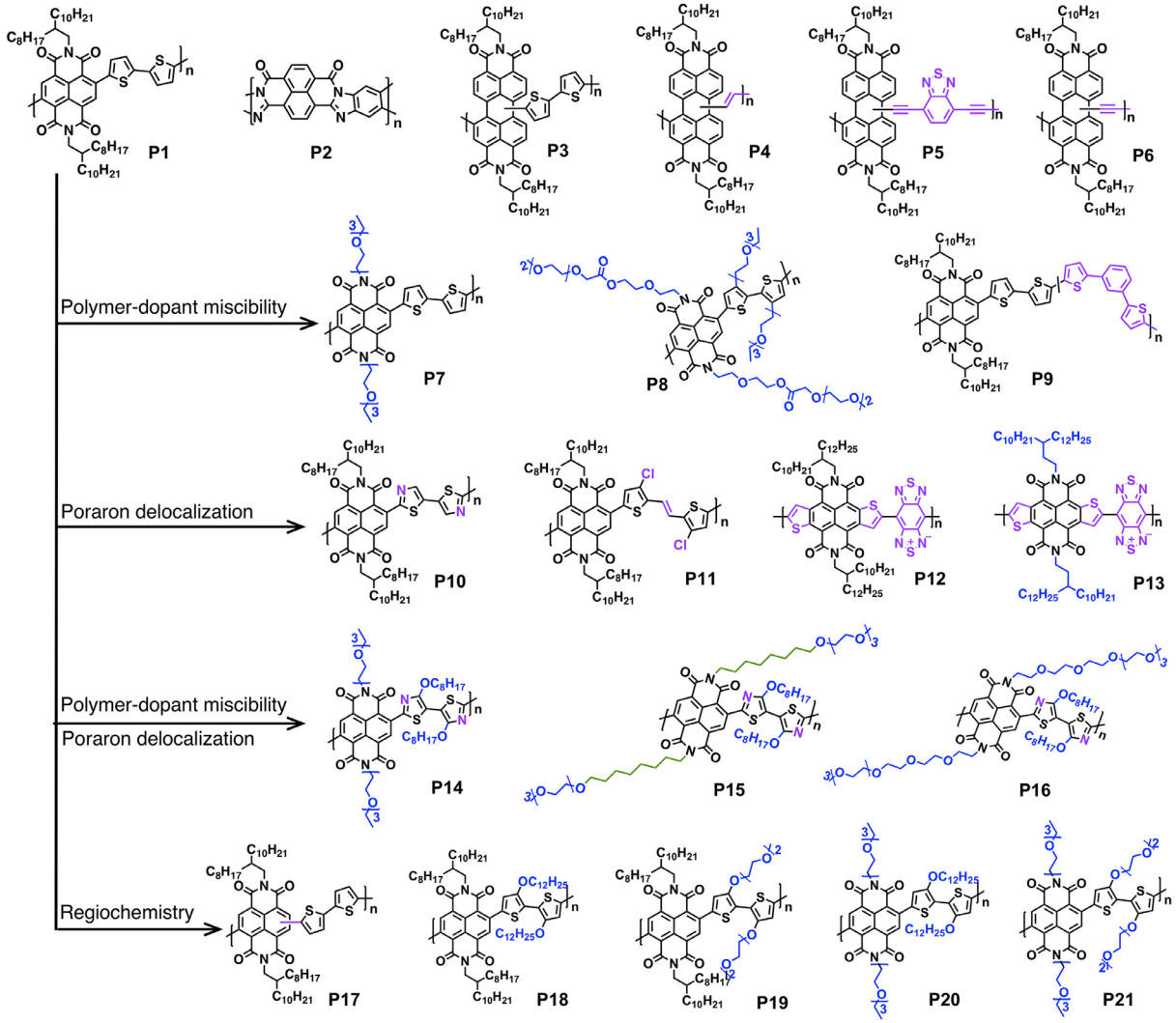

Fig. 11. Chemical structures of PNDI-based copolymers and related polymers for comparative studies.

3. Advances in n-type thermoelectric polymers and n-dopants

While the research of n-type TE conjugated polymers started much later than their p-type counterparts, thanks to the joint efforts of experimentalists and theoreticians, it has been rapid and fruitful. During the past half decade, quite a few novel n-type TE polymers and n-dopants have emerged. Here, we will comprehensively summarize the emerging empirical molecular designing rules by presenting the recent research progress of n-type TE polymers, and feature the recent advances in the development of n-dopants.

3.1. Emerging empirical molecular designing rules inspired by naphthalenediimide -based polymers

The research journey of n-type TE polymers started in 2014 from the pioneering work on n-doping the high performance electron-transporting poly((N,N′-bis(2-octyldodecyl)-naphthalene-1,4,5,8-bis(dicarboximide)-2,6-diyl)-alt-5,5′-(2,20- bithiophene)) (P(NDI2OD-T2) [148]. Since there are many analogous polymers for n-type materials, polymer abbreviations might lead to confusion, thus we use P1, P2, P3…to refer to n-type polymers, starting with P1 representing (P(NDI2OD-T2) (Fig. 11) Although P1 gives an outstanding electron mobility up to 0.85 $cm^2\ V^{-1}\ s^{-1}$ in OFETs [149], after being doped with (4-(1,3-dimethyl-2,3-dihydro-1H-benzoimidazol-2-yl)phenyl, N-DMBI) (D1, Fig. 12), its σ was only measured to be in the range of $\sim 10^{-3}$ S cm^{-1} [148].

3.1.1. Understanding the performance limitation

Phase segregation was observed in the doped film limiting the doping level, with only one percent of the dopant molecules being eventually active owing to their extremely poor solubility in the polymer matrix [148]. In a later work, P1 was doped with TDAE (D2, Fig. 12) and exhibited a similarly modest σ of ≈0.003 S cm^{-1}, whereas the ladder-type poly(benzimidazobenzophenanthroline) (BBL) (P2, Fig. 11) showed a maximum σ of 2.4 S cm^{-1} using the same dopant, ca. 3 orders of magnitude larger than that of P1 [150]. The calculated spin and polaron delocalization lengths are significantly larger in the torsion-free P2 than that in the distorted P1(Fig. 13A), well explaining the differences in the measured σ at the level of a single chain. This observation is consistent with a previous finding based on perylene diimide polymers P3-P6 (Fig. 11), that reducing D-A character increases polaron delocalization length and thus improves σ, with the acceptor-only P6 showing the largest σ of 0.45 S cm^{-1} and the D-A P3 giving only 0.001 S cm^{-1} [151]. Based on the abovementioned works, the modest σ of P1 can be attributed to both poor polymer-dopant miscibility limiting doping level and high polaron localization due to its distorted D-A feature. Keeping the performance limitations in minds,

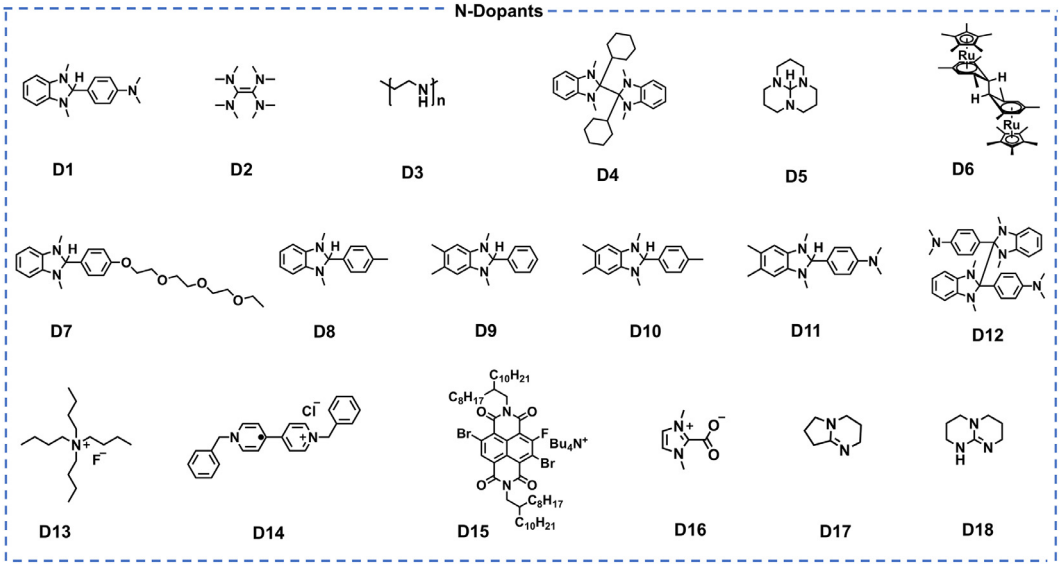

Fig. 12. Chemical structures of n-dopants.

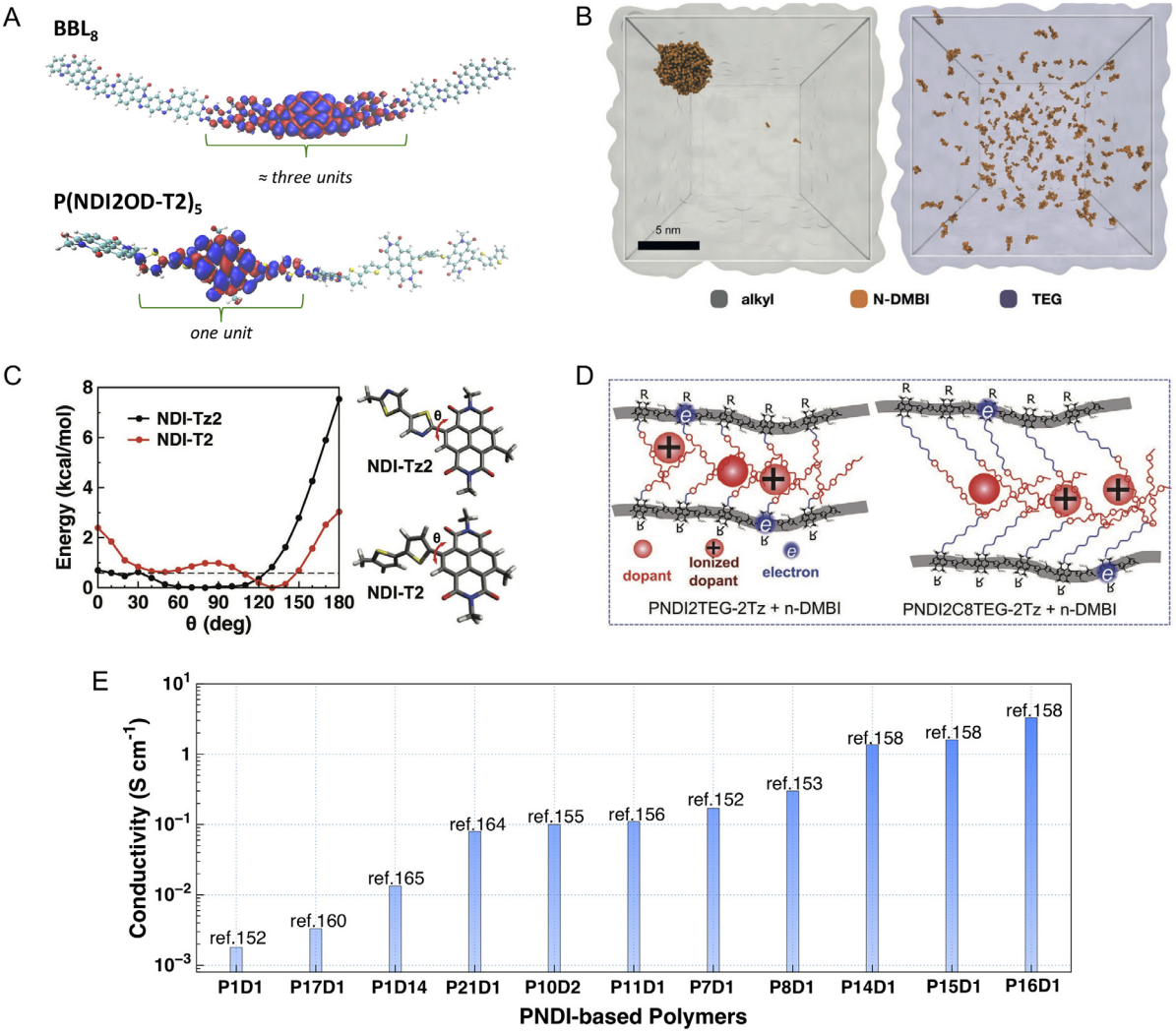

Fig. 13. Empirical molecular designing rules and performance progress on PNDI-based polymers. (A) Spin (α and β) density distributions of the longest BBL (n = 8, top) and P(NDI2OD-T2) (n = 5, bottom) oligomers, as calculated at the UDFT-BS and UDFT level, respectively. [150], Copyright 2016. Reproduced with permission from John Wiley & Sons Inc. (B) Representative snapshots of coarse-grained molecular dynamics simulations of n-DMBI molecules dissolved in a pure P1 side chain phase (left) and a pure P7 side chain phase (right). [152], Copyright 2018. Adapted with permission from John Wiley & Sons Inc. (C) ωB97X-D/6-311G** relaxed potential energy–θ profiles for the indicated structures. The dashed line denotes $k_BT \approx 0.6$ kcal mol^{-1} at 298 K. [155], Copyright 2018. Reproduced with permission from John Wiley & Sons Inc. (D) An illustration of the concept of controlling the dopant position relative to the backbone by tailoring side chains. [158], Copyright 2021. Adapted with permission from John Wiley & Sons Inc. (E) Evolution of electrical conductivities for PNDI-based polymers.

researchers have made corresponding efforts to rationally tailer the structure of PNDI-based polymers.

3.1.2. Improvement of polymer-dopant miscibility

To increase the solubility of dopants in the polymer matrix, the first attempt has been the substitute of alkyl side chain of P1 with polar triethylene glycol (TEG) side chains, yielding the new polymer P7. Thanks to the similar polarities of D1 and the TEG chains of P7, much better polymer-dopant miscibility was achieved as being observed from AFM images and confirmed by coarse-grained molecular dynamic simulation where TEG chains considerably increase the dopant's dispersion in the polymer matrix with respect to the alkyl side chains (Fig. 13B) [152]. As a result, the improved doping efficiency enabled P7 to be doped to a much higher σ of 0.17 S cm^{-1}, ca. 2 orders of magnitude higher than the analogous P1. Correspondingly, the highest PF of P7 ($\approx$0.4 μW m^{-1} K^{-2}) is 40 times higher than that of P1($\approx$0.01 μW m^{-1} K^{-2}) [152]. To further improve the solubility of the dopant in the polymer matrix, polar oligoethylene glycol side chains were inserted to both acceptor and donor sections of the polymer, generating another analogous polymer P8. After being doped with D1, P8 exhibited an even higher σ of 0.3 S cm^{-1} and an improved air stability comparing to that of P1 [153]. Besides, by incorporating kinked monomers (i.e. The meta-substituted monomer 1,3-bis(2-thienyl) benzene, TPT) into polymer backbone of P1, it is also proven to be effective to enhance the compatibility of the analogous polymer P9 and the dopant D1 [154]. However, due to the broken conjugation after the introduction of TPT, the charge carrier mobility of P9 is affected. Ultimately, the maximum σ of doped P9 is reduced as compared to P1, thus remanding researchers to take the unexpected impact of molecular engineering on charge carrier mobility into consideration while trying to achieve a higher charge carrier density.

3.1.3. Enhancement of polaron delocalization

To enhance the polaron delocalization, donor engineering has been identified as one of the effective strategies. For instance, substitution of the bithiophene (T2) unit in P1 with bithiazole (Tz2) unit generates P10, and brings 2-fold benefit: (i) the more electron-deficient Tz2 helps reduce the D-A character by elevating the electron affinity of P10; (ii) the internal steric repulsions in Tz2 moiety are significantly lower than in T2, thus promoting a more planar and rigid polymer backbone of P10 as compared to P1, as indicated by computed potential energy profile (Fig. 13C) [155]. Consequently, when exposed to the vapor of D2, P10 was doped to a higher extent and favourably packed tighter in the thin films, thus achieving a much higher σ of $\approx$0.1 S cm^{-1}, 30 times higher than that of P1. Recently, another electron-deficient dichlorodithienylethene (ClTVT) unit was employed to replace the T2 unit in P1, giving birth to a new polymer PNDIClTVT (P11). After being doped with D1, P11 shows a very decent σ of 0.11 S cm^{-1} and a highest PF of 2.6 μW m^{-1} K^{-2} [156]. Interestingly, further enhancement of electron affinity could be achieved by using more electron-efficient moieties, naphtho [2,3-b:6,7-b′]-dithiophenediimide (NDTI), benzo [1,2-c:4,5-c′]bis- [1,2,5]thiadiazole (BBT), and two polymers P12, P13 were synthesized, both of which have very low-lying LUMO energy levels($\approx$−4.4 eV). When doped with D1, P12 gives a decent σ of 0.18 S cm^{-1} and an optimal PF of 0.6 μW m^{-1} K^{-2}. Remarkably, by shifting the branching point of alkyl side chains only one C atom further away from the P12 backbone, the analogous P13 exhibits a strikingly higher σ of 5.0 S cm^{-1} and a remarkable PF of 14.2 μW m^{-1} K^{-2} [157]. The pronounced increase of over 20 times is attributed to the better crystallinity of P13 that promote a higher charge carrier mobility and simultaneously inhibit overdopping.

3.1.4. Enhancement of both polymer-dopant miscibility and polaron delocalization

Engineering side chains and the donor at the same time allows for improving the polymer-dopant miscibility/doping efficiency and simultaneously enhancing the polaron delocalization [158,159]. For instance, the TEG substituted PNDI-Tz2-based polymer P14 exhibits a largest σ of $\approx$1.4 S cm^{-1}, which is ca. 3 order of magnitude larger than the reference polymer P1, and ca. 10 times higher than TEG-modified P7 and Tz2-replaced P10 [158]. But on the other hand, the introduction of TEG chains causes a negative effect on the molecular packing of P14 as compared to P1, with higher load of dopants. To address this issue, amphipathic side chains were utilized to replace the TEG chains, that is, an alkyl side chain was inserted between the polymer backbone and the polar ethylene glycol chains, yielding the analogous P15. As a consequence, the alkyl chain segment spacer keeps the dopants further away from the backbone (Fig. 13D, right), thus greatly reducing the negative impact of counterions. Such a reduced Coulombic interaction helps enhance the S, with P15 showing comparable largest σ of $\sim$1.6 S cm^{-1} but a larger S of -326 μV K^{-1} which is nearly 2-fold that of P14 (of -167 μV K^{-1}), thus leading to an improvement of PF by $\approx$ ca. 5 times, from 3.8 to 16.5 μW m^{-1} K^{-2} [158]. By comparision, using purely longer polar side chains to replace TEG gives a even higher maximum σ of 3.3 S cm^{-1} for P16 but also decreases the S to -115 μV K^{-1} resulting in a comparable PF of 4.3 μW m^{-1} K^{-2} to that of P14, confirming that the enhancement of S for P15 is not from the increased length of the side chains but originates from the use of the amphipathic side chains [158].

3.1.4. Role of regiochemistry

Besides, regiochemistry of both backbone and pendant groups plays an essential role in the electrical properties of PNDI-based polymers. To investigate the impact of backbone chemistry, the regioirregular version of P1, namely RI-P(NDI2OD-T2) (P17) was synthesized and chemically/electrochemically doped [160,161]. Somehow counterintuitively, P17 can be doped to slightly better σ values than P1 irrespective of the dopants (D1, D2), contrasting the case of classic semicrystalline P3HT [98,100]. The higher tolerance of P17 to disorder could be ascribed to the following factors: (i) the highly aggregating nature of the PNDI-T2 polymer even in its RI form causes local aggregate regions to serve as bridges for intermolecular hopping of charges thus maintaining a decent charge carrier mobility for P17 despite its much lower levels of crystallinity [162,163](ii) the RI linkage does not cause more intrachain steric repulsions and does alter the LUMO energy of the polymer (iii) The asymmetric spin distribution and higher structural disorder of P17 facilitate a greater dopability as compared to P1, thus resulting in a much larger charge density and finally a slightly higher σ [160]. Very recently, regiochemisry and polarity of pendant groups were proven to have a huge impact on the PDNI-T2 polymer. Compared to nonpolar alkyl side chains substituted P18 which only gives an optimized σ value of $\approx 1.4\times 10^{-5}$ S cm^{-1}, the introduction of polar glycol ether groups facilitates both an improved polymer/dopant miscibility and an enhanced electron affinity, thus elevating the dopability and improving the maximum σ of the analogous polymers, with ca. 8.2×10^{-4} S cm^{-1}, 0.002 S cm^{-1}, and 0.08 S cm^{-1} being achieved for P19, P20 and P21, respectively [164]. This work emphasizes the importance of taking both identity and regiochemistry of side chains into consideration in future design of efficient conjugated polymers.

Looking back at the development of PNDI-based n-type TE polymers, research efforts of seven years has substantially improved the σ by >1000-fold (Fig. 13E) and generated a wealth of empirical molecular designing rules that will help guide the rational design of next generation high performance D-A copolymers. Table 2 summarizes the electrical and TE properties of PNDI-based polymers.

Table 2
A summary of conductivity, Seebeck coefficient and power factor of state-of-the-art PNDI-based n-type conjugated polymers.

Polymer	Dopant (Method) [a]	σ_{max} [S cm^{-1}]	S [μV K^{-1}] [b]	PF_{max} [μW m^{-1}K^{-2}]	Ref.
P1	D1(M-S)	~0.001	-290	0.010	[152]
	D2(Vapor)	0.003	-150	0.013	[150]
	D14(Sq.)	0.013	-324	0.035	[165]
	D17(Vapor)	0.004	_	0.024	[166]
P2	D1(Sq.)	1.4	-112	1.5	[167]
	D2(Vapor)	2.4	-60	0.43	[150]
	D14(Sq.)	1.63	-199	5.37	[168]
	D3(M-S)	8	~-146	12	[169]
P3	D4(M-S)	0.004	_	_	[151]
P4	D4(M-S)	0.0021	_	_	[151]
P5	D4(M-S)	0.07	_	_	[151]
P6	D4(M-S)	0.45	_	_	[151]
P7	D1(M-S)	0.17	~-157	0.4	[152]
P8	D1(M-S)	0.3	~-190	0.4	[153]
P9	D1(M-S)	0.0004	_	_	[154]
P10	D2(Vapor)	~0.1	-477	1.5	[155]
P11	D1(M-S)	0.11	-485	2.6	[156]
	D15(M-S)	0.2	-1854	67	[156]
P12	D1(M-S)	0.18	-56	0.6	[157]
P13	D1(M-S)	5	-169	14.2	[157]
P14	D1(M-S)	1.36	-167	3.8	[158]
P15	D1(M-S)	1.6	-326	16.5	[158]
P16	D1(M-S)	3.3	-115	4.3	[158]
P17	D1(M-S)	0.0033	_	_	[160]
P18	D1(M-S)	~10^{-5}	_	~10^{-6}	[164]
P19	D1(M-S)	0.00082	_	~10^{-5}	[164]
P20	D1(M-S)	0.002	_	~10^{-5}	[164]
P21	D1(M-S)	0.08	_	0.24	[164]

[a] (M-S) via mixed-solution processing, Sq.) via sequential doping
[b] S values corresponding to the PF_{max}.

3.2. Poly(p-phenylenevinylene)-based polymers and ladder-type polymers

3.2.1. Poly(p-phenylenevinylene)-based polymers

Another group of promising n-type TE polymers has been the poly(p-phenylenevinylene) (PPV) based polymers. Initially reported in 2015, three PPV derivatives, the benzodifurandione-based PPV(BDPPV) (P22, Fig. 14), and the halogen substituted ClBDPPV(P23) and FBDPPV(P24) exhibited record n-type σ values at the time [170]. Actually, P22 was firstly synthesized in 2013 with a low-lying LUMO energy level of −4.0 eV and applied in OFETs, showing an impressive electron mobility of ≈ 1 $cm^2V^{-1}s^{-1}$ [171]. When doped with D1, P22 showed an optimized σ of 0.26 S cm^{-1} and a highest PF 1.6 μW m^{-1} K^{-2}, whereas P23 and P24 exhibited significantly higher σ values of over 5 S cm^{-1} and over 10 S cm^{-1}, respectively, with a highest σ of 14 S cm^{-1} and a best PF of 28 μW m^{-1} K^{-2} being achieved for P24 [170]. The observed much better electrical performance is ascribed to: (i) the of electron-withdrawing halogen atoms helps reduce the LUMO energy, leading to a higher dopability of the analogous polymers; (ii) the incorporation of fluorine atoms promotes a higher charge carrier mobility by a factor of 2-fold, thus contributing to a higher σ under similar doping level. Interestingly, it is observed that the addition of D1 enhanced the molecular packing which is favorable for charge carrier mobility in the doped state [172]. The record σ value (14 S cm^{-1}) of P24 has been kept for 5 years until the same research group synthesized a trisaminomethane derivative (TAM) (D5, Fig. 12) as more efficient n-dopant, and D5-doped P24 gives a maximum σ of 21 S cm^{-1} [37]. Hereby, the impact of dopants is discussed in further depth in chapter 3.4. Soon after, the new record value is refreshed when the same group incorporated a linear glycol-based side chain into the backbone of P24, yielding the analogous P25. When doped with D1, P25 gives a optimal σ of ca. 18 S cm^{-1} a highest PF of 11.6 μW m^{-1} K^{-2}, whereas when doped with D5, P25 exhibits a highest σ of ca. 25 S cm^{-1} a maximum PF as high as 80 μW m^{-1} K^{-2} [36].

Using FBDOPV as an acceptor unit, two analogous PPV-based polymers were synthesized by incorporating different donor units, 9,9-dioctyl-fluorene and 3-dodecyl-2,2′-bithiophene, yielding P(FBDOPV-F) and (P(FBDOPV-2T-C12)) (P26, P27). When doped with D1, P27 exhibited σ values that are ca. 4 orders of magnitudes larger than that of P26. The superior performance of P27 is rationalized by the computed significantly smaller torsional angle favoring better intermolecular packing and more delocalized polarons, thus leading to both high electron mobility and much higher σ values [173]. Recently, an analogous polymer of P23 (P28) was synthesized by incorporating bithiophene as donor. When doped with D1, P28 exhibited a high σ of 8.1 S cm^{-1} and a maximum PF 21μW m^{-1} K^{-2}, slightly superior to that of P23 [156]. Very recently, further step forward has been taken by developing a series of extended and planar thiophene-based PPV derivatives (P29, P30) exhibiting new record σ values [40]. Although the thin films of P29 and P30 are substantially disordered as detected by GIWAXS measurement, after being doped with D1, the films exhibit exceptionally high σ of 90 S cm^{-1}. The high tolerance to disorder is attributed to their exceptionally delocalized polarons induced by high degree of planarity along the polymer backbone (Fig. 15A), and to their intrinsically good miscibility with the dopant molecules. Remarkably, the spin density of P29 extends over nearly 5 repeating units (Fig. 15B). The extensive intrachain conformational order of P29 and P30 endows them with efficient charge transport properties as evidenced by the Hall-effect measurement of the doped films. This finding is consistent with prior reports that polymers with strong rigidity are more resilent to disorder [174,175]. By contrast, the structurally distorted P30 shows a much lower maximum σ of 2 S cm^{-1}, still quite decent as an n-doped polymer. By far, the extraordinarily high σ of P29 has been the newest record value, ca. 1-2 orders of magnitudes higher than the majority of n-doped polymers.

3.2.2. Ladder-type polymers

Polycondensation of bis-lactone and bis-isatin creates the double-stranded, quasi-torsion-free PPV derivatives P32 and P33 [177]. When doped with D1, a maximum σ of 1.1 S cm^{-1} and a highest PF of 1.96 μW m^{-1} K^{-2} [177] were recorded for the P32 films. According to the computed spin density distribution, it is convincing that the polarons are strongly delocalized along the flat backbone of the doped P32. Also, the low-lying LUMO (−4.49 eV) makes it thermodynamically favorable for an efficient doping and endows the polymer with good air-stability. Note that when doped with D5, P32 gives an even higher σ of 4.0 S cm^{-1} and a significantly better PF of 33.9 μW m^{-1} K^{-2} [36] Longer side chains of P33 lead to larger π–π stacking distance, inferior electron mobility and thus much lower maximum σ of 0.07 S cm^{-1} and an inferior PF of 0.25 μW m^{-1} K^{-2} as compared to P32. Later, another two conformationally locked bis-lactone-alternating-bis-isatine polymers were synthesized via metal-free aldol condensation (P34, P35) [178]. Thanks to the strong electron-withdrawing character of the monomers, both polymers have an exceptionally high electron affinity, creating an offset large enough for efficient doping. Consequently, when doped with D1, P34 and P35 exhibited maximum σ of 0.2 and 0.28 S cm^{-1}, and corresponding highest PF of 0.12 and 0.16 μW m^{-1} K^{-2}, respectively. Hereby, shortening the side chain length is beneficial for a higher σ, in agreement with the finding for P32 and P33 [177]. Substituting the phenyl-bis-lactone with naphthalene-bis-lactone yields P39 with extended ring size, though, this expansion of the aromatic ring diluted the density of the electron deficient groups and thus reduced the electron affinity of P36. As a result, the doped film of P36 gives a much inferior maximum σ of only 0.008 S cm^{-1} and a lower PF

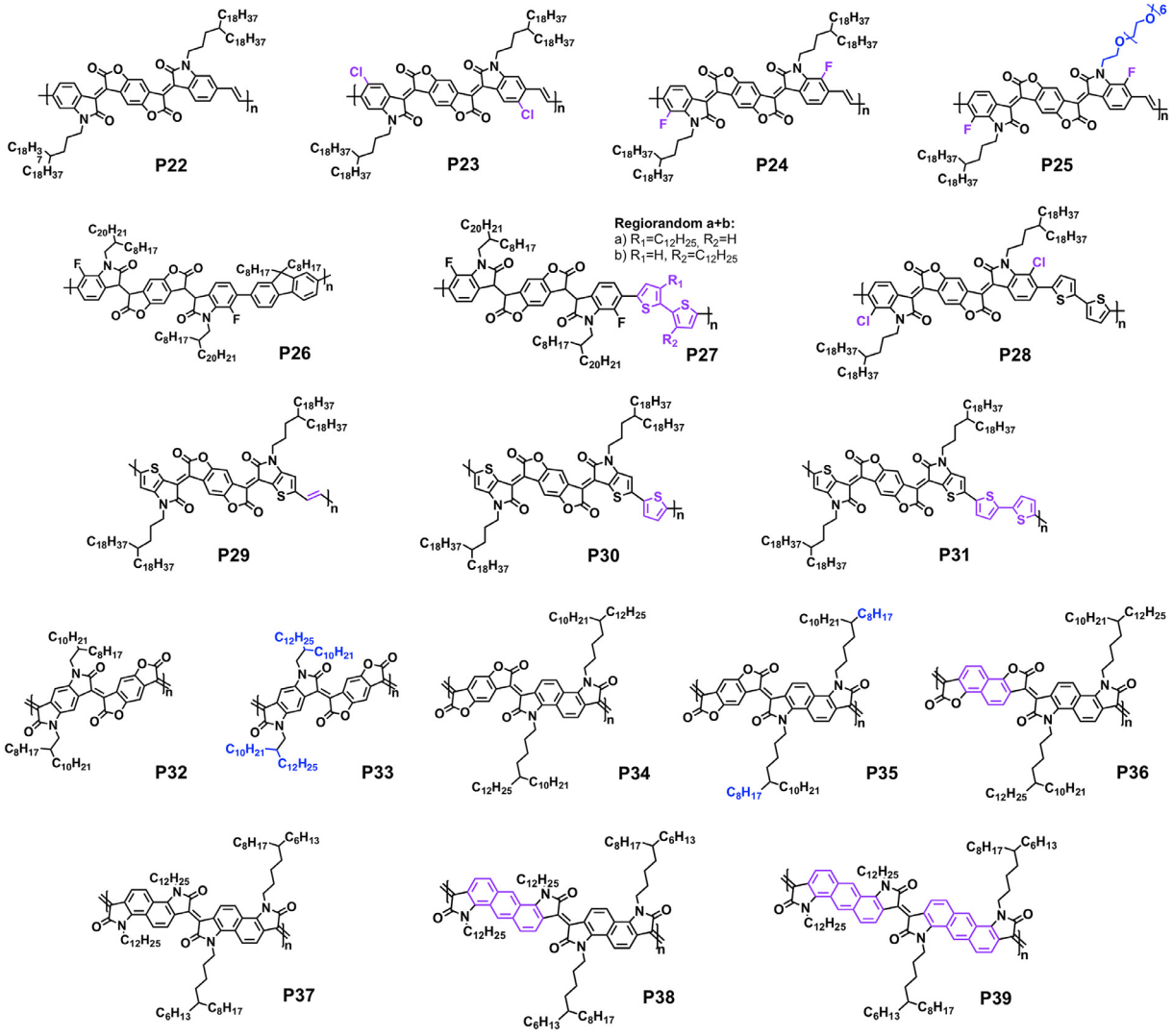

Fig. 14. Chemical structures of PPV-based copolymers and ladder-type polymers.

of 0.034 μW m^{-1} K^{-2} [178]. Very recently, three ladder-type polymers were synthesized and the impact of the size of the central acene ring were systematically investigated. Interestingly, it is observed that the electron affinities of the polymers increased as the central acenene core size was reduced from two anthracenes (P39) to mixed naphthaleneanthracene (P38) and two naphthalene cores (P37), with their TE performance of corresponding D1-doped films following the same trend, with σ from 0.018, to 0.26, and to 0.65 S cm^{-1} and PF from 0.25, to 1.6, and to 3.2 μW m^{-1} K^{-2} for P39, P38 and P37, respectively [179]. According to a recent study, the persistence length of these double-stranded rig-rod behaving could rival or even surpass their contour length and this leads to relatively long hopping distances and high charge carrier mobilities. To fully harvest the potential of these polymers, however, it will be important to further reduce the energetic disorder encountered by the charge carriers which leads to relatively slow hopping frequencies [180]. Table 3 summarizes the electrical and TE properties of PPV-based and ladder-type polymers.

3.3. Emerging conjugated polymers based on other building blocks

3.3.1. Diketopyrrolopyrrole-based polymers

Due to their planar skeleton and narrow band-gap and the ambipolar nature of their charge transport, DPP-based D-A copolymers have attracted lots of attention and have been intensively studied in the field of OFETs and OPVs during the past decade [128] and have been investigated not only for p-type (section 2.3.3), but also for n-type TE materials. Recently, two DPP-based copolymers with high electron mobility were doped with D1. Interestingly, fluorine substitution of the donor moiety in P41 (Fig. 16) resulted in an enhanced electron affinity (-4.11 eV) as compared to P40 (-3.93 eV) [181]. Moreover, the intramolecular H-bonds network in P41 helped planarize its backbone. In addition, the bimodal distribution of face-on and edge-on orientations in the films P41 promoted a favorable dopant accommodation and thus better polymer-dopant miscibility. Together, the D1-doped P41 gives a considerably large σ of 1.3 S cm^{-1} and a maximum PF of 4.65 μW m^{-1} K^{-2}, over 1000 times higher than that of P40 (0.001 S cm^{-1} and $\approx$10^{-4} μW m^{-1} K^{-2}) [181]. Later, pyrazine-flanked DPP (PzDPP) was employed as a stronger acceptor unit to copolymerize with an electron-deficient donor moiety 3,3′- dicyano-2,2′-bithiophene, yielding the new polymer P43 with a much lower LUMO than its thiophene-based reference polymer P42. The pyrazine-based P43 forms intramolecular H-bonds and displays more planar backbone conformation than P42. As a result, when doped with D1, P43 gives an excellent σ of 8.4 S cm^{-1} a maximum PF of 57.3 μW m^{-1} K^{-2}, much larger than that for P42 (0.39 S cm^{-1} and 9.3 μW m^{-1} K^{-2}) [182]. Note that through

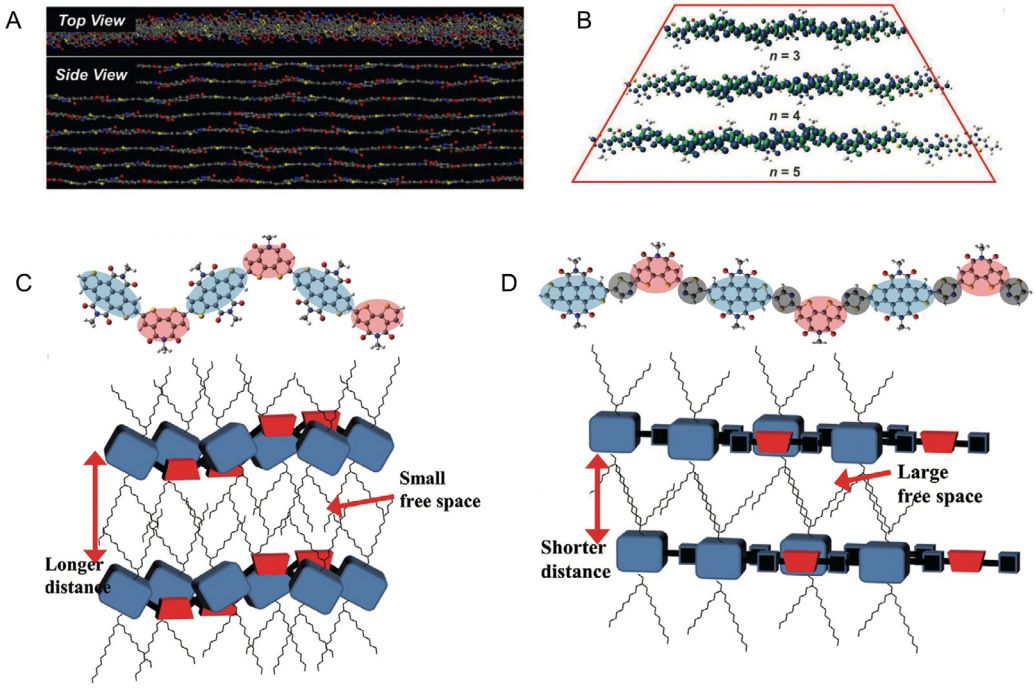

Fig. 15. (A) Molecular dynamics simulations of the backbone conformation of TBDPPV in alkyl-chains disordered region. The alkyl-chains and hydrogen atoms are omitted for clarity. Red, oxygen atoms; yellow, sulfur atoms; blue, nitrogen atoms. (B) Comparison of the spin densities on the anions of TBDPPV oligomers (n = 3, 4, and 5) calculated at the UωB97XD/6-31g(d) level. [40], Copyright 2021. Adapted with permission from John Wiley & Sons Inc. (C) DFT calculation results of backbone geometry and cartoon representations of interpolymer docking models for P49(C) and P51 (D). [176], Copyright 2020. Adapted with permission from John Wiley & Sons Inc.

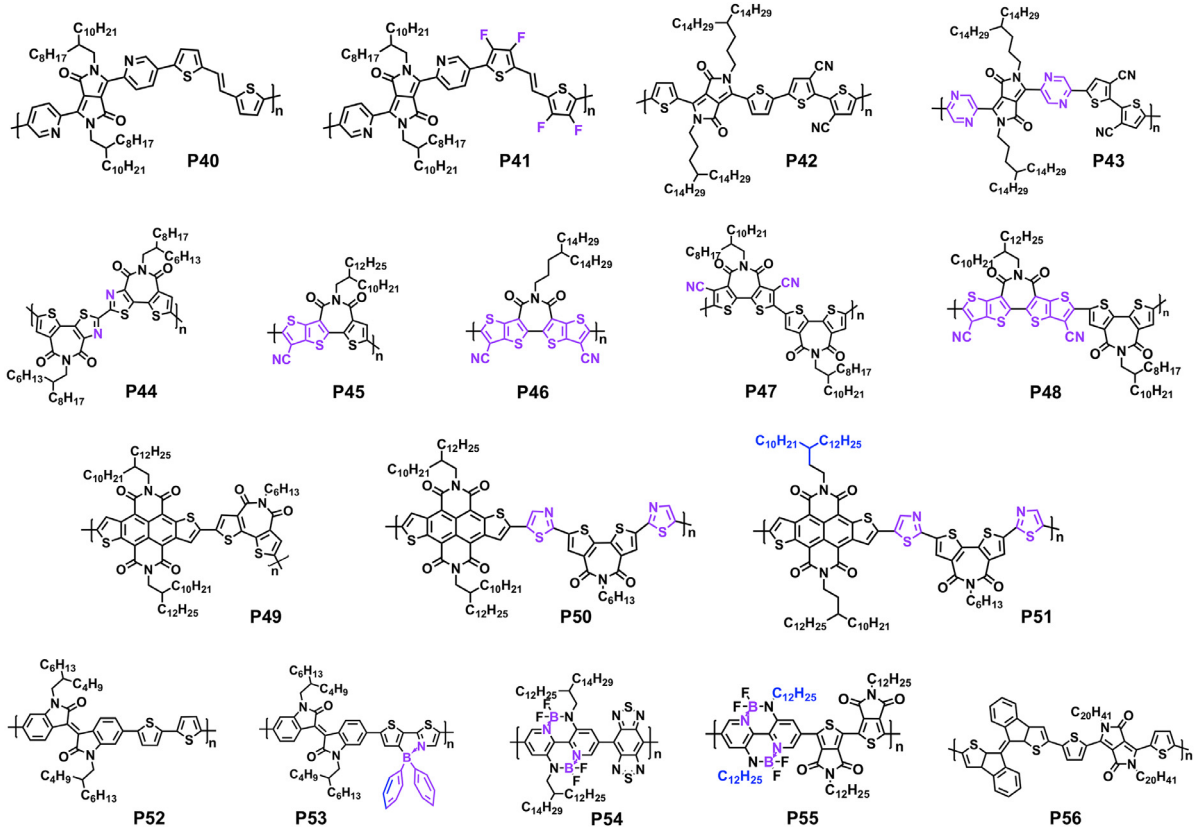

Fig. 16. Chemical structures of other n-type thermoelectric polymers.

Table 3
A summary of conductivity, Seebeck coefficient and power factor of state-of-the-art PPV-based and ladder-based n-type conjugated polymers.

Polymer	Dopant (Method) [a]	σ_{max} [S cm^{-1}]	S [μV K^{-1}] [b]	PF_{max} [μW m^{-1}K^{-2}]	Ref.
P22	D1(M-S)	0.26	_	1.6	[170]
P23	D1(M-S)	7	_	16.5	[170]
P24	D1(M-S)	14	_	28	[170]
	D5(M-S)	21	_	51	[37]
P25	D1(M-S)	18	-94	11.6	[36]
	D5(M-S)	25	-198	80	[36]
P26	D1(M-S)	0.042	-267	0.3	[173]
P27	D1(M-S)	~10^{-5}	_	_	[173]
P28	D1(M-S)	8.1	_	21	[156]
	D1+D5(M-S)	0.75	-870	56	[156]
P29	D1(M-S)	90	_	76	[40]
P30	D1(M-S)	65	_	106	[40]
P31	D1(M-S)	2.3	_	_	[40]
P32	D1(M-S)	1.1	-170	1.96	[177]
	D5(M-S)	4.0	-204	33.9	[36]
P33	D1(M-S)	0.07	_	0.25	[177]
P34	D1(M-S)	0.2	-22	0.12	[178]
P35	D1(M-S)	0.28	-21	0.16	[178]
P36	D1(M-S)	0.008	-210	0.034	[178]
P37	D1(M-S)	0.65	-256	3.2	[179]
P38	D1(M-S)	0.26	-246	1.6	[179]
P39	D1(M-S)	0.018	-368	0.25	[179]

[a](M-S) via mixed-solution processing
[b]S values corresponding to the PF_{max}.

modulating the aggregates of P43 in solution, the σ was recently pushed up to 32.1 S cm^{-1} [39].

3.3.2. Homopolymer based on functionalized (unfunctionalized) bithiophene imide

Recently, an imide-functionalized thiazole (DTzTI) was identified as excellent building block for all-acceptor polymers due to their outstanding electron transport property in OFETs. A large electron mobility up to 1.2 cm^2 V^{-1} s^{-1} as well as an extremely low off current of 10^{-10}-10^{-11}A were recorded for P44 based on its spin-coated films [183], far superior than its bithiopheneimide (BTI)-based analogous polymer [184], even outperforming that of the benchmark n-type P1 [149]. When doped with D1, P44 exhibited an outstanding σ of 4.6 S cm^{-1} and a maximum PF of 7.6 μW m^{-1} K^{-2}, about 3 orders of magnitude higher than P1 [185]. The high performance of P44 is attributed to its minimized D-A character and high planarity leading to more two-dimensionally delocalized polarons and much closer π–π stacking distance, which favourably prevent Coulomb interactions of the polymer in its doped state and facilitate the generation of free charge [185]. Very recently, a series of BTI-analogous building blocks were designed through the incorporation of cyano groups. Since these new building blocks are more electron deficient than BTI unit, the analogous P45, P46, P47, and P48 are featured with much deeper LUMO energy values (-3.63eV, -4. 11eV, -3.78eV, and -3.71eV) than that of the reference polymer PBTI (-3.48eV) [38]. When doped with D1, all these polymers exhibit high σ values of >0.1 S cm^{-1}, with P47 reaching an ultrahigh σ of 23.3 S cm^{-1} and a maximum PF of ca.10 μW m^{-1} K^{-2}, suggesting that cyano-functionalization is beneficial for conjugated polymers using BTI as building blocks.

As aforementioned, NDTI is a favorable electron-efficient acceptor for n-type TE polymers. When copolymerizing NDTI with a BTI unit, the all-acceptor polymers P49 possess a low LUMO energy level of -4.2 eV [176]. When doped with D1, P49 gives a moderate σ of 0.011 S cm^{-1} and a maximum PF of ca. 0.3 μW m^{-1} K^{-2}. DFT calculation reveals a wave-line backbone for P49 (Fig. 15C, upper), which is detrimental for molecular packing of the polymer. Incorporation of electron-deficient thiazole units into the backbone of P49 yielded P50 with a (pseudo)straight-line backbone as calculated by DFT(Fig. 15D, upper), which helped boost intermolecular packing ordering. When doped with D1, P50 gives a strikingly larger σ of 0.87 S cm^{-1} and a much higher PF of 9.9 μW m^{-1} K^{-2}. Motivated by their previous work [157], the authors shifted branching point of the alkyl side chains of P50 slightly further away from the backbone, yielding the analogous P51. Impressively, the D1-doped P51 gives a σ as large as 11.6 S cm^{-1} and a maximum PF as high as 53.4 μW m^{-1} K^{-2} [176]. The dramatically enhanced σ of P51 is attributed to the bimodal orientation of the polymer chains being able to well accommodate dopants in the 3D conduction channels without disrupting the molecular packing [176] (Fig. 15D, lower).

3.3.3. Copolymer based on organoboron chemistry

Previously, replacing C-C unit with a strong electron-withdrawing Boron-Nitrogen coordination (B←N) unit was proven to be an effective strategy to enhance the electron affinity of conjugated polymers [186]. Such an organoboron chemistry has been successfully employed in designing polymers with high electron mobility in OFETs [187] and with high efficiency in OPVs [188]. Recently, B←N unit was incorporated into the donor part of an isoindigo (IID)-based D-A copolymer P52 and was shown favorable in weakening the D-A feature and downshifting the energy levels of the polymer [189]. By comparison, the analogous organoboron P53 shows a LUMO energy of 0.27eV lower. Furthermore, the introduction of the B←N unit also makes P53 a regiorandom polymer with near-amorphous nature, thus enhancing the polymer-dopant miscibility. Consequently, although P52 is not dopable, the D1-doped P53 exhibited a σ of ≈0.001 S cm^{-1} and a maximum PF of 0.02 μW m^{-1} K^{-2} [189]. Very recently, the same research group synthesized two novel organoboron polymers (P54, P55) based on a distannylated monomer of B←N bridged bipyridine (BNBP) unit, both with ultralow LUMO energy level of ≈-4.4 eV [190]. When vapor-doped with D2, P54 shows a low σ of 6.6×10^{-5} S cm^{-1}, whereas P55 gives a significantly higher σ of 7.8 S cm^{-1} and a remarkable PF of ca. 24.8 μW m^{-1} K^{-2}. The tremendous difference in the performance originates from their disparity in electron mobility, with P54 exhibiting only 3.3×10^{-6} cm^2 V^{-1} s^{-1} and with P55 giving a much higher value of 0.029 cm^2 V^{-1} s^{-1}, respectively [190]. These reports render B←N incorporation a promising strategy to modulate the energy level and the dopability of conjugated polymers for efficient n-type thermoelectrics.

3.3.4. Surprisingly high performance observed from nonplanar polymers

While a majority of reports show that planarizing the backbone is a promising strategy to enhance the polaron delocalization and σ for conjugated polymers, σ as high as 0.45 S cm^{-1} was reported for a nonplanar, twisted DPP-based copolymer P56 when doped with D4 [191]. The authors uncovered that the nonplanar unit of P56 produces a steric space allowing for an efficient integration of the dopants, resembling the effect of kinked monomer in the backbone of P9 that help reach high doping efficiency [154]. This work broadens the designing strategies for polymers since rules that are regarded as negative factors for charge carrier mobility may not necessarily be detrimental for the ultimate σ after doping. Table 4 summarizes the electrical and TE properties of other emerging n-type conjugated polymers.

3.4. Traditional and emerging n-dopants

3.4.1. Traditional n-dopants: N-DMBI family and TDAE

As a most widely used air-stable n-dopant in organic thermoelectrics, N-DMBI(D1) was initially developed to dope semiconduc-

Table 4
A summary of conductivity, Seebeck coefficient and power factor of other state-of-the-art n-type conjugated polymers.

Polymer	Dopant (Method)[a]	σ_{max} [S cm^{-1}]	S [μV K^{-1}][b]	PF$_{max}$[μW m^{-1}K^{-2}]	Ref.
P40	D1(M-S)	0.001	_	~10^{-4}	[181]
P41	D1(M-S)	1.3	_	4.65	[181]
P42	D1(M-S)	0.39	_	9.3	[182]
P43	D1(M-S)	8.4	_	57.3	[182]
	D1(M-S)	32.1	_	_	[39]
P44	D2(Vapor)	4.6	-129	7.6	[185]
P45	D1(M-S)	0.19	-123	0.25	[38]
P46	D1(M-S)	0.28	-73	0.1	[38]
P47	D1(M-S)	23.3	-83	10	[38]
P48	D1(M-S)	0.56	-94	0.33	[38]
P49	D1(M-S)	0.011	_	0.3	[176]
P50	D1(M-S)	0.87	_	9.9	[176]
P51	D1(M-S)	11.6	_	53.4	[176]
P52	D1(M-S)	~10^{-8}	_	_	[189]
P53	D1(M-S)	0.0011	-454	0.02	[189]
P54	D2(Vapor)	~10^{-5}	_	_	[190]
P55	D2(Vapor)	7.8	-179	24.8	[190]
P56	D6(M-S)	0.45	_	_	[191]

[a] (M-S) via mixed-solution processing
[b] S values corresponding to the PF$_{max}$.

tors in OFETs to enhance the air-stability of n-channel OFETs by compensating environmentally trapped electrons [192]. Being a hydride donor, although the doping mechanism of D1 has been inconclusive, it is acknowledged that the doping is caused by an interaction between the host and the dopant that starts with hydride/hydrogen atom transfer and ends with the generation of host radical anions [193]. A recent study show that in polar media, the doping is dominated by direct hydride H$^-$ transfer, whereas in apolar media, it is more thermodynamically preferred for doping to be mediated by the singly occupied molecular orbital (SOMO) after H$^\bullet$ release [194]. Introducing TEG chains to the DMBI (D7) helps enhance the miscibility between the dopant and the host, leading to noticeably higher doping efficiency as compared to D1 [195]. On the other hand, the SOMO energy levels were observed to have a noticeable effect on n-doping by comparing several benzimidazole derivatives with different SOMO energy levels (D8 (−3.02 eV), D9 (−2.99 eV), D10 (−2.91 eV), D1 (−2.82 eV), D11 (−2.73 eV)). Raising the dopant SOMO energy by ≈0.3 eV (from D8 to D11, the SOMO became less negative) resulted in an improved σ by >10 times for doped P1(Fig. 17A) [196]. Remarkably, the dimer version D12 was proven to be a direct electron donor, and its smaller and planar counterion makes it a stronger dopant than D1 [197].

As a strong electron donor, TDAE (D2) has a sufficiently high HOMO level and is used as a vapor dopant owing to its low boiling point. Previously, D2 was employed to optimize the oxidation levels and thus the TE performance for p-type PEDOT-Tos [5]. Later, D2 was used to dope a variety of n-type conjugated polymers via straightforward electron transfer from the dopant to the polymers [150,155,160,161,185,190]. The versatility of D2 makes it appealing for simultaneously regulating the doping levels of both p- and n-type polymers, which is highly desirable for the production of thermoelectric generators. However, due to its high volatility, D2 could diffuse out of the doped films at room temperature, not to mention practically operating in a thermoelectric generator at higher temperature [167]. As shown in Fig. 17B, upon annealing D2-doped P2 at 190°C for 10h, the σ of the film declined by over 100 times, whereas the σ of D1-doped P2 films is observed to be invariant even upon 20h's annealing, showing the strikingly different ther-

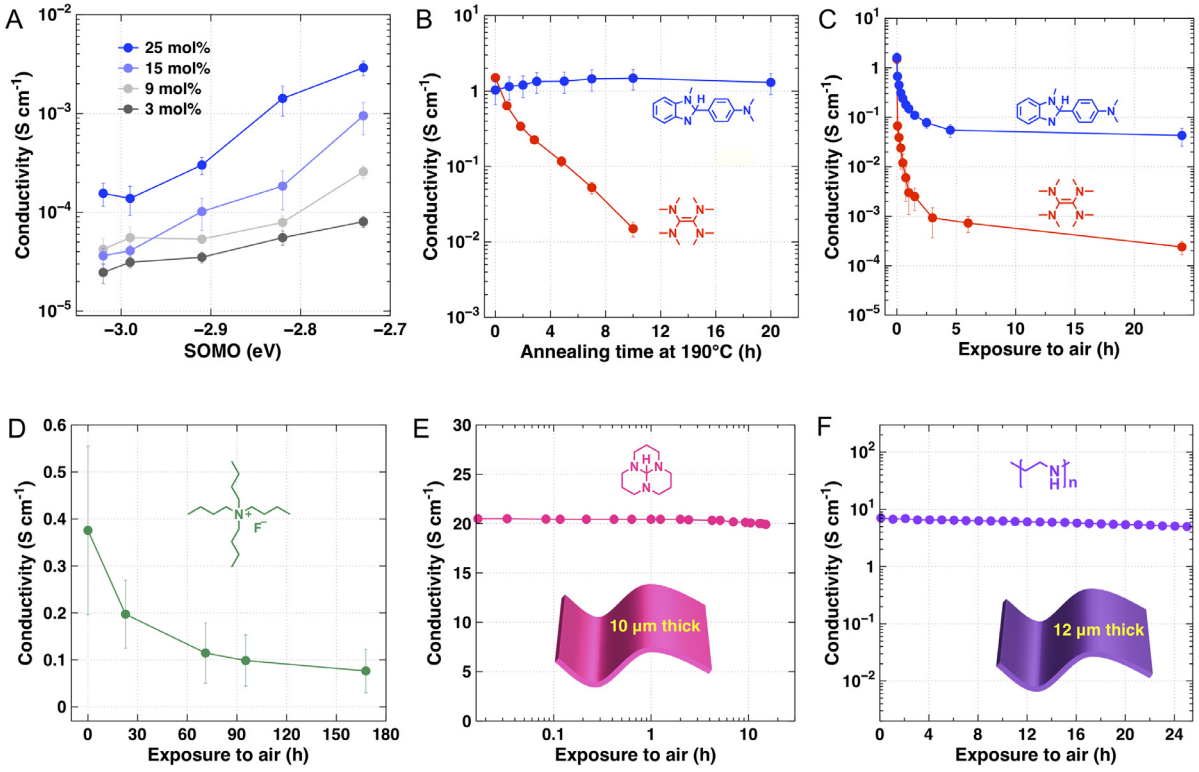

Fig. 17. (A) Electrical conductivity of doped P1 as a function of SOMO energy of dopants with different concentrations. [196], Copyright 2019. Reproduced with permission from American Chemical Society. Electrical stability test of D2 vapor-doped and D1 sequentially doped P2 films by (B) annealing at 190°C for 20 h in N2 and (C) exposing to air. [167], Copyright 2020. Reproduced with permission from American Chemical Society. (D) Air stability of 25 mol% D13-doped P23 films. [198], Copyright 2017. Reproduced with permission from John Wiley & Sons Inc. (E) Air stability of D5-doped P24 thick films without encapsulation. [37], Copyright 2020. Reproduced with permission from Macmillan Publishers Ltd. (F) Evolution of electrical conductivity of D3-doped P2 in air for 24 h. [169], Copyright 2021. Reproduced with permission from Macmillan Publishers Ltd.

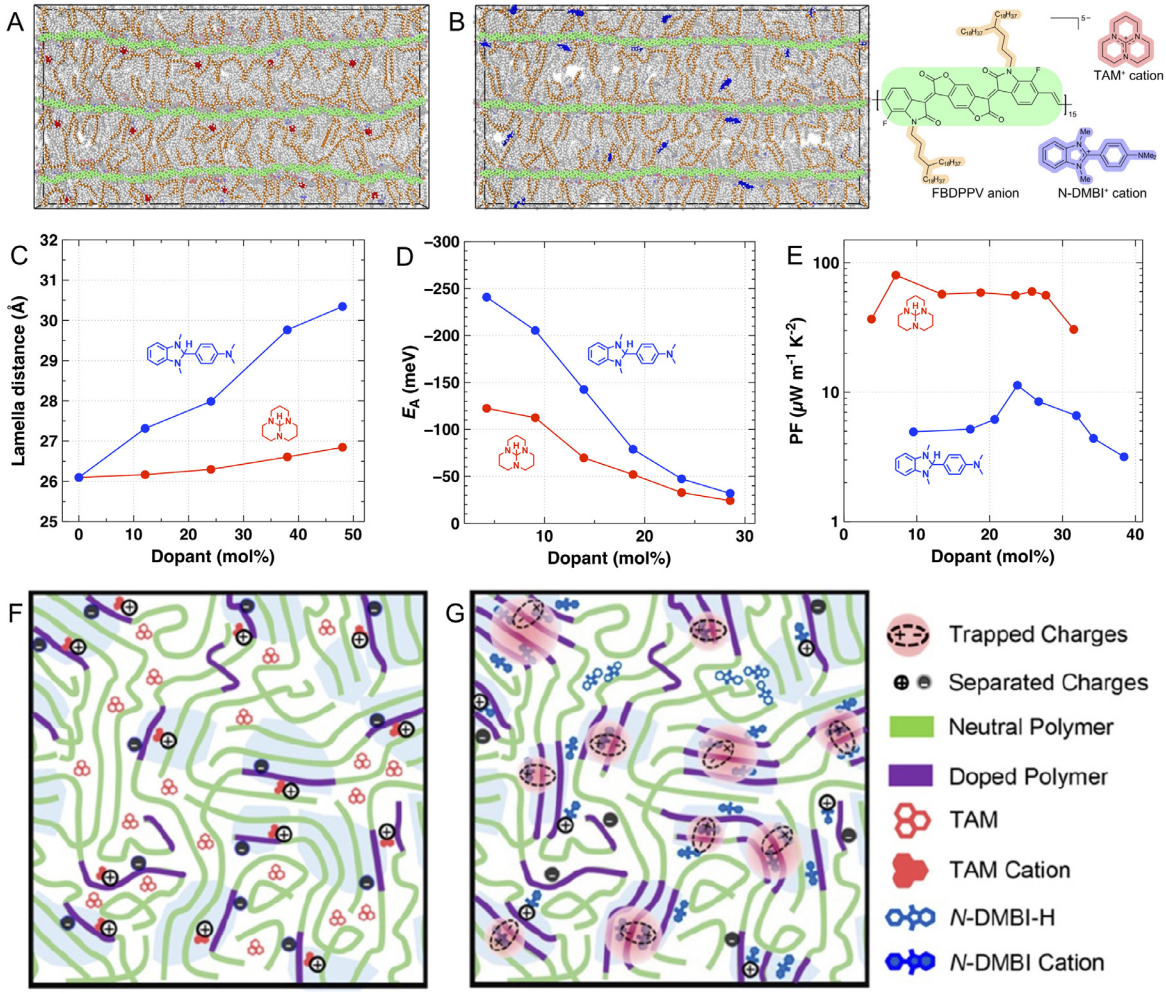

Fig. 18. Equilibrium configurations of n-doped FBDPPV by TAM (A) and N-DMBI (B) (top right: Chemical structures of FBDPPV anions, TAM+, and N-DMBI+ cations.) [37], Copyright 2020. Reproduced with permission from Macmillan Publishers Ltd. (C) Lamellar distance, (D) Measured E_A values, and (E) PFs of doped UFBDPPV (P25) with two n-dopants as a function of dopant concentration. [36], Copyright 2020. Reproduced with permission from American Chemical Society. Schematic of TAM-doped (F) and N-DMBI-H-doped (G) UFBDPPV (P25) films. [36], Copyright 2020. Adapted with permission from American Chemical Society.

mal stability of D1 and D2 [167]. Another noticeable disadvantage of D2 is its intrinsically poor air-stability due to chemiluminescence when exposed to oxygen [199]. As a result, the σ of D2-doped P2 films dropped instantly by ca. 2 orders of magnitude upon exposure to ambient for half hour, and finally decreased by ca. 4 orders of magnitude after exposure for 24h. In contrast, while the σ of D1-doped P2 also decreased over 1 order of magnitude after 1 day of exposure, it exhibited much better ambient stability (Fig. 17C) [167].

3.4.2. Tetrabutylammonium fluoride

Initially, a small dose of tetrabutylammonium fluoride (TBAF, D13) was incorporated to the P1-based solution-processed OFETs to fill the charge trap sites, resulting in a noticeable improvement in electron mobility and a simultaneous enhancement in air-stability of the devices [200]. The doping occurs through electron transfer from radical anions to the polymer. Later, D13 was employed to dope the electron-deficient PPV-based P23 for stable TE performance in ambient [198]. According to experimental evidence, the n-doping takes place through electron transfer from F^- anions to P23 via anion–π electronic interactions [198,201]. Although the D13-doped P23 film exhibits lower σ (0.6 S cm^{-1}) as compared to the D1-doped P23, it shows a satisfying air-stability, being able to retain σ of ca. 0.1 S cm^{-1} after 7 days of ambient exposure (Fig. 17D) [198].

3.4.3. Triaminomethane: the importance of smaller size

The triaminomethane-type dopant D5 was recently synthesized with the assistance of DFT calculations, showing high n-doping ability, good solubility and excellent stability [37]. In contrast to D1-doped P24 that the overall σ declines as film thickness increases, the σ of D5-doped P24 increases as film thickness increases and eventually reaches 21 S cm^{-1} at a film thickness of 10 μm. Thanks to the self-encapsulation effect, the D5-doped P24 shows a good staiblity in ambient that after 16h of exposure to air, and only a modest drop (ca. 5%) in its σ values could be seen (Fig. 17E) [37]. It is worth mentioning that a very recent work based on 12 μm-thick BBL films also indicated the favorable effect of self-encapsulation (Fig. 17F) [169]. MD simulation suggests that D3 with smaller size prefers to stay together with alky side chains of P24 due to the decent dopant-side chain miscibility, whereas D1 tends to interact with the polymer backbone leading to undesired Coulomb interactions. As shown in Fig. 18A and 18B, a majority of $D5^+$ cations located within the alkyl side-chain packing zones, whereas a considerable number of $D1^+$ cations stayed close to backbones [37]. The MD simulation was corroborated by GIWAXS measurement for solid-state microstructure, which revealed that

the distance of both lamellar packing and π–π stacking remains nearly invariant before and after incorporation of D5, whereas both distances increase after the addition of D1.

Similarly, when the TEG substituted P25 was doped with D1 and D5 separately, the lamellar distance of the D5-doped P25 only altered slightly between 26 Å and 27 Å, whereas it increased distinctly from 26 Å to 30.5 Å for D1-doped P25 (Fig. 18C). At a dopant ratio of 1mol%, D1-doped P25 had a high EA value (243meV) that is 2 times greater than that of the D5-doped P25(122meV). Moreover, the EA value in the D1-doped system decreased more dramatically as the doping level increased, indicating that the coupled ion pairs had significant Coulomb interactions (Fig. 18D). Finally, D5-doped P25 exhibited a maximum PF that is ca. 7 times larger than that of D1-doped P25 (Fig. 18E). Thus, the high TE performance of D5-doped P25 is ascribed to its low ionization and high carrier delocalization features (Fig. 18F), whereas a majority of potential carriers are confined by intense Coulomb contacts and the local energy landscape for the D1-doped P25 leading to lower TE performance (Fig. 18G) [36].

3.4.4. Benzyl viologen radical cation

Originally, neutral benzyl viologen (BV^0) was employed to dope conjugated polymers to achieve high-performance OFETs [202,203]. Owing to the strong reduction potential of BV^0, a small amount of dopant could lead to remarkably higher charge density and thus much higher charge carrier mobility. To avoid using water in the synthesis of BV^0, benzyl viologen radical cation ($BV^{\cdot+}$, D14) was synthesized by reducing BV^{2+} in anhydrous acetonitrile [165]. According to a recent report, when doped with D14, P1 gives a very decent σ values of 0.013 S cm^{-1} [165], which is 3-5 times greater than that of P1 doped with D1, D2 and D5. Note that D14 has a very similar SOMO energy level as compared to D2, making it a very strong electron donor. Another advantage is that the D14-doped films show ultralow contact resistance and higher stability than D2-doped film. Later, it was reported that D14 is also an effective n-dopant for P3 and the corresponding doped films have good electrical stability that the σ remains nearly unchanged after 24h of heating at 100C in glovebox [204]. Very recently, D14 was also used as n-dopant for P2, and a decent PF together with a very good thermal-stability were achieved [168].

3.4.5. Meisenheimer complexes of NDI-TBAF as n-dopant / co-dopant

Firstly, it is worth mentioning that Meisenheimer complex is defined as “a 1:1 reaction adduct between an arene carrying electron withdrawing groups and a nucleophile”(Wikipedia). Recently, a Meisenheimer complex NDI-TBAF (D15) was readily prepared by simply blending NDI and TBAF in solution and utilized as an efficient n-dopant for thermoelectrics [156]. For instance, D15-doped P11 exhibited an obvious higher maximum σ value of 0.2 S cm^{-1} and a much larger S of -1854 μV K^{-1}, far superior to that of D1-doped P11 (0.11 S cm^{-1}, ca. -500 μV K^{-1}). Finally, D15-doped P11 gives an enhanced PF as high as 67 μW m^{-1} K^{-2}, over 20 times larger than that of D1-doped P11. Besides, when using the ionic adduct D15 together with neutral dopant D1 as co-dopants, similar enhancing effect could be observed. This work demonstrated that F^-, in the form of Meisenheimer adduct, could be used as an efficient n-dopant, or as a co-dopant for achieving high-performing n-type organic thermoelectrics.

3.4.6. Nucleophilic organic molecules as efficient n-dopant

N-heterocyclic carbenes (NHCs) with strong nucleophilic ability are recognized as excellent σ-donors and have been widely utilized in organic chemistry [205]. Recently, a NHC precursor 1,3-dime- thylimidazolium-2-carboxylate (DMImC, D16) was designed as a thermally activated air-stable n-dopant [206]. Through thermal activation, DMImC could release NHC that actually n-dope the semiconducting polymers. As two demonstrations, P1 and P24 were separately doped with D16, resulting in maximum σ values of 0.0054 S cm^{-1} and 8.4 S cm^{-1}, respectively, very comparable to those films doped with D1 [150,170,185]. Due to its limited solubility in the commonly utilized halogenated solvent, D16 was only processable through sequential doping by dissolving in acetonitrile. Since D16 is air-stable and does not interact with semiconducting polymers before thermal annealing, the sequential doping could be processed in ambient. Remarkably enough, after annealing in inert atmosphere, the doped films could reach comparable maximum σ to those deposited inside glovebox. Very recently, two nucleophilic organic bases, namely 1,5,7-Triazabicyclo [4.4.0] dec-5-ene (TBD, D17) and 1,5-Diazabicyclo [4.3.0] non-5-ene (DBN, D18) were demonstrated as efficient n-dopants for semiconducting polymers [166]. When doped with D17, P1 exhibits a maximum σ value that is almost five times higher than that of P1 doped with D1 or D2. Strikingly, D17 and D18 are both very cheap in the cost, with a price as low as <20 $/gram, much cheaper than that of D1 which costs > 200 $/gram.

4. Enhancing thermoelectric performance: strategies beyond molecular design

Beyond molecular design, there are two major strategies to decouple S and σ: one is to utilize advanced solution processing (i.e., polymer chain alignment) to boost μ and thus the σ while keeping S invariant under a given doping level; another is to use DOS engineering to enhance S without sacrificing σ.

4.1. Polymer chain alignment: boosting electrical conductivity without degrading Seebeck coefficient

The first approach to decouple σ and S is to increase the σ by improving μ while keeping the n invariant in order to leave the S unaffected. Due to the fact that charge transport is a lot faster along the backbone direction than that along π–π stacking and alkyl stacking directions, polymer chain alignment has been well-recognized to have a remarkable impact on enhancing μ [207,208]. During the last two decades, a group of meniscus-guided coating (MGC) approaches has been developed to achieve molecular alignment for conjugated molecules, including zone-casting [209–212], solution shearing [27,213-216], dip coating [120,217-220], bar-coating [221,222], etc. An important feature of MGC methods is that they are well suited to steady-state, continuous, and large area deposition, such as R2R processing. For instance, when the pre-aggregating solution of P1 was bar-coated (Fig. 19A), the resulting film were highly aligned (Fig. 19B), displaying a considerably greater μ than that of identical polymer produced by spin coating and resulting in a large anisotropic ratio of ≈30 [221] (Fig. 19C).

Polymer chain alignment has recently been demonstrated to be beneficial in improving TE performance of conjugated polymers. Taking the case of PEDOT:PSS as an example, when processed via solution shearing approach (Fig. 19D), well-controlled phase separation and backbone alignment were achieved, with a σ value up to 4600 S cm^{-1} recorded [27]. In addition, the corresponding films preserved excellent optical transparency. As a result, in terms of both device performance and figure of merit for transparent conductors, the solution-sheared films significantly outperform the spin-coated films. Very recently, by combining of solution-shearing and a postdeposition solvent shearing treatment (Fig. 19E), quasi-metallic record-high σ values of 8500 ± 400 S cm^{-1} and a very large PF of ≈800 μW m^{-1} K^{-2} were achieved for PEDOT:PSS films along the shearing direction [34]. Based on X-ray scattering and optical measurements, the considerably improved σ is attributed to chain alignment of PEDOT and larger-sized domains (Fig. 19F).

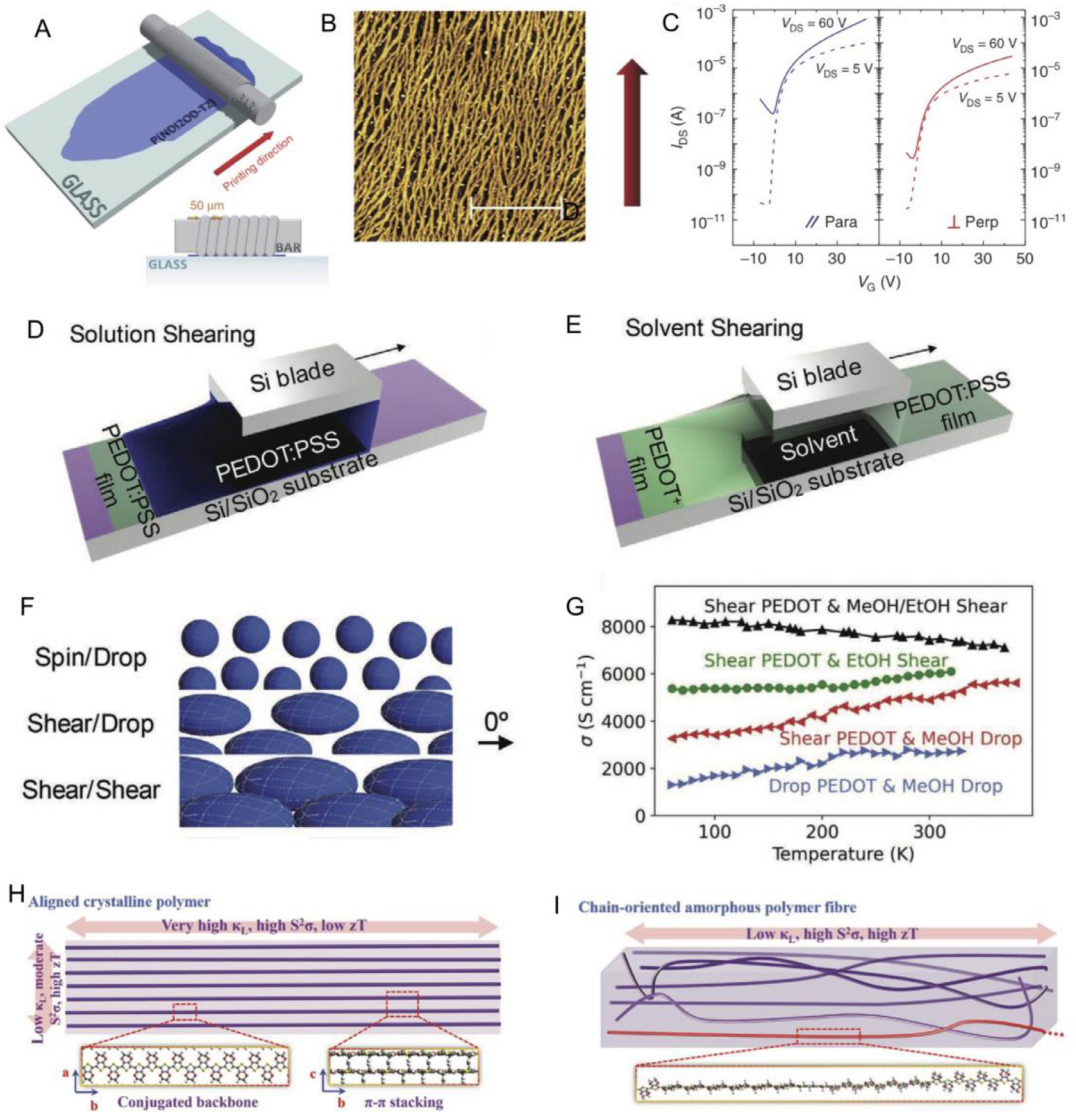

Fig. 19. (A) Sketch of the bar-coating process. (B) AFM picture of a submonolayer deposited by bar-coating a 0.5 g l^{-1} solution in mesitylene. (C) Typical transfer characteristic plots in linear (dashed) and saturation (solid) regimes of OFETs with the fibrils axis oriented parallel (blue) and perpendicular (red) to the probing direction. [221], Copyright 2015. Adapted with permission from Macmillan Publishers Ltd. Schematic illustration of sheared deposition of PEDOT:PSS (D) and postdeposition sheared solvent (E). (F) Schematic depicting the shearing-induced domain elongation; dark blue circles represent PEDOT-rich domains. (G) Temperature dependence of the conductivity of individual PEDOT: PSS films deposited by different methods and subjected to different solvent treatments. [34], Copyright 2021. Reproduced with permission from John Wiley & Sons Inc. (H) Anisotropic thermoelectric transport properties of crystalline polymers in the conjugated backbone and $\pi-\pi$ stacking directions, respectively. (I) Suppression of phonon transport in chain-oriented amorphous polymer fibers. [223], Copyright 2017. Adapted with permission from John Wiley & Sons Inc.

As shown in Fig. 19G, the σ values of PEDOT films are highly dependent on various deposition procedures and different solvent treatments.

In addition, when sequentially doped with F4TCNQ solution, the aligned P3HT film gives a $\sigma_{//}$ of ≈22 S cm^{-1} and $\sigma_{\perp}$ of ≈3 S cm^{-1} [138]. Remarkably, during a temperature gradient crystallization process, highly oriented P3HT films was fabricated using 1,3,5-trichlorobenzene (TCB) as a template, exhibiting low defects and high degree of charge delocalization. When doped with $Fe(TFSI)_3$, these highly oriented films give outstanding maximum σ of ≈320 S cm^{-1} [139], the highest ever reported for doped P3HT.

Mechanical alignment techniques [224, 225] have also been applied to PBTTT to enhance TE properties [226]. When aligned PBTTT film was doped by immersing in F4TCNQ solution, a large σ of 193 S cm^{-1} were recorded [140]. Using a recently developed ion-exchange doping method combined with alignment of the polymer chains by mechanical rubbing, excellent σ of > 4000 S cm^{-1} and PF of 137 μW m^{-1} K^{-2} were reported in PBTTT for transport parallel to the polymer alignment direction [35].

It is noteworthy that according to a recent computational investigation, while polymer chain alignment could help improve both σ and PF of conjugated polymers, the high degree of crystallinity and ultra-high molecular weight could lead to undesired large thermal conductivity (Fig. 19H) [223]. Such an effect is due to the fact that charge carriers and phonons flow along the polymer chains on different length scales, with the former having a shorter mean free path. It is therefore essential to tune the grain size of crystallites such that thermal and charge transport could be decoupled. As suggested by the authors, moderately shortening the length of polymer chain and reducing the crystallinity could significantly decrease thermal conductivity, and effectively increase energy conversion efficiency by ca. one order of magnitude (Fig. 19I). Favorably, the emerging class of conjugated poly-

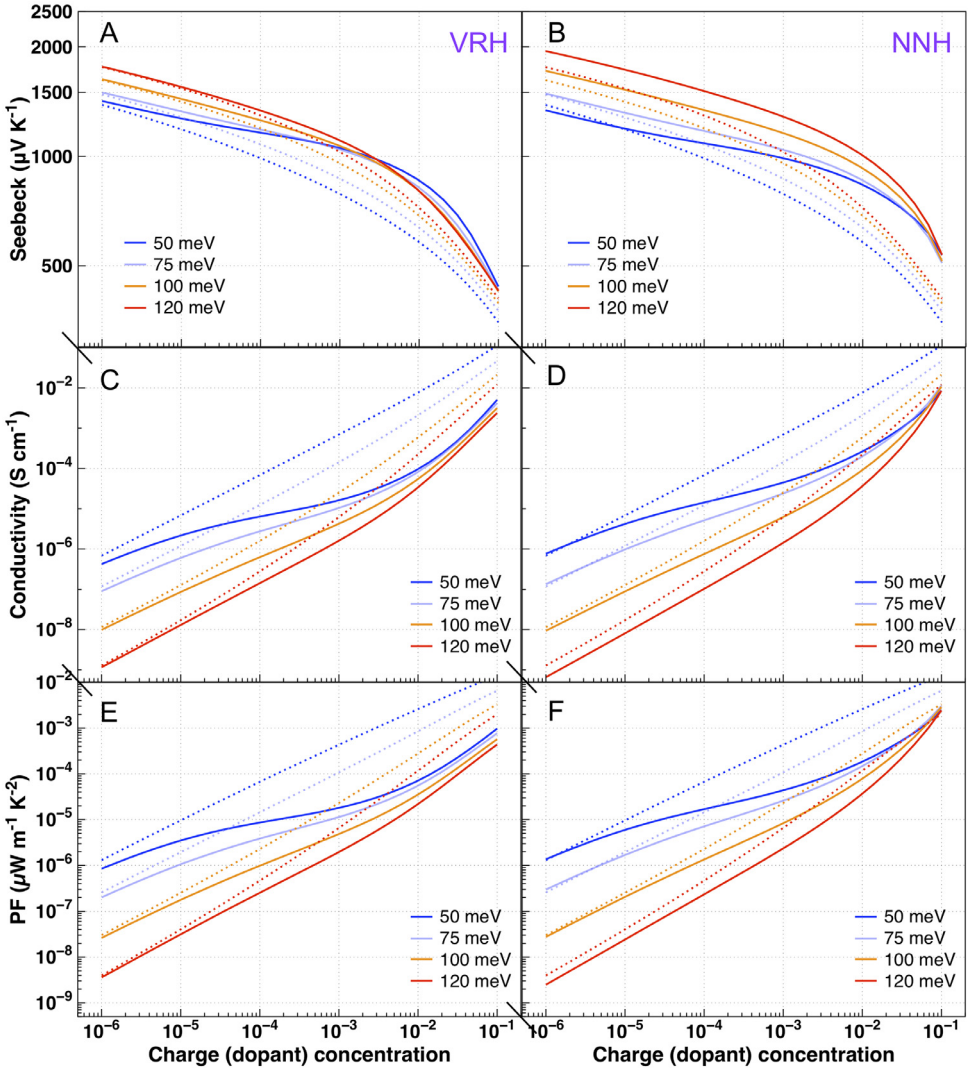

Fig. 20. Seebeck coefficient, conductivity, and power factor for both pristine and doped OSC calculated from Model II with variable range hopping (a-c) and nearest neighbour hopping (d-e). Parameters used $\nu_0 = 10^{13}$ s^{-1}, $a_{NN} = 1.8$ nm, $\sigma_{DOS} = 50$ - 120 meV, $T = 300$ K, and $\alpha = 2e9$ nm^{-1}. [234], Copyright 2018. Reproduced with permission from Linköping University Electronic Press.

mers is highly suitable for the strategy of chain alignment as most of them are high-performing low-crystalline donor-acceptor polymers [227,228]. The short-range intermolecular aggregation in these polymers is good enough to maintain efficient charge transport [175,229,230], whereas it helps restrain the thermal transport as it is typically shorter than the mean free path of phonon. Very recently, experimental evidence shows that when long alkyl side chains were attached to the aromatic rings of semiconducting molecule, the in-plane thermal conductivity was strongly suppressed as a result of a stronger localization of vibration modes [231]. Whether this technique for decoupling thermal and charge transport can be applied to polymeric systems remains an open question.

4.2. DOS engineering: enhancing Seebeck coefficient without sacrificing electrical conductivity

Theoretically, the DOS is typically believed to be of a specific shape and to have only one single Gaussian peak. In a framework considering hopping transport within a specified, sole Gaussian DOS, S and σ are mainly affected by disorder and concentration. Generally, the energetic disorder has a strong effect on S at low carrier concentrations. With respect to unperturbed DOS, enlarging the disorder tends to result in an increase in S due to the broadened gap between the Fermi and transport energy. The remaining parameters in the system either have a trivial effect, such as the typical inter-site distance and the dielectric constant, or act as an insubstantial scaling factor, like the attempt-to-hop frequency.

According to the model in doped OSC systems described recently [232], charge transport is highly influenced by the induced tail of DOS, which is caused by the Coulomb potential of dopant ions at high doping fractions [232,233]. As shown in Fig. 20, the σ, S and PF were calculated within a variable-range hopping (VRH) and nearest-neighbor hopping (NNH) framework as a function of carrier/doping concentration. Regardless of whether the hopping process is VRH or NNH, the PF increases significantly with increased charge concentration due to the large improvement in σ, whilst the S declines. However, the energetic disorder has negligible effect on the TE properties at high concentration over $\sim 10^{-2}$, as shown in Fig. 20. It indicates that, for a specified sole DOS, there is limitation to modulating the TE characteristics by tuning disorder and concentration in both pristine and doped OSCs.

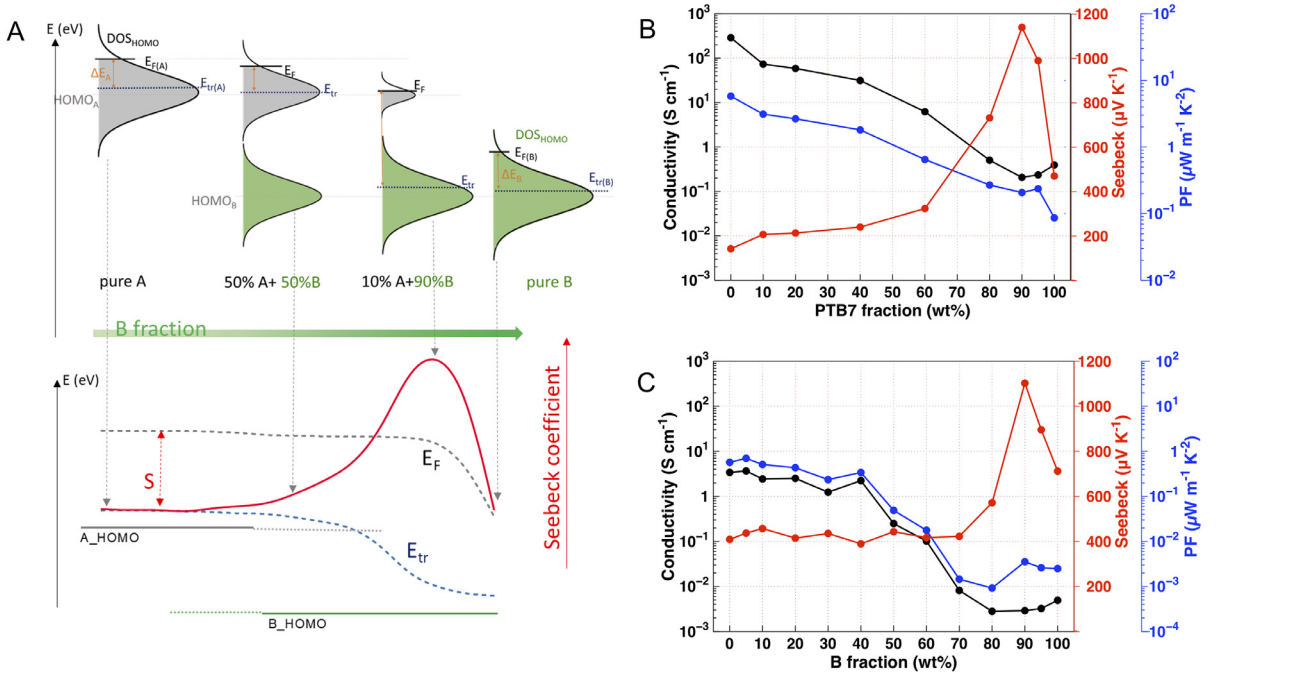

Fig. 21. Illustration of DOS engineering to achieve a high Seebeck coefficient. Upper part: hole density of states for a binary mixture A:B. White and shaded regions indicate hole- and electron-filled parts of the DOS, respectively. Lower part: corresponding relative positions of the Fermi energy E_F and the transport energy E_{tr} and the Seebeck coefficient S that is proportional to their difference (A). Conductivity, Seebeck coefficient and power factor for experimental data for P3HT$_x$:PTB7$_{1-x}$ (B). NNH kinetic Monte Carlo simulations for A$_x$:B$_{1-x}$ mixtures with HOMO energy differences of 0.3 eV, dependent on active layer composition (C). Parameters used $\nu_0 = 10^{-13}$ s^{-1}, $a_{NN} = 1.8$ nm, $\sigma_{DOS} = 75$ meV, $T = 300$ K, HOMO$_A$ - LUMO$_{dopant} = 0.24$ eV. [237], Copyright 2018. Reproduced with permission from John Wiley & Sons Inc.

The concept of a delta-shaped transport distribution situated somewhere above the Fermi energy was theoretically described [235] and shown to achieve the optimal TE properties. Later, the abovementioned delta-shaped transport distribution was experimentally confirmed by P3HT blending in a small fraction of P3HTT and then doped by F4TCNQ, with negligible decrease in σ while obviously increasing S from ~580 to 700 μV/K [236]. Recently, this strategy of DOS engineering was revisited and the physical understanding of this concept was enriched for systems consisting of two blended OSCs [237]. As shown in Fig. 21A, assuming that there is no interaction between the intrinsic DOS of CPs, the overall DOS distribution of two blended CPs simply mixes the respective DOS distributions at the energy of the respective HOMO/LUMO levels; the altitude of the DOS sub-peaks is exactly proportionate to the respective volume fraction. Fig. 21A also indicates the evolution of overall HOMO DOS for distinct materials A and B as the blend fraction changes. In principle, E_F is dictated by the charge concentration, whereas E_{tr} is correlated to the segment of the entire DOS that supports or carries the charge transport. With tuning the A:B ratio, somewhere the E_F and E_{tr} will be located on distinct materials, resulting in a noticeable increase in splitting between the two, allowing for a high S being achieved, as illustrated in Fig. 21A. Moreover, this concept was further tested by both experimentally and theoretically investigating the σ, S and PF for blends of P3HT with PTB7, where PTB7 with a full fraction from 0% to 100% [237]. As shown in Fig. 21B, indeed, there came out an obvious peak value of ~ 1200 of μV/K in S at 10% P3HT mixed 90% PTB7. The calculated result showed the similar trend and the value in S, from the kinetic Monte Carlo (kMC) simulations done with parameters corresponding to the taken experimental P3HT mixed PTB7 system, as shown in Fig. 21C. It indicated a good concurrence between the results of experiments and kMC simulations, confirming the validity of the DOS engineering. That is, DOS strategy with two blended OSCs is an effective solution with more freedom to modulate the TE properties, compared to a given single DOS.

5. Emerging applications of thermoelectric polymers

Since conjugated polymers have at present lower performance and are not resilient at extremely high temperatures, they are not currently able to compete with their inorganic counterparts in terms of providing large output power and high waste-heat to electricity efficiency. In spite of this, their many advantages such as softness, mechanical flexibility, and even stretchability make them more beneficial for powering wearable/portable electronic devices through the conversion of low-grade heat into electricity with typical power output at the level of nW to μW, by harvesting heat from human body or infrared radiation. Fig. 22 shows the power consumption of various emerging devices. For instance, an integrated temperature sensor consumes less than 100 nW [238], whereas an Internet of things (IoT) consumes energy at the level of μW. The state-of-the-art polymer-based TEGs could generate powers density in the range of 10^1-10^2 μW cm^{-2} [34,239]. Remarkably, using novel radial device architecture and model, the most efficient polymer-based TEGs are estimated to generate power density in the range of ~1 mW cm^{-2} [240]. Embedding TE polymers for power harvesting and supplying into a trillion node IoTs and various other applications will overcome the scalability and cost problem of changing batteries in such huge numbers. Especially, since conjugated polymers can be readily produced in large scale using solution processing, they hold significant potential for future commercialization. Here, we briefly highlight some examples of potential applications.

5.1. Self-powered/multiparameter sensors

In 2015, the first flexible dual-functional sensor was reported with the ability of concurrent sensing of both temperature and pressure (Fig. 23A, B) [241]. The sensors, based on PEDOT:PSS deposited on a polyurethane (PU) frame foam via dip coating method, on one hand can detect temperature change by reading

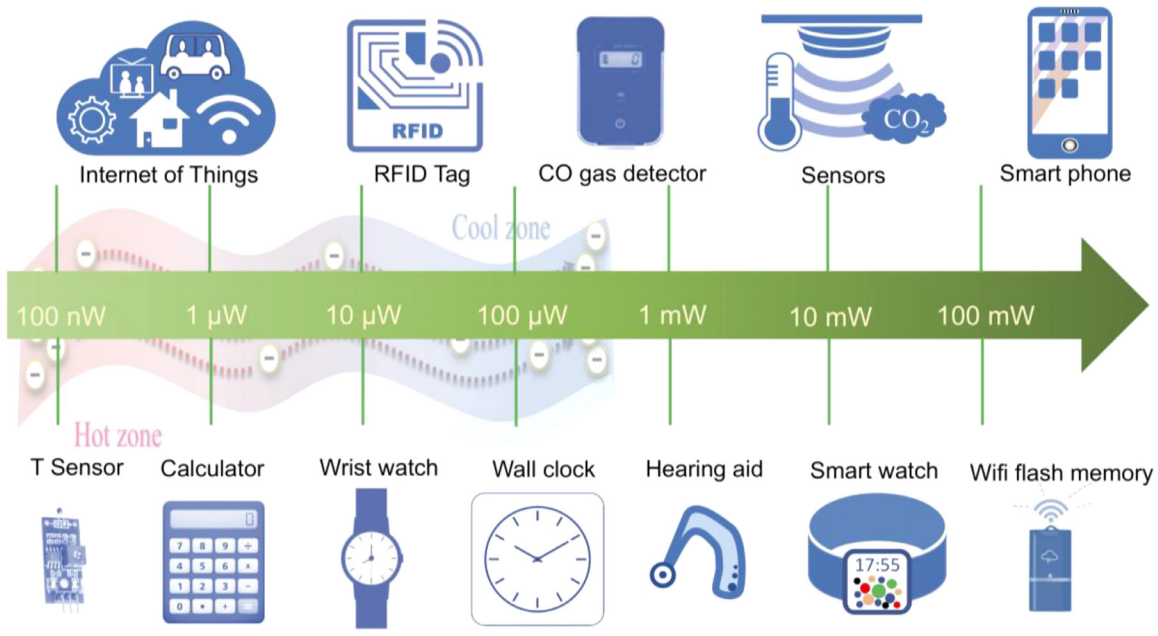

Fig. 22. Power consumption associated with various applications.

the voltage shift in the current-voltage graph based on Seebeck effect, and on the other hand are able to read the pressure-induced resistance change in the I-V curve as a result of the porous structure of the PU form. Under such strategy, temperature and pressure stimuli can be dissociated from each other. Strikingly, these sensors can be self-powered. Besides, polymeric thermoelectric aerogel, namely PEDOT:PSS aerogel reinforced by glycidoxypropyl trimethoxysilane (GOPS) and mechanical enhancer such nanofibrillated cellulose(NFC)) [242], has also been exemplified to be a favourable choice for pressure/temperature dual parameter sensors [243]. However, due to their inherent transport properties [72], such kind of devices typically experience substantial crosstalk in their sensing operation (Fig. 23C) [244]. To address this issue, DMSO vapor treatment was utilized to tune the properties of PEDOT:PSS aerogel to a unique activated free transport regime (Fig. 23D), and finally decoupled reading of the two parameters was achieved (Fig. 23E) [244].

Recently, mixed ionic–electronic conductors (MIECs) have been demonstrated with the ability to transport both ions and electrons, thus being able to sense temperature gradients and humidity [71]. Very recently, multiparameter sensor based on polymeric MIEC aerogels (PEDOT:PSS and nanofibrillated cellulose) was fabricated to sense pressure (read as a resistance shift, Fig. 23F), temperature gradient (read as a stable thermovoltage, Fig. 23G), and humidity (read as a thermovoltage peak, Fig. 23H) without significant crosstalk [245]. These achievements bring up new avenues for multipurpose IoT technology that is less complex and much cheaper to manufacture, which is highly desirable for monitoring, diagnostics and safety applications.

5.2. Stretchable conducting polymers/thermoelectric generators

Recent advances in stretchable electronics opened up new opportunities for various emerging applications, such as stretchable PLEDS [246], soft batteries [246], stretchable sensors and supercapacitors [247], connecting humans and machines in a variety of possible ways, such as wearable and implantable electronic devices [247–250]. One of the most attractive and widely used materials in the field of stretchable electronics is PEDOT:PSS [251]. It is worth mentioning that the brittleness of pristine PEDOT:PSS, i. e. high Young's modulus and low fracture strain, makes it impractical for wearable electronics when used alone [252]. During the past half decade, several powerful strategies have been shown effective in enhancing the stretchability of PEDOT: PSS, including blending the polymer with volatile surfactant plasticizers such as Zonyl or Triton [253–255], adding ionic liquids (ILs) [32,256], etc. Note that adding plasticizers enhanced the stretchability by sacrificing conductivities over one order of magnitude. In comparison, ionic additives are proven to be boosters for both stretchability and conductivity. For instance, Bao and co-workers employed several ionic additives to blend with PEDOT:PSS (Fig. 24A-E), and at optimized conditions, the polymer film exhibit conductivities exceeding 4100 S cm^{-1}under 100% strain, even higher than that in its unstretched state, 3100 S cm^{-1} [32]. Despite the aforementioned progress, these approaches are highly dependent on their supporting elastomer substrates, and the films are affected by buckles in the out-of-plane direction after multiple stretching. Moreover, as film thickness increases, their stretchability suffers from deterioration.

Recently, water borne polyurethane (WPU) was discovered as an effective enhancer when blended with the dispersion of PEDOT:PSS, yielding conducting elastic composites with both intrinsic stretchability and water processability [258]. However, to achieve good stretchability, a substantial amount of insulating WPU is required, leading to a low electrical performance, ca. a few tens of S cm^{-1}. Very recently, an intrinsically stretchable TE module was developed for the first time to have the capability of capturing energy from body heat. The system is based on the addition of IL into the WPU/PEDOT:PSS system, creating unique functions i.e., TE capabilities thanks to the PEDOT:PSS, stretchability thanks to the water-soluble WPU, and softness thanks to the IL (EMIM) (Fig. 24F) [257]. Remarkably, it is possible to stretch such a free-standing composite film to over 600% and have it return to its original shape with negligible hysteresis (Fig. 24G). Although the strain-dependent resistances somehow affect the output power upon applying strain, this work does open a new avenue for intrinsically stretchable thermoelectrics. Especially, such water-based solution-blending composite may be printed on a variety of surfaces in a cost-effective and en-

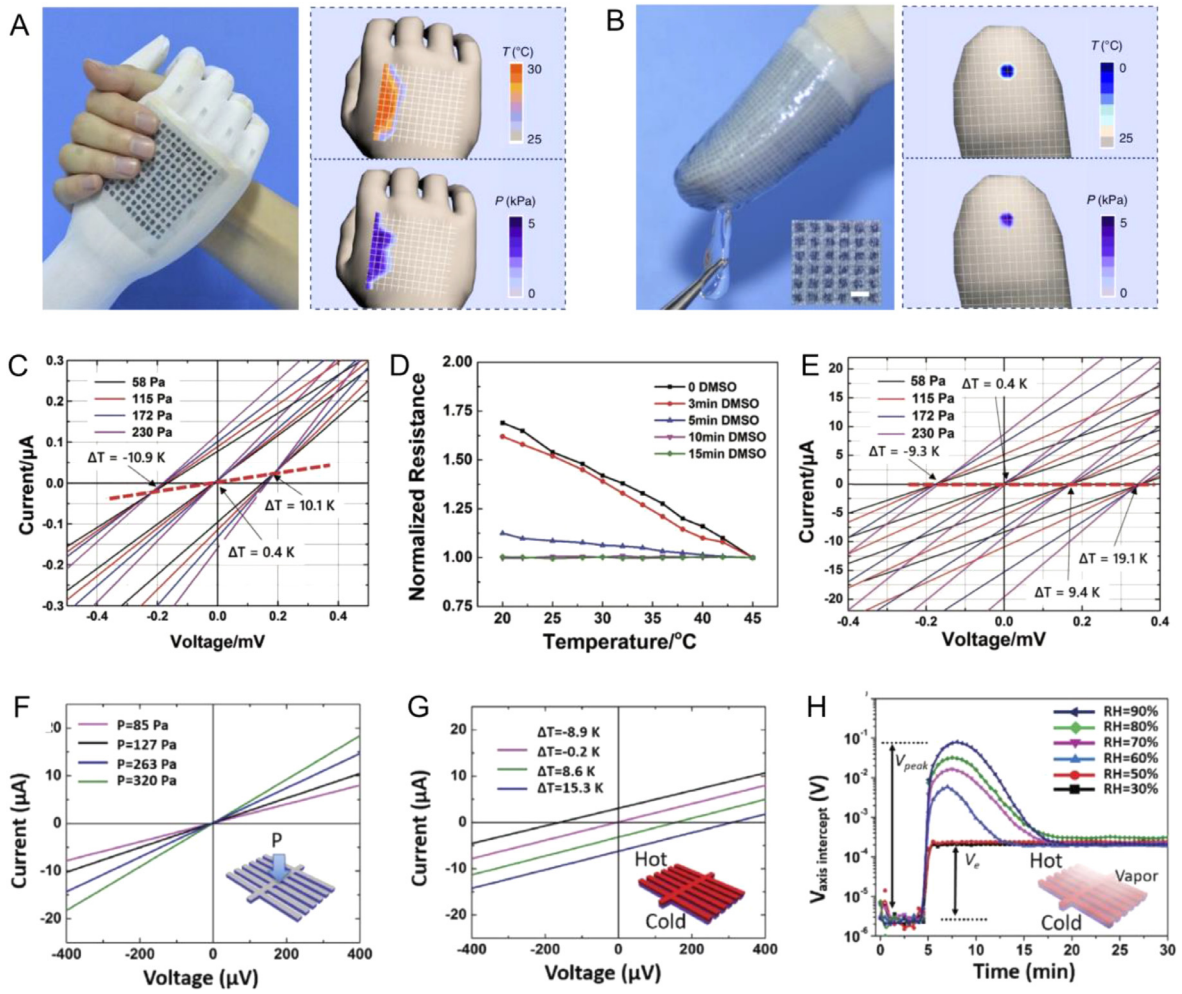

Fig. 23. (A) Left: photograph of a prosthetic hand arm-wrestling with an adult woman. Right: temperature and pressure mapping profiles of pixel signals on the back of the prosthetic hand. (B) Left: photograph of an e-finger touching an ice cube. The inset shows the optical microscope image of the inkjet-printed MFSOTE matrix. Scale bar, 1 mm. Right: temperature and pressure mappings of the sensing array. [241], Copyright 2015. Adapted with permission from Macmillan Publishers Ltd. (C) Measured I–V curves with different temperatures and pressures. (D) Normalized resistance as a function of temperature after DMSO vapor treatment in different time. (E) The measured I–V curves of PNG aerogel after 10 min DMSO vapor treatment. [244], Copyright 2017. Reproduced with permission from John Wiley & Sons Inc. (F) I–V curves measured under various pressures possess different slopes. The inserted sketch illustrates the aerogel under applied pressure. (G) I–V curves measured under various temperature differences display different voltage axis intercepts. The inserted sketch illustrates the aerogel submitted to a temperature gradient, oriented in the normal direction of the device structure. (H) Voltage axis intercept of I–V curves as a function of time, under different humidity. 10 K of temperature gradient was loaded at 4 min. The insert sketch illustrates the aerogel in a humid environment and submitted to an applied temperature gradient. [245], Copyright 2019. Reproduced with permission from John Wiley & Sons Inc.

vironmentally sustainable manner, holding promise for widespread use.

5.3. Other emerging applications

Photo-thermal effect is attracting more and more attention as it allows for utilizing the inexhaustible solar energy more efficiently. Since photovoltaics (PV) typically absorb only visible energy within band-gap, the remaining part of sunlight is converted into thermal energy, which could be harvested by a TEG. Therefore, developing PV/TEG integrated devices is currently considered to be an important research direction. Previously, integrated PV/TEG devices have been demonstrated by using inorganic TE materials [259], and a better overall efficiency was achieved, though, under severe conditions. Reducing coupling losses must be taken into consideration when integrating the devices. Similarly, infrared light was also directly used as the source for illuminating the photothermal materials so as to power the integrated TEG [260]. Interestingly, in addition to being used as TE materials, conjugated polymers can simultaneously serve as solar absorbers, thereby simplifying the device architecture and lowering the coupling losses. Recently, a polymer-based solar TEG device was demonstrated for the first time. In the case of two sun illumination, a 50K temperature gradient is established between the illuminated side and the unilluminated side of a PEDOT:PSS film and finally such kind of a proof-of-concept device could output 180 nW from 6 legs when driven by two suns [261,262]. These advances show huge potential that researchers will devote more efforts to develop next-generation conjugated polymers simultaneously capturing solar energy and converting it into electricity.

Besides, the thermoelectrics community is looking into other emerging applications for TE materials, such as triboelectric–thermoelectric hybrid nanogenerators where both mechanical energy and thermal energy (produced by friction) could be harvested [263], thermoelectric papers [264], etc. Hereby, rather than try to report the literature comprehensively, we showcased in the review several most striking applications of TE polymers, and for readers' further interests, we recommend a most recent review summarizing the emerging applications of TE polymers [265].

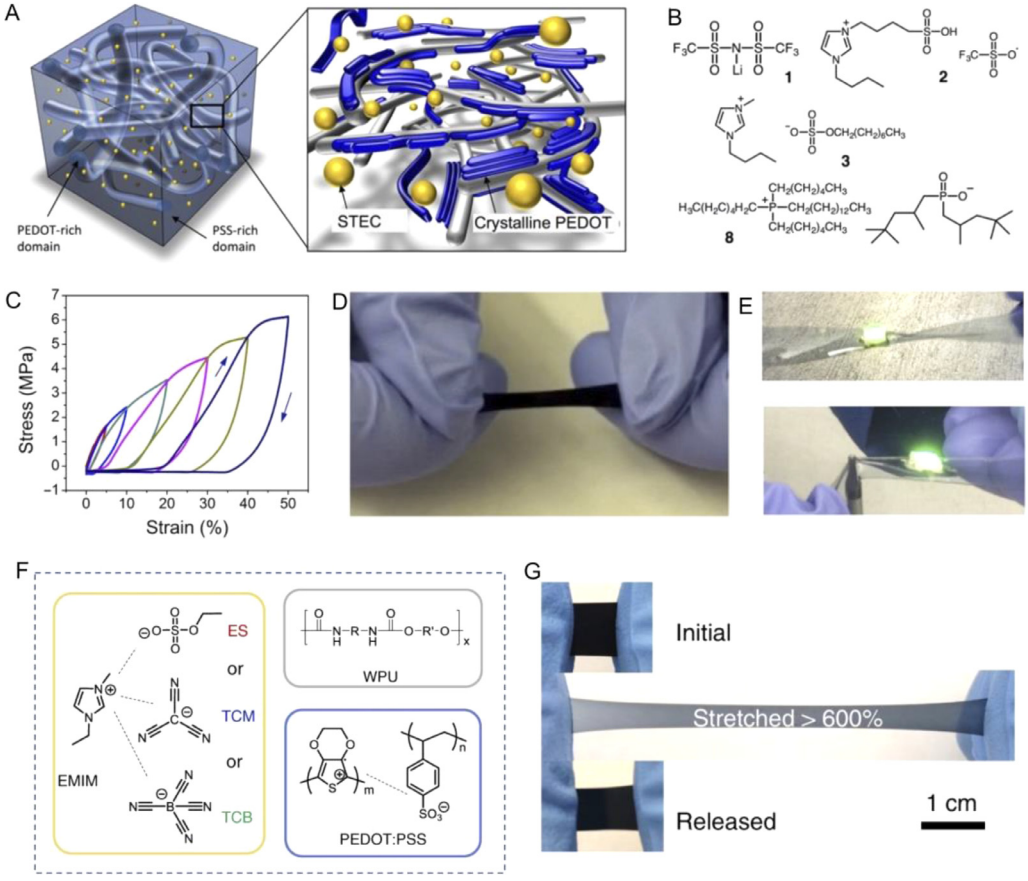

Fig. 24. (A) Schematic diagram representing the morphology of a stretchable PEDOT film with STEC enhancers. (B) Chemical structures of STEC enhancers. (C) Strain cycling behaviour of freestanding PEDOT/STEC films. (D) Photograph showing a freestanding PEDOT/STEC film being stretched. (E) Photographs illustrating the minimal change in LED brightness as the device is stretched under twisting (upper) and poked with a sharp object (lower), respectively. [32], Copyright 2017. Adapted with permission from American Association for the Advancement of Science. (F) Chemical structures of elastic conducting polymer composites. (G) A free-standing composite film (CP: TCM: WPU = 15:25:85, w/w) can be stretched to over 600% and relax to its original shape with little hysteresis. [257], Copyright 2020. Adapted with permission from Macmillan Publishers Ltd.

6. Conclusions and Outlook

In the past few decades, especially in the preceding decade, commendable progress has been made in the field of TE polymers. In this review, we offered a summary of molecular designing principles of TE polymers by reviewing the most promising state-of-the-art polymers, as well as insights into power factor improvement strategies beyond molecular design, especially the methodologies of decoupling the electrical conductivity and Seebeck coefficient of TE polymers. We've also showcased some of the most relevant potential applications for TE polymers that appear achievable with current performance levels. Particularly, the cost of polymeric TE materials is significantly lower than that of their inorganic counterparts. Today, the price of 25g high-conductivity PEDOT:PSS solution is less than 200 $ (Sigma-Aldrich), which can be utilized to fabricate thermoelectric films over large areas by solution processing under room temperature. By contrast, 25g Bismuth(III) telluride powder costs as high as over 300 $ (Sigma-Aldrich). Moreover, for inorganic TE materials, much higher manufacturing cost should also be taken into consideration. Although it is a fact that thermoelectrics will never outperform steam engines in the terms of energy conversion efficiency [266], with the future rapid advancements of science and technology, there is hope that TE polymers could be widely used in ever-present sensor networks, self-powered IoT, wearable electronics, smart clothes, and in the long-term potentially a wider range of applications for converting otherwise waste low-grade heat into useful electricity. Before, however the TE polymers can be utilized in such applications, the organic electrics community needs to overcome a number of obstacles and challenges.

First, the performance of TE polymers, especially the n-type polymers, is still far from satisfactory. There is still a large space for further enhancement of both electrical conductivity and Seebeck coefficient. Another long-lasting challenge for TE polymers has been their poor stability, including both air stability and operational stability [267,268], especially for the n-doped polymers. Upon exposure to ambient, the charge-carrying electrons are susceptible to being quenched by the redox interaction with oxygen and water, resulting in a rapid loss of their TE performance. The inherently poor stability of most n-type polymers is the major barrier. Deepening the LUMO level of n-type polymers is an effective strategy to enhance air stability. Recently, replacing the imide oxygen of a PNDI-based polymer with sulfur, the thionation, reduced the LUMO of the polymer by 0.2 eV leading to better conductivity and a significantly improved air stability. The thionated polymer exhibited a decrease in electrical conductivity of less than 2 times after 16h of exposure to the ambient, whereas the reference polymer showed a drop of 3 orders of magnitude after only 1h of exposure [269]. More recently, dichloro-substitution of the electron-deficient BDOPV and copolymerization with weak donor dichlorodithienylethene (ClTVT) yielded a highly conductive (16.1 S cm^{-1}) n-type donor-acceptor copolymer PCIC-ITVT showing remarkably high air stability, with 4.9 S cm^{-1} being recorded after storing in ambient for over 200 days [270]. Besides,

thermally assisted de-doping effect is a severe concern for doped polymers during high-temperature operations. In this regard, self-capsulation effect can be utilized to improve air-stability of polymers. Thus, developing stable n-type polymers with low LUMO and stable n-dopants are pressing necessities in the field of TE polymers.

In spite of the existence of the aforementioned challenges, conjugated polymers are now intensively studied as TE materials as a result of their advantages such as mechanical flexibility, stretchability and large-area fabrication at much lower cost, etc. It can be foreseen that with the help of a better understanding of molecular-structure relationship and the further advances of organic synthesis, materials processing, better comprehension of the relevant thermoelectric physics and device engineering, significant progress will be achieved by the scientific community in the years to come.

Declaration of Competing Interest

The authors declare that they have no known competing financial interests or personal relationships that could have appeared to influence the work reported in this paper.

CRediT authorship contribution statement

Suhao Wang: Conceptualization, Supervision, Visualization, Writing – original draft, Writing – review & editing. **Guangzheng Zuo:** Writing – original draft. **Jongho Kim:** Visualization. **Henning Sirringhaus:** Writing – review & editing.

Acknowledgments

Suhao Wang acknowledges the financial support from CY Initiative of Excellence (Talent project: Thermoelectric Green Energy) and EUTOPIA Young Leaders Academy. **Guangzheng Zuo** acknowledges support from the Alexander von Humboldt Foundation. **Henning Sirringhaus** acknowledges funding from the Royal Society through a Royal Society Research Professorship. The Authors acknowledge Prof. Martijn Kemerink for proofreading section 4.2.

Abbreviations

BBL, poly(benzimidazobenzophenanthroline); BBT, Benzo[1,2-c;4,5-c′]bisthiadiazole; BMP TFSI, 1-butyl-1- methylpyrrolidinium bis(trifluoromethylsulfonyl)imide; B←N, Boron-Nitrogen coordination; BT, benzothiadiazole; BV0, neutral benzyl viologen; $BV^{\cdot}+$, benzyl viologen radical cation; CDT, cyclopentadithiophene; ClTVT, dichlorodithienylethene; DPP, diketopyrrolopyrrole; D-A, donor-acceptor; DBN,1,5-Diazabicyclo [4.3.0] non-5-ene; DMSO, dimethyl sulfoxide; DMImC, 1,3-dime- thylimidazolium-2-carboxylate; DOS, density of states; DTzTI, imide-functionalized thiazole; EDOT, 3,4-ethylenedioxythiophene; EG, ethylene glycol; $EMIMBF_4$, 1-ethyl-3-methylimidazolium tetrafluoroborate; F4TCNQ, 2,3,5,6-Tetrafluoro-7,7,8,8-tetracyanoquinodimethane; Fe(TFSI)3, ferric salt with triflimide anion; FTS, (tride-cafluoro-1,1,2,2,-tetrahydrooctyl)-trichlorosilane; GIWAXS, Grazing-Incidence Wide-Angle X-ray Scattering; H_2SO_4, Sulfuric acid; HOMO, Highest Occupied Molecular Orbital; IE, ionization energy; IL, ionic liquid; kMC, kinetic Monte Carlo; LUMO, Lowest Unoccupied Molecular Orbital; Mw, molecular weight; MIECs, mixed ionic–electronic conductors; Na_2SO_3, sodium sulfite; NaBH4, sodium borohydride; N-DMBI, 4-(1,3-dimethyl-2,3-dihydro-1H-benzoimidazol-2-yl)phenyl; NDTI, naphtho[2,3-b:6,7-b′]-dithiophenediimide; NHCs, N-heterocyclic carbenes; NOPF6, nitrosonium hexafluorophosphate; OCL, orientation correlation lift; OFETs, organic field-effect transistors; OTE, organic thermoelectric; OSC, organic semiconductor; OSCs, organic solar cells; P37S, poly(3-heptylselenophene); P3HT, poly(3-heylthiophene); P3RSe, poly(3-alkylselenophene); P3RT, poly(3-alkylthiophene); P3RTe, Poly(3-alkyltellurophene); PA, Polyacetylene; PBTTT, poly(2,5-bis(thiophen-2-yl)thieno-[3,2-b]thiophene); PDI, polydispersity; PEDOT, poly(3,4-ethylenedioxythiophene); PEO, poly(ethylene oxide); PF, power factor; PV, photovoltaics; P(NDI2OD-T2), poly((N,N′-bis(2-octyldodecyl)-naphthalene-1,4,5,8-bis(dicarboximide)-2,6-diyl)-alt-5,5′-(2,20- bithiophene)); PNDI, polynaphthalenediimide; PPV, poly(p-phenylenevinylene); PQT, poly(3,3'-dialkyl-quaterthiophene); PSS, poly(styrenesulfonate); PT, pyridinethiadiazole; p(g42T-T), bithiophene-thienothiophene copolymer with tetraethylene glycol side chains; PU, polyurethane; GOPS, glycidoxypropyl trimethoxysilane; RI, regioirregular; SOMO, singly occupied molecular orbital; RSoXs, resonant soft x-ray scattering; T2, bithiophene; TAM, trisaminomethane derivative; TBAF, tetrabutylammonium fluoride; TBD, 1,5,7-Triazabicyclo [4.4.0] dec-5-ene; TCB, 1,3,5-trichlorobenzene; TDAE, tetrakis(dimethylamino)ethylene; TE, thermoelectric; TEG, triethylene glycol; TEGs, thermoelectric generators; TSA, p-toluenesulfonic acid monohydrate; Tos, tosylate; TPT, meta-substituted monomer 1,3-bis(2-thienyl) benzene; Tz2, bithiazole; WPU, water borne polyurethane.

Reference

[1] Forman C, Muritala IK, Pardemann R, Meyer B. Estimating the global waste heat potential. Renew Sustain Energy Rev 2016;57:1568–79.
[2] Beretta D, Neophytou N, Hodges JM, Kanatzidis MG, Narducci D, Martin- Gonzalez M, Beekman M, Balke B, Cerretti G, Tremel W, Zevalkink A, Hofmann AI, Müller C, Dörling B, Campoy-Quiles M, Caironi M. Thermoelectrics: From history, a window to the future. Mater Sci Eng R Rep 2019;138:100501.
[3] Tan G, Zhao LD, Kanatzidis MG. Rationally Designing High-Performance Bulk Thermoelectric Materials. Chem Rev 2016;116:12123–49.
[4] Snyder GJ, Toberer ES. Complex thermoelectric materials. Nat Mater 2008;7:105–14.
[5] Bubnova O, Khan ZU, Malti A, Braun S, Fahlman M, Berggren M, Crispin X. Optimization of the thermoelectric figure of merit in the conducting polymer poly(3,4-ethylenedioxythiophene). Nat Mater 2011;10:429–33.
[6] Bubnova O, Crispin X. Towards polymer-based organic thermoelectric generators. Energy Environ Sci 2012;5:9345–62.
[7] Kroon R, Mengistie DA, Kiefer D, Hynynen J, Ryan JD, Yu L, Muller C. Thermoelectric plastics: from design to synthesis, processing and structure-property relationships. Chem Soc Rev 2016;45:6147–64.
[8] Russ B, Glaudell A, Urban JJ, Chabinyc ML, Segalman RA. Organic thermoelectric materials for energy harvesting and temperature control. Nat Rev Mater 2016;1:16050.
[9] Zhao W, Ding J, Zou Y, Di CA, Zhu D. Chemical doping of organic semiconductors for thermoelectric applications. Chem Soc Rev 2020;49:7210–28.
[10] Reddy P, Jang S-Y, Segalman RA, Majumdar A. Thermoelectricity in Molecular Junctions. Science 2007;315:1568–71.
[11] Berggren M, Nilsson D, Robinson ND. Organic materials for printed electronics. Nat Mater 2007;6:3–5.
[12] Yvenou E, Sandroni M, Carella A, Gueye MN, Faure-Vincent J, Pouget S, Demadrille R, Simonato J-P. Spray-coated PEDOT:OTf films: thermoelectric properties and integration into a printed thermoelectric generator. Mater Chem Front 2020;4:2054–63.
[13] Hossain MS, Li T, Yu Y, Yong J, Bahk J-H, Skafidas E. Recent advances in printable thermoelectric devices: materials, printing techniques, and applications. RSC Adv 2020;10:8421–34.
[14] Fan Z, Zhang Y, Pan L, Ouyang J, Zhang Q. Recent developments in flexible thermoelectrics: From materials to devices. Renew Sustain Energy Rev 2021;137:110448.
[15] Du Y, Xu J, Paul B, Eklund P. Flexible thermoelectric materials and devices. Appl Mater Today 2018;12:366–88.
[16] Zhang L, Shi X-L, Yang Y-L, Chen Z-G. Flexible thermoelectric materials and devices: From materials to applications. Mater Today 2021;46:62–108.
[17] Prunet G, Pawula F, Fleury G, Cloutet E, Robinson AJ, Hadziioannou G. Pakdel A. A review on conductive polymers and their hybrids for flexible and wearable thermoelectric applications. Mater Today Phys 2021;18:100402.
[18] Chen Y, Zhao Y, Liang Z. Solution processed organic thermoelectrics: towards flexible thermoelectric modules. Energy Environ Sci 2015;8:401–22.
[19] Wang Y, Yang L, Shi X-L, Shi X, Chen L, Dargusch MS, Zou J, Chen Z-G. Flexible Thermoelectric Materials and Generators: Challenges and Innovations. Adv Mater 2019;31:1807916.
[20] Eryilmaz IH, Chen Y-F, Mattana G, Orgiu E, Cosseddu P, Caironi M. 11 - Flexible organic thermoelectric generators. In: Organic Flexible Electronics. Woodhead Publishing; 2021. p. 335–51.
[21] Qiu Z, Hammer BAG, Müllen K. Conjugated polymers – Problems and promises. Prog Polym Sci 2020;100:101179.

[22] Sun H, Guo X, Facchetti A. High-Performance n-Type Polymer Semiconductors: Applications, Recent Development, and Challenges. Chem 2020;6:1310–26.
[23] Sun Y, Di C-A, Xu W, Zhu D. Advances in n-Type Organic Thermoelectric Materials and Devices. Adv Electron Mater 2019;5:1800825.
[24] Thomas EM, Popere BC, Fang H, Chabinyc ML, Segalman RA. Role of Disorder Induced by Doping on the Thermoelectric Properties of Semiconducting Polymers. Chem Mater 2018;30:2965–72.
[25] Kim N, Kee S, Lee SH, Lee BH, Kahng YH, Jo Y-R, Kim B-J, Lee K. Highly Conductive PEDOT:PSS Nanofibrils Induced by Solution-Processed Crystallization. Adv Mater 2014;26:2268–72.
[26] Gueye MN, Carella A, Massonnet N, Yvenou E, Brenet S, Faure-Vincent J, Pouget S, Rieutord F, Okuno H, Benayad A, Demadrille R, Simonato J-P. Structure and Dopant Engineering in PEDOT Thin Films: Practical Tools for a Dramatic Conductivity Enhancement. Chem Mater 2016;28:3462–8.
[27] Worfolk BJ, Andrews SC, Park S, Reinspach J, Liu N, Toney MF, Mannsfeld SCB, Bao Z. Ultrahigh electrical conductivity in solution-sheared polymeric transparent films. Proc Natl Acad Sci U S A 2015;112:14138–43.
[28] Jin Bae E, Hun Kang Y, Jang K-S, Yun Cho S. Enhancement of Thermoelectric Properties of PEDOT:PSS and Tellurium-PEDOT:PSS Hybrid Composites by Simple Chemical Treatment. Sci Rep 2016;6:18805.
[29] Cho B, Park KS, Baek J, Oh HS, Koo Lee Y-E, Sung MM. Single-Crystal Poly(3,4-ethylenedioxythiophene) Nanowires with Ultrahigh Conductivity. Nano Lett 2014;14:3321–7.
[30] Wang X, Zhang X, Sun L, Lee D, Lee S, Wang M, Zhao J, Shao-Horn Y, Dincă M, Palacios T, Gleason KK. High electrical conductivity and carrier mobility in oCVD PEDOT thin films by engineered crystallization and acid treatment. Sci Adv 2018;4:eaat5780.
[31] Farka D, Coskun H, Gasiorowski J, Cobet C, Hingerl K, Uiberlacker LM, Hild S, Greunz T, Stifter D, Sariciftci NS, Menon R, Schoefberger W, Mardare CC, Hassel AW, Schwarzinger C, Scharber MC, Stadler P. Anderson-Localization and the Mott–Ioffe–Regel Limit in Glassy-Metallic PEDOT. Adv Electron Mater 2017;3:1700050.
[32] Wang Y, Zhu C, Pfattner R, Yan H, Jin L, Chen S, Molina-Lopez F, Lissel F, Liu J, Rabiah NI, Chen Z, Chung JW, Linder C, Toney MF, Murmann B, Bao Z. A highly stretchable, transparent, and conductive polymer. Sci Adv 2017;3:e1602076.
[33] Schultheiss A, Carella A, Pouget S, Faure-Vincent J, Demadrille R, Revaux A, Simonato J-P. Water content control during solution-based polymerization: a key to reach extremely high conductivity in PEDOT thin films. J Mater Chem C 2020;8:17254–60.
[34] Hinckley AC, Andrews SC, Dunham MT, Sood A, Barako MT, Schneider S, Toney MF, Goodson KE, Bao Z. Achieving High Thermoelectric Performance and Metallic Transport in Solvent-Sheared PEDOT:PSS. Adv Electron Mater 2021;7 2001190.
[35] Huang Y, Tjhe DHL, Jacobs IE, Jiao X, He Q, Statz M, Ren X, Huang X, McCulloch I, Heeney M, McNeill C, Sirringhaus H. Design of experiment optimization of aligned polymer thermoelectrics doped by ion-exchange. Appl Phys Lett 2021;119:111903.
[36] Lu Y, Yu ZD, Liu Y, Ding YF, Yang CY, Yao ZF, Wang ZY, You HY, Cheng XF, Tang B, Wang JY, Pei J. The Critical Role of Dopant Cations in Electrical Conductivity and Thermoelectric Performance of n-Doped Polymers. J Am Chem Soc 2020;142:15340–8.
[37] Yang CY, Ding YF, Huang D, Wang J, Yao ZF, Huang CX, Lu Y, Un HI, Zhuang FD, Dou JH, Di CA, Zhu D, Wang JY, Lei T, Pei J. A thermally activated and highly miscible dopant for n-type organic thermoelectrics. Nat Commun 2020;11:3292.
[38] Feng K, Guo H, Wang J, Shi Y, Wu Z, Su M, Zhang X, Son JH, Woo HY, Guo X. Cyano-Functionalized Bithiophene Imide-Based n-Type Polymer Semiconductors: Synthesis, Structure–Property Correlations, and Thermoelectric Performance. J Am Chem Soc 2021;143:1539–52.
[39] Xiong M, Yan X, Li JT, Zhang S, Cao Z, Prine N, Lu Y, Wang JY, Gu X, Lei T. Efficient n-Doping of Polymeric Semiconductors through Controlling the Dynamics of Solution-State Polymer Aggregates. Angew Chem Int Ed 2021;60:8189–97.
[40] Lu Y, Yu ZD, Un HI, Yao ZF, You HY, Jin W, Li L, Wang ZY, Dong BW, Barlow S, Longhi E, Di CA, Zhu D, Wang JY, Silva C, Marder SR, Pei J. Persistent Conjugated Backbone and Disordered Lamellar Packing Impart Polymers with Efficient n-Doping and High Conductivities. Adv Mater 2021;33 2005946.
[41] Lu G, Blakesley J, Himmelberger S, Pingel P, Frisch J, Lieberwirth I, Salzmann I, Oehzelt M, Di Pietro R, Salleo A, Koch N, Neher D. Moderate doping leads to high performance of semiconductor/insulator polymer blend transistors. Nat Commun 2013;4:1588.
[42] Khim D, Baeg K-J, Caironi M, Liu C, Xu Y, Kim D-Y, Noh Y-Y. Control of Ambipolar and Unipolar Transport in Organic Transistors by Selective Inkjet-Printed Chemical Doping for High Performance Complementary Circuits. Adv Funct Mater 2014;24:6252–61.
[43] Xu Y, Sun H, Liu A, Zhu H-H, Li W, Lin Y-F, Noh Y-Y. Doping: A Key Enabler for Organic Transistors. Adv Mater 2018;30:1801830.
[44] Zhang Y, Zhou H, Seifter J, Ying L, Mikhailovsky A, Heeger AJ, Bazan GC. Nguyen T-Q. Molecular Doping Enhances Photoconductivity in Polymer Bulk Heterojunction Solar Cells. Adv Mater 2013;25:7038–44.
[45] Lin Y, Firdaus Y, Nugraha MI, Liu F, Karuthedath S, Emwas A-H, Zhang W, Seitkhan A, Neophytou M, Faber H, Yengel E, McCulloch I, Tsetseris L, Laquai F, Anthopoulos TD. 17.1% Efficient Single-Junction Organic Solar Cells Enabled by n-Type Doping of the Bulk-Heterojunction. Adv Sci 2020;7:1903419.
[46] Yamashita Y, Tsurumi J, Ohno M, Fujimoto R, Kumagai S, Kurosawa T, Okamoto T, Takeya J, Watanabe S. Efficient molecular doping of polymeric semiconductors driven by anion exchange. Nature 2019;572:634–8.
[47] Jacobs IE, Lin Y, Huang Y, Ren X, Simatos D, Chen C, Tjhe D, Statz M, Lai L, Finn PA, Neal WG, D'Avino G, Lemaur V, Fratini S, Beljonne D, Strzalka J, Nielsen CB, Barlow S, Marder SR, McCulloch I, Sirringhaus H. High-Efficiency Ion-Exchange Doping of Conducting Polymers. Adv Mater 2021 n/a:e2102988.
[48] Chiang CK, Fincher CR, Park YW, Heeger AJ, Shirakawa H, Louis EJ, Gau SC, MacDiarmid AG. Electrical Conductivity in Doped Polyacetylene. Phys Rev Lett 1977;39:1098–101.
[49] Basescu N, Liu ZX, Moses D, Heeger AJ, Naarmann H, Theophilou N. High electrical conductivity in doped polyacetylene. Nature 1987;327:403–5.
[50] Naarmann H, Theophilou N. New process for the production of metal-like, stable polyacetylene. Synth Met 1987;22:1–8.
[51] Zuzok R, Kaiser AB, Pukacki W, Roth S. Thermoelectric power and conductivity of iodine-doped "new" polyacetylene. J Chem Phys 1991;95:1270–5.
[52] Kaneko H, Ishiguro T, Takahashi A, Tsukamoto J. Magnetoresistance and thermoelectric power studies of metal-nonmetal transition in iodine-doped polyacetylene. Synth Met 1993;57:4900–5.
[53] Park YW, Yoon CO, Na BC, Shirakawa H, Akagi K. Metallic properties of transition metal halides doped polyacetylene: The soliton liquid state. Synth Met 1991;41:27–32.
[54] Münstedt H. Ageing of electrically conducting organic materials. Polymer 1988;29:296–302.
[55] Heywang G, Jonas F. Poly(alkylenedioxythiophene)s—new, very stable conducting polymers. Adv Mater 1992;4:116–18.
[56] Jonas F, Morrison JT. 3,4-polyethylenedioxythiophene (PEDT): Conductive coatings technical applications and properties. Synth Met. 1997;85:1397–8.
[57] Kirchmeyer S, Reuter K. Scientific importance, properties and growing applications of poly(3,4-ethylenedioxythiophene). J Mater Chem 2005;15:2077–88.
[58] Xia Y, Ouyang J. Significant Different Conductivities of the Two Grades of Poly(3,4-ethylenedioxythiophene):Poly(styrenesulfonate), Clevios P and Clevios PH1000, Arising from Different Molecular Weights. ACS Appl Mater Interfaces 2012;4:4131–40.
[59] Luo J, Billep D, Waechtler T, Otto T, Toader M, Gordan O, Sheremet E, Martin J, Hietschold M, Zahn DRT, Gessner T. Enhancement of the thermoelectric properties of PEDOT:PSS thin films by post-treatment. J Mater Chem A 2013;1:7576–83.
[60] Wei Q, Mukaida M, Naitoh Y, Ishida T. Morphological Change and Mobility Enhancement in PEDOT:PSS by Adding Co-solvents. Adv Mater 2013;25:2831–6.
[61] Kumar SRS, Kurra N, Alshareef HN. Enhanced high temperature thermoelectric response of sulphuric acid treated conducting polymer thin films. J Mater Chem C 2016;4:215–21.
[62] Palumbiny CM, Schlipf J, Hexemer A, Wang C, Müller-Buschbaum P. The Morphological Power of Soap: How Surfactants Lower the Sheet Resistance of PEDOT:PSS by Strong Impact on Inner Film Structure and Molecular Interface Orientation. Adv Electron Mater 2016;2:1500377.
[63] Park H, Lee SH, Kim FS, Choi HH, Cheong IW, Kim JH. Enhanced thermoelectric properties of PEDOT:PSS nanofilms by a chemical dedoping process. J Mater Chem A 2014;2:6532–9.
[64] Yi C, Wilhite A, Zhang L, Hu R, Chuang SSC, Zheng J, Gong X. Enhanced Thermoelectric Properties of Poly(3,4-ethylenedioxythiophene):poly(styrenesulfonate) by Binary Secondary Dopants. ACS Appl Mater Interfaces 2015;7:8984–9.
[65] Mengistie DA, Chen C-H, Boopathi KM, Pranoto FW, Li L-J, Chu C-W. Enhanced Thermoelectric Performance of PEDOT:PSS Flexible Bulky Papers by Treatment with Secondary Dopants. ACS Appl Mater Interfaces 2015;7:94–100.
[66] Poehler TO, Katz HE. Prospects for polymer-based thermoelectrics: state of the art and theoretical analysis. Energy Environ Sci 2012;5:8110–15.
[67] Upadhyaya M, Boyle CJ, Venkataraman D, Aksamija Z. Effects of Disorder on Thermoelectric Properties of Semiconducting Polymers. Sci Rep. 2019;9:5820.
[68] Massonnet N, Carella A, Jaudouin O, Rannou P, Laval G, Celle C, Simonato J-P. Improvement of the Seebeck coefficient of PEDOT:PSS by chemical reduction combined with a novel method for its transfer using free-standing thin films. J Mater Chem C 2014;2:1278–83.
[69] Lee SH, Park H, Kim S, Son W, Cheong IW, Kim JH. Transparent and flexible organic semiconductor nanofilms with enhanced thermoelectric efficiency. J Mater Chem A 2014;2:7288–94.
[70] Saxena N, Keilhofer J, Maurya AK, Fortunato G, Overbeck J, Müller-Buschbaum P. Facile Optimization of Thermoelectric Properties in PEDOT:PSS Thin Films through Acido-Base and Redox Dedoping Using Readily Available Salts. ACS Appl Energy Mater 2018;1:336–42.
[71] Wang H, Ail U, Gabrielsson R, Berggren M, Crispin X. Ionic Seebeck Effect in Conducting Polymers. Adv Energy Mater 2015;5:1500044.
[72] Bubnova O, Khan ZU, Wang H, Braun S, Evans DR, Fabretto M, Hojati-Talemi P, Dagnelund D, Arlin JB, Geerts YH, Desbief S, Breiby DW, Andreasen JW, Lazzaroni R, Chen WM, Zozoulenko I, Fahlman M, Murphy PJ, Berggren M, Crispin X. Semi-metallic polymers. Nat Mater 2014;13:190–4.
[73] Fabretto MV, Evans DR, Mueller M, Zuber K, Hojati-Talemi P, Short RD, Wallace GG, Murphy PJ. Polymeric Material with Metal-Like Conductivity for Next Generation Organic Electronic Devices. Chem Mater 2012;24:3998–4003.

[74] Petsagkourakis I, Pavlopoulou E, Portale G, Kuropatwa BA, Dilhaire S, Fleury G, Hadziioannou G. Structurally-driven Enhancement of Thermoelectric Properties within Poly(3,4-ethylenedioxythiophene) thin. Films. Sci Rep. 2016;6:30501.
[75] Lee YH, Oh J, Lee S-S, Kim H, Son JG. Highly Ordered Nanoconfinement Effect from Evaporation-Induced Self-Assembly of Block Copolymers on In Situ Polymerized PEDOT:Tos. ACS Macro Lett 2017;6:386–92.
[76] Petsagkourakis I, Pavlopoulou E, Cloutet E, Chen YF, Liu X, Fahlman M, Berggren M, Crispin X, Dilhaire S, Fleury G, Hadziioannou G. Correlating the Seebeck coefficient of thermoelectric polymer thin films to their charge transport mechanism. Org Electron 2018;52:335–41.
[77] Petsagkourakis I, Kim N, Tybrandt K, Zozoulenko I, Crispin X. Poly(3,4-ethylenedioxythiophene): Chemical Synthesis, Transport Properties, and Thermoelectric Devices. Adv Electron Mater. 2019;5:1800918.
[78] Gueye MN, Carella A, Faure-Vincent J, Demadrille R, Simonato J-P. Progress in understanding structure and transport properties of PEDOT-based materials: A critical review. Prog Mater Sci 2020;108:100616.
[79] Xu Y, Jia Y, Liu P, Jiang Q, Hu D, Ma Y. Poly(3,4-ethylenedioxythiophene) (PEDOT) as promising thermoelectric materials and devices. Chem Eng J 2021;404:126552.
[80] Fan Z, Ouyang J. Thermoelectric Properties of PEDOT:PSS. Adv Electron Mater 2019;5:1800769.
[81] Bao Z, Dodabalapur A, Lovinger AJ. Soluble and processable regioregular poly(3-hexylthiophene) for thin film field-effect transistor applications with high mobility. Appl Phys Lett 1996;69:4108–10.
[82] Sirringhaus H, Brown PJ, Friend RH, Nielsen MM, Bechgaard K, Langeveld-Voss BMW, Spiering AJH, Janssen RAJ, Meijer EW, Herwig P, de Leeuw DM. Two-dimensional charge transport in self-organized, high-mobility conjugated polymers. Nature 1999;401:685–8.
[83] Sirringhaus H, Tessler N, Friend RH. Integrated Optoelectronic Devices Based on Conjugated Polymers. Science 1998;280:1741–4.
[84] Kline RJ, McGehee MD, Kadnikova EN, Liu J, Fréchet JMJ, Toney MF. Dependence of Regioregular Poly(3-hexylthiophene) Film Morphology and Field-Effect Mobility on Molecular Weight. Macromolecules 2005;38:3312–19.
[85] Himmelberger S, Vandewal K, Fei Z, Heeney M, Salleo A. Role of Molecular Weight Distribution on Charge Transport in Semiconducting Polymers. Macromolecules 2014;47:7151–7.
[86] Xuan Y, Liu X, Desbief S, Leclère P, Fahlman M, Lazzaroni R, Berggren M, Cornil J, Emin D, Crispin X. Thermoelectric properties of conducting polymers: The case of poly(3-hexylthiophene). Phys Rev B 2010;82:115454.
[87] Zhang Q, Sun Y, Xu W, Zhu D. Thermoelectric energy from flexible P3HT films doped with a ferric salt of triflimide anions. Energy Environ Sci 2012;5:9639.
[88] Wang C, Duong DT, Vandewal K, Rivnay J, Salleo A. Optical measurement of doping efficiency in poly(3-hexylthiophene) solutions and thin films. Phys Rev B 2015;91 085205.
[89] Méndez H, Heimel G, Winkler S, Frisch J, Opitz A, Sauer K, Wegner B, Oehzelt M, Röthel C, Duhm S, Többens D, Koch N, Salzmann I. Charge-transfer crystallites as molecular electrical dopants. Nat Commun 2015;6:8560.
[90] Duong DT, Wang C, Antono E, Toney MF, Salleo A. The chemical and structural origin of efficient p-type doping in P3HT. Org Electron 2013;14:1330–6.
[91] Aziz EF, Vollmer A, Eisebitt S, Eberhardt W, Pingel P, Neher D, Koch N. Localized Charge Transfer in a Molecularly Doped Conducting Polymer. Adv Mater 2007;19:3257–60.
[92] Zuo G, Li Z, Andersson O, Abdalla H, Wang E, Kemerink M. Molecular Doping and Trap Filling in Organic Semiconductor Host–Guest Systems. J Phys Chem C 2017;121:7767–75.
[93] Scholes DT, Hawks SA, Yee PY, Wu H, Lindemuth JR, Tolbert SH, Schwartz BJ. Overcoming Film Quality Issues for Conjugated Polymers Doped with F4TCNQ by Solution Sequential Processing: Hall Effect, Structural, and Optical Measurements. J Phys Chem Lett 2015;6:4786–93.
[94] Jacobs IE, Aasen EW, Oliveira JL, Fonseca TN, Roehling JD, Li J, Zhang G, Augustine MP, Mascal M, Moulé AJ. Comparison of solution-mixed and sequentially processed P3HT:F4TCNQ films: effect of doping-induced aggregation on film morphology. J Mater Chem C 2016;4:3454–66.
[95] Scholes DT, Yee PY, Lindemuth JR, Kang H, Onorato J, Ghosh R, Luscombe CK, Spano FC, Tolbert SH, Schwartz BJ. The Effects of Crystallinity on Charge Transport and the Structure of Sequentially Processed F4 TCNQ-Doped Conjugated Polymer Films. Adv Funct Mater 2017;27:1702654.
[96] Fontana MT, Stanfield DA, Scholes DT, Winchell KJ, Tolbert SH, Schwartz BJ. Evaporation vs Solution Sequential Doping of Conjugated Polymers: F4TCNQ Doping of Micrometer-Thick P3HT Films for Thermoelectrics. J Phys Chem C 2019;123:22711–24.
[97] Lim E, Peterson KA, Su GM, Chabinyc ML. Thermoelectric Properties of Poly(3-hexylthiophene) (P3HT) Doped with 2,3,5,6-Tetrafluoro-7,7,8,8-tetracyanoquinodimethane (F4TCNQ) by Vapor-Phase Infiltration. Chem Mater 2018;30:998–1010.
[98] Hynynen J, Kiefer D, Yu L, Kroon R, Munir R, Amassian A, Kemerink M, Müller C. Enhanced Electrical Conductivity of Molecularly p-Doped Poly(3-hexylthiophene) through Understanding the Correlation with Solid-State Order. Macromolecules 2017;50:8140–8.
[99] Kroon R, Kiefer D, Stegerer D, Yu L, Sommer M, Muller C. Polar Side Chains Enhance Processability, Electrical Conductivity, and Thermal Stability of a Molecularly p-Doped Polythiophene. Adv Mater 2017;29:1700930.
[100] Lim E, Glaudell AM, Miller R, Chabinyc ML. The Role of Ordering on the Thermoelectric Properties of Blends of Regioregular and Regiorandom Poly(3-hexylthiophene). Adv Electron Mater 2019;5:1800915.
[101] Mardi S, Pea M, Notargiacomo A, Yaghoobi Nia N, Di Carlo A, Reale A. The Molecular Weight Dependence of Thermoelectric Properties of Poly (3-Hexylthiophene). Materials (Basel, Switzerland) 2020;13:1404.
[102] Gregory SA, Menon AK, Ye S, Seferos DS, Reynolds JR, Yee SK. Effect of Heteroatom and Doping on the Thermoelectric Properties of Poly(3-alkylchalcogenophenes). Adv Energy Mater 2018;8:1802419.
[103] Scholes DT, Yee PY, McKeown GR, Li S, Kang H, Lindemuth JR, Xia X, King SC, Seferos DS, Tolbert SH, Schwartz BJ. Designing Conjugated Polymers for Molecular Doping: The Roles of Crystallinity, Swelling, and Conductivity in Sequentially-Doped Selenophene-Based Copolymers. Chem Mater 2019;31:73–82.
[104] Ong BS, Wu Y, Liu P, Gardner S. Structurally Ordered Polythiophene Nanoparticles for High-Performance Organic Thin-Film Transistors. Adv Mater 2005;17:1141–4.
[105] Li H, DeCoster ME, Ireland RM, Song J, Hopkins PE, Katz HE. Modification of the Poly(bisdodecylquaterthiophene) Structure for High and Predominantly Nonionic Conductivity with Matched Dopants. J Am Chem Soc 2017;139:11149–57.
[106] McCulloch I, Heeney M, Bailey C, Genevicius K, MacDonald I, Shkunov M, Sparrowe D, Tierney S, Wagner R, Zhang W, Chabinyc ML, Kline RJ, McGehee MD, Toney MF. Liquid-crystalline semiconducting polymers with high charge-carrier mobility. Nat Mater 2006;5:328–33.
[107] Hamadani BH, Gundlach DJ, McCulloch I, Heeney M. Undoped polythiophene field-effect transistors with mobility of 1cm2V−1s−1. Appl Phys Lett 2007;91:243512.
[108] Kline RJ, DeLongchamp DM, Fischer DA, Lin EK, Richter LJ, Chabinyc ML, Toney MF, Heeney M, McCulloch I. Critical Role of Side-Chain Attachment Density on the Order and Device Performance of Polythiophenes. Macromolecules 2007;40:7960–5.
[109] Zhang Q, Sun Y, Jiao F, Zhang J, Xu W, Zhu D. Effects of structural order in the pristine state on the thermoelectric power-factor of doped PBTTT films. Synth Met 2012;162:788–93.
[110] Zhang Q, Sun Y, Xu W, Zhu D. What To Expect from Conducting Polymers on the Playground of Thermoelectricity: Lessons Learned from Four High-Mobility Polymeric Semiconductors. Macromolecules 2014;47:609–15.
[111] Kang K, Watanabe S, Broch K, Sepe A, Brown A, Nasrallah I, Nikolka M, Fei Z, Heeney M, Matsumoto D, Marumoto K, Tanaka H, Kuroda S, Sirringhaus H. 2D coherent charge transport in highly ordered conducting polymers doped by solid state diffusion. Nat Mater 2016;15:896–902.
[112] Glaudell AM, Cochran JE, Patel SN, Chabinyc ML. Impact of the Doping Method on Conductivity and Thermopower in Semiconducting Polythiophenes. Adv Energy Mater 2015;5:1401072.
[113] Cochran JE, Junk MJN, Glaudell AM, Miller PL, Cowart JS, Toney MF, Hawker CJ, Chmelka BF, Chabinyc ML. Molecular Interactions and Ordering in Electrically Doped Polymers: Blends of PBTTT and F4TCNQ. Macromolecules 2014;47:6836–46.
[114] Kang K, Schott S, Venkateshvaran D, Broch K, Schweicher G, Harkin D, Jellett C, Nielsen CB, McCulloch I. Sirringhaus H. Investigation of the thermoelectric response in conducting polymers doped by solid-state diffusion. Mater Today Phys 2019;8:112–22.
[115] Patel SN, Glaudell AM, Peterson KA, Thomas EM, O'Hara KA, Lim E, Chabinyc ML. Morphology controls the thermoelectric power factor of a doped semiconducting polymer. Sci Adv 2017;3:e1700434.
[116] Patel SN, Glaudell AM, Kiefer D, Chabinyc ML. Increasing the Thermoelectric Power Factor of a Semiconducting Polymer by Doping from the Vapor Phase. ACS Macro Lett 2016;5:268–72.
[117] Zhu Z, Waller D, Gaudiana R, Morana M, Mühlbacher D, Scharber M, Brabec C. Panchromatic Conjugated Polymers Containing Alternating Donor/Acceptor Units for Photovoltaic Applications. Macromolecules 2007;40:1981–6.
[118] Mühlbacher D, Scharber M, Morana M, Zhu Z, Waller D, Gaudiana R, Brabec C. High Photovoltaic Performance of a Low-Bandgap Polymer. Adv Mater 2006;18:2884–9.
[119] Zhang M, Tsao HN, Pisula W, Yang C, Mishra AK. Müllen K. Field-Effect Transistors Based on a Benzothiadiazole−Cyclopentadithiophene Copolymer. J Am Chem Soc 2007;129:3472–3.
[120] Tsao HN, Cho D, Andreasen JW, Rouhanipour A, Breiby DW, Pisula W, Müllen K. The Influence of Morphology on High-Performance Polymer Field–Effect Transistors. Adv Mater 2009;21:209–12.
[121] Aïch RB, Blouin N, Bouchard A, Leclerc M. Electrical and Thermoelectric Properties of Poly(2,7-Carbazole) Derivatives. Chem Mater 2009;21:751–7.
[122] Suh EH, Jeong YJ, Oh JG, Lee K, Jung J, Kang YS, Jang J. Doping of donor-acceptor polymers with long side chains via solution mixing for advancing thermoelectric properties. Nano Energy 2019;58:585–95.
[123] Guo J, Li G, Reith H, Jiang L, Wang M, Li Y, Wang X, Zeng Z, Zhao H, Lu X, Schierning G, Nielsch K, Liao L, Hu Y. Doping High-Mobility Donor–Acceptor Copolymer Semiconductors with an Organic Salt for High-Performance Thermoelectric Materials. Adv Electron Mater 2020;6:1900945.
[124] Dexter Tam TL, Ng CK, Lim SL, Yildirim E, Ko J, Leong WL, Yang S-W, Xu J. Proquinoidal-Conjugated Polymer as an Effective Strategy for the Enhancement of Electrical Conductivity and Thermoelectric Properties. Chem Mater 2019;31:8543–50.
[125] Fan J, Yuen JD, Wang M, Seifter J, Seo J-H, Mohebbi AR, Zakhidov D, Heeger A, Wudl F. High-Performance Ambipolar Transistors and Inverters from an Ultralow Bandgap Polymer. Adv Mater 2012;24:2186–90.
[126] Fan J, Yuen JD, Cui W, Seifter J, Mohebbi AR, Wang M, Zhou H, Heeger A, Wudl F. High-Hole-Mobility Field-Effect Transistors Based on Co-Benzobisthiadiazole-Quaterthiophene. Adv Mater 2012;24:6164–8.

[127] Tam TLD, Wu G, Chien SW, Lim SFV, Yang S-W, Xu J. High Spin Pro-Quinoid Benzo[1,2-c;4,5-c′]bisthiadiazole Conjugated Polymers for High--Performance Solution-Processable Polymer Thermoelectrics. ACS Mater Lett 2020;2:147–52.
[128] Nielsen CB, Turbiez M, McCulloch I. Recent advances in the development of semiconducting DPP-containing polymers for transistor applications. Adv Mater 2013;25:1859–80.
[129] Zhang X, Richter LJ, DeLongchamp DM, Kline RJ, Hammond MR, McCulloch I, Heeney M, Ashraf RS, Smith JN, Anthopoulos TD, Schroeder B, Geerts YH, Fischer DA, Toney MF. Molecular packing of high-mobility diketo pyrrolo-pyrrole polymer semiconductors with branched alkyl side chains. J Am Chem Soc 2011;133:15073–84.
[130] Jung IH, Hong CT, Lee U-H, Kang YH, Jang K-S, Cho SY. High Thermoelectric Power Factor of a Diketopyrrolopyrrole-Based Low Bandgap Polymer via Finely Tuned Doping Engineering. Sci Rep 2017;7:44704.
[131] Liu Z, Hu Y, Li P, Wen J, He J, Gao X. Enhancement of the thermoelectric performance of DPP based polymers by introducing one 3,4-ethylenedioxythiophene electron-rich building block. J Mater Chem C 2020;8:10859–67.
[132] Ding J, Liu Z, Zhao W, Jin W, Xiang L, Wang Z, Zeng Y, Zou Y, Zhang F, Yi Y, Diao Y, McNeill CR, Di CA, Zhang D, Zhu D. Selenium-Substituted Diketopyrrolopyrrole Polymer for High-Performance p-Type Organic Thermoelectric Materials. Angew Chem Int Ed 2019;58:18994–9.
[133] Ashraf RS, Meager I, Nikolka M, Kirkus M, Planells M, Schroeder BC, Holliday S, Hurhangee M, Nielsen CB, Sirringhaus H, McCulloch I. Chalcogenophene Comonomer Comparison in Small Band Gap Diketopyrrolopyrrole-Based Conjugated Polymers for High-Performing Field-Effect Transistors and Organic Solar Cells. J Am Chem Soc 2015;137:1314–21.
[134] Fei Z, Han Y, Gann E, Hodsden T, Chesman ASR, McNeill CR, Anthopoulos TD, Heeney M. Alkylated Selenophene-Based Ladder-Type Monomers via a Facile Route for High-Performance Thin-Film Transistor Applications. J Am Chem Soc 2017;139:8552–61.
[135] Wang Z, Liu Z, Ning L, Xiao M, Yi Y, Cai Z, Sadhanala A, Zhang G, Chen W, Sirringhaus H, Zhang D. Charge Mobility Enhancement for Conjugated DPP-Selenophene Polymer by Simply Replacing One Bulky Branching Alkyl Chain with Linear One at Each DPP Unit. Chem Mater 2018;30:3090–100.
[136] Li H, Song J, Xiao J, Wu L, Katz HE, Chen L. Synergistically Improved Molecular Doping and Carrier Mobility by Copolymerization of Donor–Acceptor and Donor–Donor Building Blocks for Thermoelectric Application. Adv Funct Mater 2020;30 2004378.
[137] Hu Y, Gao Y, Li P, Gao X, Liu Z. Enhancement of thermoelectric properties of D-A conjugated polymer through constructing random copolymers with more electronic donors. J Polym Sci 2020 10.1002/pol.20210604.
[138] Hamidi-Sakr A, Biniek L, Bantignies J-L, Maurin D, Herrmann L, Leclerc N, Lévêque P, Vijayakumar V, Zimmermann N, Brinkmann M. A Versatile Method to Fabricate Highly In-Plane Aligned Conducting Polymer Films with Anisotropic Charge Transport and Thermoelectric Properties: The Key Role of Alkyl Side Chain Layers on the Doping Mechanism. Adv Funct Mater 2017;27:1700173.
[139] Qu S, Yao Q, Wang L, Chen Z, Xu K, Zeng H, Shi W, Zhang T, Uher C, Chen L. Highly anisotropic P3HT films with enhanced thermoelectric performance via organic small molecule epitaxy. NPG Asia Materials 2016;8 e292-e.
[140] Vijayakumar V, Zaborova E, Biniek L, Zeng H, Herrmann L, Carvalho A, Boyron O, Leclerc N, Brinkmann M. Effect of Alkyl Side Chain Length on Doping Kinetics, Thermopower, and Charge Transport Properties in Highly Oriented F4TCNQ-Doped PBTTT Films. ACS Appl Mater Interfaces 2019;11:4942–53.
[141] Parthasarathy G, Shen C, Kahn A, Forrest SR. Lithium doping of semiconducting organic charge transport materials. J Appl Phys 2001;89:4986–92.
[142] Koech PK, Padmaperuma AB, Wang L, Swensen JS, Polikarpov E, Darsell JT, Rainbolt JE, Gaspar DJ. Synthesis and Application of 1,3,4,5,7,8-Hexafluorotetracyanonaphthoquinodimethane (F6-TNAP): A Conductivity Dopant for Organic Light-Emitting Devices. Chem Mater 2010;22:3926–32.
[143] Li J, Zhang G, Holm DM, Jacobs IE, Yin B, Stroeve P, Mascal M, Moulé AJ. Introducing Solubility Control for Improved Organic P-Type Dopants. Chem Mater 2015;27:5765–74.
[144] Rainbolt JE, Koech PK, Polikarpov E, Swensen JS, Cosimbescu L, Von Ruden A, Wang L, Sapochak LS, Padmaperuma AB, Gaspar DJ. Synthesis and characterization of p-type conductivity dopant 2-(3-(adamantan-1-yl)propyl)-3,5,6-trifluoro-7,7,8,8-tetracyanoquinodimethane. J Mater Chem C 2013;1:1876–84.
[145] Kiefer D, Kroon R, Hofmann AI, Sun H, Liu X, Giovannitti A, Stegerer D, Cano A, Hynynen J, Yu L, Zhang Y, Nai D, Harrelson TF, Sommer M, Moulé AJ, Kemerink M, Marder SR, McCulloch I, Fahlman M, Fabiano S, Müller C. Double doping of conjugated polymers with monomer molecular dopants. Nat Mater 2019;18:149–55.
[146] Karpov Y, Erdmann T, Raguzin I, Al-Hussein M, Binner M, Lappan U, Stamm M, Gerasimov KL, Beryozkina T, Bakulev V, Anokhin DV, Ivanov DA, Günther F, Gemming S, Seifert G, Voit B, Di Pietro R, Kiriy A. High Conductivity in Molecularly p-Doped Diketopyrrolopyrrole-Based Polymer: The Impact of a High Dopant Strength and Good Structural Order. Adv Mater 2016;28:6003–10.
[147] Saska J, Gonel G, Bedolla-Valdez ZI, Aronow SD, Shevchenko NE, Dudnik AS, Moulé AJ, Mascal M. A Freely Soluble, High Electron Affinity Molecular Dopant for Solution Processing of Organic Semiconductors. Chem Mater 2019;31:1500–6.
[148] Schlitz RA, Brunetti FG, Glaudell AM, Miller PL, Brady MA, Takacs CJ, Hawker CJ, Chabinyc ML. Solubility-limited extrinsic n-type doping of a high electron mobility polymer for thermoelectric applications. Adv Mater 2014;26:2825–30.
[149] Yan H, Chen Z, Zheng Y, Newman C, Quinn JR, Dötz F, Kastler M, Facchetti A. A high-mobility electron-transporting polymer for printed transistors. Nature 2009;457:679–86.
[150] Wang S, Sun H, Ail U, Vagin M, Persson PO, Andreasen JW, Thiel W, Berggren M, Crispin X, Fazzi D, Fabiano S. Thermoelectric Properties of Solution-Processed n-Doped Ladder-Type Conducting Polymers. Adv Mater 2016;28:10764–71.
[151] Naab BD, Gu X, Kurosawa T, To JWF, Salleo A, Bao Z. Role of Polymer Structure on the Conductivity of N-Doped Polymers. Adv Electron Mater 2016;2:1600004.
[152] Liu J, Qiu L, Alessandri R, Qiu X, Portale G, Dong J, Talsma W, Ye G, Sengrian AA, Souza PCT, Loi MA, Chiechi RC, Marrink SJ, Hummelen JC, Koster LJA. Enhancing Molecular n-Type Doping of Donor-Acceptor Copolymers by Tailoring Side Chains. Adv Mater 2018;30:1704630.
[153] Kiefer D, Giovannitti A, Sun H, Biskup T, Hofmann A, Koopmans M, Cendra C, Weber S, Anton Koster LJ, Olsson E, Rivnay J, Fabiano S, McCulloch I, Muller C. Enhanced n-Doping Efficiency of a Naphthalenediimide-Based Copolymer through Polar Side Chains for Organic Thermoelectrics. ACS Energy Lett 2018;3:278–85.
[154] Shin Y, Massetti M, Komber H, Biskup T, Nava D, Lanzani G, Caironi M, Sommer M. Improving Miscibility of a Naphthalene Diimide-Bithiophene Copolymer with n-Type Dopants through the Incorporation of “Kinked” Monomers. Adv Electron Mater 2018;4:1700581.
[155] Wang S, Sun H, Erdmann T, Wang G, Fazzi D, Lappan U, Puttisong Y, Chen Z, Berggren M, Crispin X, Kiriy A, Voit B, Marks TJ, Fabiano S, Facchetti A. A Chemically Doped Naphthalenediimide-Bithiazole Polymer for n-Type Organic Thermoelectrics. Adv Mater 2018;30:e1801898.
[156] Han J, Ganley C, Hu Q, Zhao X, Clancy P, Russell TP, Katz HE. Using Preformed Meisenheimer Complexes as Dopants for n-Type Organic Thermoelectrics with High Seebeck Coefficients and Power Factors. Adv Funct Mater 2021;31:2010567.
[157] Wang Y, Nakano M, Michinobu T, Kiyota Y, Mori T, Takimiya K. Naphthodithiophenediimide–Benzobisthiadiazole-Based Polymers: Versatile n–Type Materials for Field-Effect Transistors and Thermoelectric Devices. Macromolecules 2017;50:857–64.
[158] Liu J, Ye G, Potgieser HGO, Koopmans M, Sami S, Nugraha MI, Villalva DR, Sun H, Dong J, Yang X, Qiu X, Yao C, Portale G, Fabiano S, Anthopoulos TD, Baran D, Havenith RWA, Chiechi RC, Koster LJA. Amphipathic Side Chain of a Conjugated Polymer Optimizes Dopant Location toward Efficient N-Type Organic Thermoelectrics. Adv Mater 2021;33:e2006694.
[159] Liu J, Ye G, Zee BV, Dong J, Qiu X, Liu Y, Portale G, Chiechi RC, Koster LJA. N-Type Organic Thermoelectrics of Donor-Acceptor Copolymers: Improved Power Factor by Molecular Tailoring of the Density of States. Adv Mater 2018;30:e1804290.
[160] Wang S, Fazzi D, Puttisong Y, Jafari MJ, Chen Z, Ederth T, Andreasen JW, Chen WM, Facchetti A, Fabiano S. Effect of Backbone Regiochemistry on Conductivity, Charge Density, and Polaron Structure of n-Doped Donor-Acceptor Polymers. Chem Mater 2019;31:3395–406.
[161] Gross YM, Trefz D, Dingler C, Bauer D, Vijayakumar V, Untilova V, Biniek L, Brinkmann M, Ludwigs S. From Isotropic to Anisotropic Conductivities in P(NDI2OD-T2) by (Electro-)Chemical Doping Strategies. Chem Mater 2019;31:3542–55.
[162] Steyrleuthner R, Di Pietro R, Collins BA, Polzer F, Himmelberger S, Schubert M, Chen Z, Zhang S, Salleo A, Ade H, Facchetti A, Neher D. The role of regioregularity, crystallinity, and chain orientation on electron transport in a high-mobility n-type copolymer. J Am Chem Soc 2014;136:4245–56.
[163] Gross YM, Trefz D, Tkachov R, Untilova V, Brinkmann M, Schulz GL, Ludwigs S. Tuning Aggregation by Regioregularity for High-Performance n-Type P(NDI2OD-T2) Donor–Acceptor Copolymers. Macromolecules 2017;50:5353–66.
[164] Ye G, Liu J, Qiu X, Stäter S, Qiu L, Liu Y, Yang X, Hildner R, Koster LJA, Chiechi RC. Controlling n-Type Molecular Doping via Regiochemistry and Polarity of Pendant Groups on Low Band Gap Donor–Acceptor Copolymers. Macromolecules 2021;54:3886–96.
[165] Dexter Tam TL, Lin TT, Omer MI, Wang X, Xu J. The benzyl viologen radical cation: an effective n-dopant for poly(naphthalenediimide-bithiophene). J Mater Chem A 2020;8:18916–24.
[166] Wei H, Chen PA, Guo J, Liu Y, Qiu X, Chen H, Zeng Z, Nguyen TQ, Hu Y. Low–Cost Nucleophilic Organic Bases as n-Dopants for Organic Field-Effect Transistors and Thermoelectric Devices. Adv Funct Mater 2021:2102768.
[167] Wang S, Ruoko TP, Wang G, Riera-Galindo S, Hultmark S, Puttisong Y, Moro F, Yan H, Chen WM, Berggren M, Muller C, Fabiano S. Sequential Doping of Ladder-Type Conjugated Polymers for Thermally Stable n-Type Organic Conductors. ACS Appl Mater Interfaces 2020;12:53003–11.
[168] Tam TLD, Lin M, Handoko AD, Lin TT, Xu J. High-performance & thermally stable n-type polymer thermoelectrics based on a benzyl viologen radical cation-doped ladder-type conjugated polymer. J Mater Chem A 2021;9:11787–93.
[169] Yang C-Y, Stoeckel M-A, Ruoko T-P, Wu H-Y, Liu X, Kolhe NB, Wu Z, Puttisong Y, Musumeci C, Massetti M, Sun H, Xu K, Tu D, Chen WM, Woo HY,

Fahlman M, Jenekhe SA, Berggren M. Fabiano S. A high-conductivity n-type polymeric ink for printed electronics. Nat Commun 2021;12:2354.
[170] Shi K, Zhang F, Di CA, Yan TW, Zou Y, Zhou X, Zhu D, Wang JY, Pei J. Toward High Performance n-Type Thermoelectric Materials by Rational Modification of BDPPV Backbones. J Am Chem Soc 2015;137:6979–82.
[171] Lei T, Dou J-H, Cao X-Y, Wang J-Y, Pei J. Electron-Deficient Poly(p-phenylene vinylene) Provides Electron Mobility over 1 cm2 V–1 s–1 under Ambient Conditions. Journal of the American Chemical Society 2013;135:12168–71.
[172] Ma W, Shi K, Wu Y, Lu Z-Y, Liu H-Y, Wang J-Y, Pei J. Enhanced Molecular Packing of a Conjugated Polymer with High Organic Thermoelectric Power Factor. ACS Appl Mater Interfaces 2016;8:24737–43.
[173] Bardagot O, Kubik P, Marszalek T, Veyre P, Medjahed AA, Sandroni M, Grévin B, Pouget S, Nunes Domschke T, Carella A, Gambarelli S, Pisula W, Demadrille R. Impact of Morphology on Charge Carrier Transport and Thermoelectric Properties of N-Type FBDOPV-Based Polymers. Adv Funct Mater 2020;30 2000449.
[174] Zhang X, Bronstein H, Kronemeijer AJ, Smith J, Kim Y, Kline RJ, Richter LJ, Anthopoulos TD, Sirringhaus H, Song K, Heeney M, Zhang W, McCulloch I, DeLongchamp DM. Molecular origin of high field-effect mobility in an indacenodithiophene-benzothiadiazole copolymer. Nat Commun 2013;4:2238.
[175] Venkateshvaran D, Nikolka M, Sadhanala A, Lemaur V, Zelazny M, Kepa M, Hurhangee M, Kronemeijer AJ, Pecunia V, Nasrallah I, Romanov I, Broch K, McCulloch I, Emin D, Olivier Y, Cornil J, Beljonne D, Sirringhaus H. Approaching disorder-free transport in high-mobility conjugated polymers. Nature 2014;515:384–8.
[176] Wang Y, Takimiya K. Naphthodithiophenediimide-Bithiopheneimide Copolymers for High-Performance n-Type Organic Thermoelectrics: Significant Impact of Backbone Orientation on Conductivity and Thermoelectric Performance. Adv Mater 2020;32 2002060.
[177] Lu Y, Yu ZD, Zhang RZ, Yao ZF, You HY, Jiang L, Un HI, Dong BW, Xiong M, Wang JY, Pei J. Rigid Coplanar Polymers for Stable n-Type Polymer Thermoelectrics. Angew Chem Int Ed Engl 2019;58:11390–4.
[178] Alsufyani M, Hallani RK, Wang S, Xiao M, Ji X, Paulsen BD, Xu K, Bristow H, Chen H, Chen X, Sirringhaus H, Rivnay J, Fabiano S, McCulloch I. The effect of aromatic ring size in electron deficient semiconducting polymers for n-type organic thermoelectrics. J Mater Chem C 2020;8:15150–7.
[179] Chen H, Moser M, Wang S, Jellett C, Thorley K, Harrison GT, Jiao X, Xiao M, Purushothaman B, Alsufyani M, Bristow H, De Wolf S, Gasparini N, Wadsworth A, McNeill CR, Sirringhaus H, Fabiano S, McCulloch I. Acene Ring Size Optimization in Fused Lactam Polymers Enabling High n-Type Organic Thermoelectric Performance. J Am Chem Soc 2021;143:260–268.
[180] Xiao M, Carey RL, Chen H, Jiao X, Lemaur V, Schott S, Nikolka M, Jellett C, Sadhanala A, Rogers S, Senanayak SP, Onwubiko A, Han S, Zhang Z, Abdi-Jalebi M, Zhang Y, Thomas TH, Mahmoudi N, Lai L, Selezneva E, Ren X, Nguyen M, Wang Q, Jacobs I, Yue W, McNeill CR, Liu G, Beljonne D, McCulloch I, Sirringhaus H. Charge transport physics of a unique class of rigid-rod conjugated polymers with fused-ring conjugated units linked by double carbon-carbon bonds. Sci Adv 2021;7:eabe5280.
[181] Yang CY, Jin WL, Wang J, Ding YF, Nong S, Shi K, Lu Y, Dai YZ, Zhuang FD, Lei T, Di CA, Zhu D, Wang JY, Pei J. Enhancing the n-Type Conductivity and Thermoelectric Performance of Donor-Acceptor Copolymers through Donor Engineering. Adv Mater 2018;30:1802850.
[182] Yan X, Xiong M, Li JT, Zhang S, Ahmad Z, Lu Y, Wang ZY, Yao ZF, Wang JY, Gu X, Lei T. Pyrazine-Flanked Diketopyrrolopyrrole (DPP): A New Polymer Building Block for High-Performance n-Type Organic Thermoelectrics. J Am Chem Soc 2019;141:20215–21.
[183] Shi Y, Guo H, Qin M, Zhao J, Wang Y, Wang H, Wang Y, Facchetti A, Lu X, Guo X. Thiazole Imide-Based All-Acceptor Homopolymer: Achieving High-Performance Unipolar Electron Transport in Organic Thin-Film Transistors. Adv Mater 2018:30.
[184] Guo X, Ortiz RP, Zheng Y, Hu Y, Noh YY, Baeg KJ, Facchetti A, Marks TJ. Bithiophene-imide-based polymeric semiconductors for field-effect transistors: synthesis, structure-property correlations, charge carrier polarity, and device stability. J Am Chem Soc 2011;133:1405–18.
[185] Liu J, Shi Y, Dong J, Nugraha MI, Qiu X, Su M, Chiechi RC, Baran D, Portale G, Guo X, Koster LJA. Overcoming Coulomb Interaction Improves Free-Charge Generation and Thermoelectric Properties for n-Doped Conjugated Polymers. ACS Energy Letters 2019;4:1556–64.
[186] Dou C, Ding Z, Zhang Z, Xie Z, Liu J, Wang L. Developing Conjugated Polymers with High Electron Affinity by Replacing a C C Unit with a B←N Unit. Angew Chem Int Ed 2015;54:3648–52.
[187] Long X, Gao Y, Tian H, Dou C, Yan D, Geng Y, Liu J, Wang L. Electron-transporting polymers based on a double B<–N bridged bipyridine (BNBP) unit. Chem Commun 2017;53:1649–52.
[188] Long X, Ding Z, Dou C, Zhang J, Liu J, Wang L. Polymer Acceptor Based on Double B<–N Bridged Bipyridine (BNBP) Unit for High-Efficiency All-Polymer Solar Cells. Adv Mater 2016;28:6504–8.
[189] Dong C, Meng B, Liu J, Wang L. B <– N Unit Enables n-Doping of Conjugated Polymers for Thermoelectric Application. ACS Appl Mater Interfaces 2020;12:10428–33.
[190] Dong C, Deng S, Meng B, Liu J, Wang L. Distannylated Monomer of Strong Electron-Accepting Organoboron Building Block: Enabling Acceptor-Acceptor Type Conjugated Polymers for n-Type Thermoelectric Applications. Angew Chem Int Ed 2021;60:16184–90.
[191] Perry EE, Chiu C-Y, Moudgil K, Schlitz RA, Takacs CJ, O'Hara KA, Labram JG, Glaudell AM, Sherman JB, Barlow S, Hawker CJ, Marder SR, Chabinyc ML. High Conductivity in a Nonplanar n-Doped Ambipolar Semiconducting Polymer. Chem Mater 2017;29:9742–50.
[192] Wei P, Oh JH, Dong G, Bao Z. Use of a 1H-Benzoimidazole Derivative as an n–Type Dopant and To Enable Air-Stable Solution-Processed n-Channel Organic Thin-Film Transistors. J Am Chem Soc 2010;132:8852–3.
[193] Naab BD, Guo S, Olthof S, Evans EG, Wei P, Millhauser GL, Kahn A, Barlow S, Marder SR, Bao Z. Mechanistic study on the solution-phase n-doping of 1,3-dimethyl-2-aryl-2,3-dihydro-1H-benzoimidazole derivatives. J Am Chem Soc 2013;135:15018–25.
[194] Bardagot O, Aumaître C, Monmagnon A, Pécaut J, Bayle P-A, Demadrille R. Revisiting doping mechanisms of n-type organic materials with N-DMBI for thermoelectric applications: Photo-activation, thermal activation, and air stability. Appl Phys Lett 2021;118:203904.
[195] Qiu L, Liu J, Alessandri R, Qiu X, Koopmans M, Havenith Remco WA, Marrink SJ, Chiechi RC, Anton Koster LJ, Hummelen JC. Enhancing doping efficiency by improving host-dopant miscibility for fullerene-based n-type thermoelectrics. J Mater Chem A 2017;5:21234–41.
[196] Riera-Galindo S, Orbelli Biroli A, Forni A, Puttisong Y, Tessore F, Pizzotti M, Pavlopoulou E, Solano E, Wang S, Wang G, Ruoko TP, Chen WM, Kemerink M, Berggren M, di Carlo G, Fabiano S. Impact of Singly Occupied Molecular Orbital Energy on the n-Doping Efficiency of Benzimidazole Derivatives. ACS Appl Mater Interfaces 2019;11:37981–90.
[197] Un HI, Gregory SA, Mohapatra SK, Xiong M, Longhi E, Lu Y, Rigin S, Jhulki S, Yang CY, Timofeeva TV, Wang JY, Yee SK, Barlow S, Marder SR, Pei J. Understanding the Effects of Molecular Dopant on n-Type Organic Thermoelectric Properties. Adv Energy Mater 2019;9:1900817.
[198] Zhao X, Madan D, Cheng Y, Zhou J, Li H, Thon SM, Bragg AE, DeCoster ME, Hopkins PE, Katz HE. High Conductivity and Electron-Transfer Validation in an n-Type Fluoride-Anion-Doped Polymer for Thermoelectrics in Air. Adv Mater 2017;29:1606928.
[199] Winberg HE, Carnahan JE, Coffman DD, Brown M. Tetraaminoethylenes. J Am Chem Soc 1965;87:2055–6.
[200] Kim J, Khim D, Baeg K-J, Park W-T, Lee S-H, Kang M, Noh Y-Y, Kim D-Y. Systematic Study of Widely Applicable N-Doping Strategy for High--Performance Solution-Processed Field-Effect Transistors. Adv Funct Mater 2016;26:7886–94.
[201] Guha S, Saha S. Fluoride Ion Sensing by an Anion−π Interaction. J Am Chem Soc 2010;132:17674–7.
[202] Lee D-H, Kang M, Lim D-H, Kim Y, Lee J, Kim D-Y, Baeg K-J. Simultaneous enhancement of charge density and molecular stacking order of polymer semiconductors by viologen dopants for high performance organic field-effect transistors. J Mater Chem C 2018;6:5497–505.
[203] Huseynova G, Shrestha NK, Xu Y, Shin E-Y, Park W-T, Ji D, Noh Y-Y. Benzyl viologen as an n-type dopant for organic semiconductors. Org Electron 2018;62:572–80.
[204] Tam TLD, Xu J. Benzyl viologen radical cation: an effective n-dopant for poly(perylenediimide-bithiophene). J Mater Chem C 2020;8:17261–8.
[205] Hopkinson MN, Richter C, Schedler M, Glorius F. An overview of N-heterocyclic carbenes. Nature 2014;510:485–96.
[206] Ding YF, Yang CY, Huang CX, Lu Y, Yao ZF, Pan CK, Wang JY, Pei J. Thermally Activated n-Doping of Organic Semiconductors Achieved by N-Heterocyclic Carbene Based Dopant. Angew Chem Int Ed 2021;60:5816–20.
[207] Khim D, Luzio A, Bonacchini GE, Pace G, Lee M-J, Noh Y-Y, Caironi M. Uniaxial Alignment of Conjugated Polymer Films for High-Performance Organic Field-Effect Transistors. Adv Mater 2018;30:1705463.
[208] Diao Y, Shaw L, Bao Z, Mannsfeld SCB. Morphology control strategies for solution-processed organic semiconductor thin films. Energy Environ Sci 2014;7:2145–59.
[209] Pisula W, Menon A, Stepputat M, Lieberwirth I, Kolb U, Tracz A, Sirringhaus H, Pakula T, Müllen K. A Zone-Casting Technique for Device Fabrication of Field-Effect Transistors Based on Discotic Hexa-peri-hexabenzocoronene. Adv Mater 2005;17:684–9.
[210] Tang C, Wu W, Smilgies D-M, Matyjaszewski K, Kowalewski T. Robust Control of Microdomain Orientation in Thin Films of Block Copolymers by Zone Casting. J Am Chem Soc 2011;133:11802–9.
[211] Michels JJ, Zhang K, Wucher P, Beaujuge PM, Pisula W, Marszalek T. Predictive modelling of structure formation in semiconductor films produced by meniscus-guided coating. Nat Mater 2021;20:68–75.
[212] Zhang K, Borkowski M, Wucher P, Beaujuge PM, Michels JJ, Blom PWM, Marszalek T, Pisula W. Relation between Spherulitic Growth, Molecular Organization, and Charge Carrier Transport in Meniscus-Guided Coated Organic Semiconducting Films. Adv Electron Mater 2021;7:2100397.
[213] Giri G, Verploegen E, Mannsfeld SCB, Atahan-Evrenk S, Kim DH, Lee SY, Becerril HA, Aspuru-Guzik A, Toney MF, Bao Z. Tuning charge transport in solution-sheared organic semiconductors using lattice strain. Nature 2011;480:504–8.
[214] Diao Y, Tee BCK, Giri G, Xu J, Kim DH, Becerril HA, Stoltenberg RM, Lee TH, Xue G, Mannsfeld SCB, Bao Z. Solution coating of large-area organic semiconductor thin films with aligned single-crystalline domains. Nat Mater 2013;12:665–71.
[215] Galindo S, Tamayo A, Leonardi F. Mas-Torrent M. Control of Polymorphism and Morphology in Solution Sheared Organic Field-Effect Transistors. Adv Funct Mater 2017;27:1700526.

[216] Xiao M, Kang B, Lee SB, Perdigão LMA, Luci A, Warr DA, Senanayak SP, Nikolka M, Statz M, Wu Y, Sadhanala A, Schott S, Carey R, Wang Q, Lee M, Kim C, Onwubiko A, Jellett C, Liao H, Yue W, Cho K, Costantini G, McCulloch I. Sirringhaus H. Anisotropy of Charge Transport in a Uniaxially Aligned Fused Electron-Deficient Polymer Processed by Solution Shear Coating. Adv Mater 2020;32 2000063.
[217] Sele CW, Kjellander BKC, Niesen B, Thornton MJ, van der Putten JBPH, Myny K, Wondergem HJ, Moser A, Resel R, van Breemen AJJM, van Aerle N, Heremans P, Anthony JE, Gelinck GH. Controlled Deposition of Highly Ordered Soluble Acene Thin Films: Effect of Morphology and Crystal Orientation on Transistor Performance. Adv Mater 2009;21:4926–31.
[218] Wang S, Kivala M, Lieberwirth I, Kirchhoff K, Feng X, Pisula W, Mullen K. Dip–coating-induced fiber growth of a soluble heterotriangulene. Chemphyschem 2011;12:1648–51.
[219] Li Q-Y, Yao Z-F, Lu Y, Zhang S, Ahmad Z, Wang J-Y, Gu X, Pei J. Achieving High Alignment of Conjugated Polymers by Controlled Dip-Coating. Adv Electron Mater 2020;6 2000080.
[220] Zhang K, Wang Z, Marszalek T, Borkowski M, Fytas G, Blom PWM, Pisula W. Key role of the meniscus shape in crystallization of organic semiconductors during meniscus-guided coating. Mater Horiz 2020;7:1631–40.
[221] Bucella SG, Luzio A, Gann E, Thomsen L, McNeill CR, Pace G, Perinot A, Chen Z, Facchetti A, Caironi M. Macroscopic and high-throughput printing of aligned nanostructured polymer semiconductors for MHz large-area electronics. Nat Commun 2015;6:8394.
[222] Yabuuchi Y, Minowa Y, Kajii H, Nagano S, Fujii A, Ozaki M. Direction-Selectable Ultra-Highly Oriented State of Donor–Acceptor Conjugated Polymer Induced by Slow Bar Coating Process. Adv Electron Mater 2021;7:2100313.
[223] Shi W, Shuai Z, Wang D. Tuning Thermal Transport in Chain-Oriented Conducting Polymers for Enhanced Thermoelectric Efficiency: A Computational Study. Adv Funct Mater 2017;27:1702847.
[224] Biniek L, Leclerc N, Heiser T, Bechara R, Brinkmann M. Large Scale Alignment and Charge Transport Anisotropy of pBTTT Films Oriented by High Temperature Rubbing. Macromolecules 2013;46:4014–23.
[225] Hamidi-Sakr A, Biniek L, Fall S, Brinkmann M. Precise Control of Lamellar Thickness in Highly Oriented Regioregular Poly(3-Hexylthiophene) Thin Films Prepared by High-Temperature Rubbing: Correlations with Optical Properties and Charge Transport. Adv Funct Mater 2016;26:408–20.
[226] Vijayakumar V, Zhong Y, Untilova V, Bahri M, Herrmann L, Biniek L, Leclerc N, Brinkmann M. Bringing Conducting Polymers to High Order: Toward Conductivities beyond 105 S cm−1 and Thermoelectric Power Factors of 2 mW m−1 K−2. Adv Energy Mater 2019;9:1900266.
[227] Noriega R. Efficient Charge Transport in Disordered Conjugated Polymer Microstructures. Macromol Rapid Commun 2018;39:e1800096.
[228] Wang S. Emerging efficient charge-transport landscape based on short-range order in conjugated polymers. Synth Met 2019;251:104–19.
[229] Noriega R, Rivnay J, Vandewal K, Koch FP, Stingelin N, Smith P, Toney MF, Salleo A. A general relationship between disorder, aggregation and charge transport in conjugated polymers. Nat Mater 2013;12:1038–44.
[230] Wang S, Fabiano S, Himmelberger S, Puzinas S, Crispin X, Salleo A, Berggren M. Experimental evidence that short-range intermolecular aggregation is sufficient for efficient charge transport in conjugated polymers. Proc Natl Acad Sci U S A 2015;112:10599–604.
[231] Selezneva E, Vercouter A, Schweicher G, Lemaur V, Broch K, Antidormi A, Takimiya K, Coropceanu V, Brédas J-L, Melis C, Cornil J, Sirringhaus H. Strong Suppression of Thermal Conductivity in the Presence of Long Terminal Alkyl Chains in Low-Disorder Molecular Semiconductors. Adv Mater 2021;33 2008708.
[232] Zuo G, Abdalla H, Kemerink M. Impact of doping on the density of states and the mobility in organic semiconductors. Phys Rev B 2016;93:235203.
[233] Abdalla H, Zuo G, Kemerink M. Range and energetics of charge hopping in organic semiconductors. Phys Rev B 2017;96:241202.
[234] Zuo G. Doping and Density of States Engineering for Organic Thermoelectrics. Linköping University; 2018. doi:103384/dissdiva-147778.
[235] Mahan GD, Sofo JO. The best thermoelectric. Proc Natl Acad Sci U S A 1996;93:7436–9.
[236] Sun J, Yeh ML, Jung BJ, Zhang B, Feser J, Majumdar A, Katz HE. Simultaneous Increase in Seebeck Coefficient and Conductivity in a Doped Poly(alkylthiophene) Blend with Defined Density of States. Macromolecules 2010;43:2897–903.
[237] Zuo G, Liu X, Fahlman M, Kemerink M. High Seebeck Coefficient in Mixtures of Conjugated Polymers. Adv Funct Mater 2018;28:1703280.
[238] Jeong S, Foo Z, Lee Y, Sim J, Blaauw D, Sylvester D. A Fully-Integrated 71 nW CMOS Temperature Sensor for Low Power Wireless Sensor Nodes. IEEE J Solid-State Circuits 2014;49:1682–93.
[239] Mukaida M, Kirihara K, Wei Q. Enhanced Power Output in Polymer Thermoelectric Devices through Thermal and Electrical Impedance Matching. ACS Appl Energy Mater 2019;2:6973–8.
[240] Menon AK, Yee SK. Design of a polymer thermoelectric generator using radial architecture. J Appl Phys 2016;119 055501.
[241] Zhang F, Zang Y, Huang D, C-a Di, Zhu D. Flexible and self-powered temperature–pressure dual-parameter sensors using microstructure-frame-supported organic thermoelectric materials. Nat Commun 2015;6:8356.
[242] Malti A, Edberg J, Granberg H, Khan ZU, Andreasen JW, Liu X, Zhao D, Zhang H, Yao Y, Brill JW, Engquist I, Fahlman M, Wågberg L, Crispin X, Berggren M. An Organic Mixed Ion–Electron Conductor for Power Electronics. Adv Sci 2016;3:1500305.
[243] Khan ZU, Edberg J, Hamedi MM, Gabrielsson R, Granberg H, Wågberg L, Engquist I, Berggren M, Crispin X. Thermoelectric Polymers and their Elastic Aerogels. Adv Mater 2016;28:4556–62.
[244] Han S, Jiao F, Khan ZU, Edberg J, Fabiano S, Crispin X. Thermoelectric Polymer Aerogels for Pressure-Temperature Sensing Applications. Adv Funct Mater 2017;27:1703549.
[245] Han S, Alvi NUH, Granlof L, Granberg H, Berggren M, Fabiano S, Crispin X. A Multiparameter Pressure-Temperature-Humidity Sensor Based on Mixed Ionic-Electronic Cellulose Aerogels. Adv Sci 2019;6:1802128.
[246] White MS, Kaltenbrunner M, Głowacki ED, Gutnichenko K, Kettlgruber G, Graz I, Aazou S, Ulbricht C, Egbe DAM, Miron MC, Major Z, Scharber MC, Sekitani T, Someya T, Bauer S, Sariciftci NS. Ultrathin, highly flexible and stretchable PLEDs. Nature Photonics 2013;7:811–16.
[247] Zhao Y, Zhang B, Yao B, Qiu Y, Peng Z, Zhang Y, Alsaid Y, Frenkel I, Youssef K, Pei Q, He X. Hierarchically Structured Stretchable Conductive Hydrogels for High-Performance Wearable Strain Sensors and Supercapacitors. Matter 2020;3:1196–210.
[248] Ashizawa M, Zheng Y, Tran H, Bao Z. Intrinsically stretchable conjugated polymer semiconductors in field effect transistors. Prog Polym Sci 2020;100:101181.
[249] Oh JY, Rondeau-Gagné S, Chiu Y-C, Chortos A, Lissel F, Wang G-JN, Schroeder BC, Kurosawa T, Lopez J, Katsumata T, Xu J, Zhu C, Gu X, Bae W-G, Kim Y, Jin L, Chung JW, Tok JBH, Bao Z. Intrinsically stretchable and healable semiconducting polymer for organic transistors. Nature 2016;539:411–15.
[250] Xu J, Wang S, Wang G-JN, Zhu C, Luo S, Jin L, Gu X, Chen S, Feig VR, To JWF, Rondeau-Gagné S, Park J, Schroeder BC, Lu C, Oh JY, Wang Y, Kim Y-H, Yan H, Sinclair R, Zhou D, Xue G, Murmann B, Linder C, Cai W, Tok JB-H, Chung JW, Bao Z. Highly stretchable polymer semiconductor films through the nanoconfinement effect. Science 2017;355:59–64.
[251] Fan X, Nie W, Tsai H, Wang N, Huang H, Cheng Y, Wen R, Ma L, Yan F, Xia Y. PEDOT:PSS for Flexible and Stretchable Electronics: Modifications, Strategies, and Applications. Adv Sci 2019;6:1900813.
[252] Lang U, Naujoks N, Dual J. Mechanical characterization of PEDOT:PSS thin films. Synth Met 2009;159:473–9.
[253] Kayser LV, Lipomi DJ. Stretchable Conductive Polymers and Composites Based on PEDOT and PEDOT:PSS. Adv Mater 2019;31:1806133.
[254] Oh JY, Kim S, Baik H-K, Jeong U. Conducting Polymer Dough for Deformable Electronics. Adv Mater 2016;28:4455–61.
[255] Savagatrup S, Chan E, Renteria-Garcia SM, Printz AD, Zaretski AV, O'Connor TF, Rodriquez D, Valle E, Lipomi DJ. Plasticization of PEDOT:PSS by Common Additives for Mechanically Robust Organic Solar Cells and Wearable Sensors. Adv Funct Mater 2015;25:427–36.
[256] Teo MY, Kim N, Kee S, Kim BS, Kim G, Hong S, Jung S, Lee K. Highly Stretchable and Highly Conductive PEDOT:PSS/Ionic Liquid Composite Transparent Electrodes for Solution-Processed Stretchable Electronics. ACS Appl Mater Interfaces 2017;9:819–26.
[257] Kim N, Lienemann S, Petsagkourakis I, Alemu Mengistie D, Kee S, Ederth T, Gueskine V, Leclere P, Lazzaroni R, Crispin X, Tybrandt K. Elastic conducting polymer composites in thermoelectric modules. Nat Commun 2020;11:1424.
[258] Li P, Du D, Guo L, Guo Y, Ouyang J. Stretchable and conductive polymer films for high-performance electromagnetic interference shielding. J Mater Chem C 2016;4:6525–32.
[259] Fisac M, Villasevil FX, López AM. High-efficiency photovoltaic technology including thermoelectric generation. J Power Sources 2014;252:264–9.
[260] He M, Lin Y-J, Chiu C-M, Yang W, Zhang B, Yun D, Xie Y, Lin Z-H. A flexible photo-thermoelectric nanogenerator based on MoS2/PU photothermal layer for infrared light harvesting. Nano Energy 2018;49:588–95.
[261] Jurado JP, Dörling B, Zapata-Arteaga O, Roig A, Mihi A, Campoy-Quiles M. Solar Harvesting: a Unique Opportunity for Organic Thermoelectrics? Adv Energy Mater 2019;9:1902385.
[262] Jurado JP, Dörling B, Zapata-Arteaga O, Goñi AR. Campoy-Quiles M. Comparing different geometries for photovoltaic-thermoelectric hybrid devices based on organics. J Mater Chem C 2021;9:2123–32.
[263] Wu Y, Kuang S, Li H, Wang H, Yang R, Zhai Y, Zhu G, Wang ZL. Triboelectric–Thermoelectric Hybrid Nanogenerator for Harvesting Energy from Ambient Environments. Adv Mater Technol 2018;3:1800166.
[264] Abol-Fotouh D, Dorling B, Zapata-Arteaga O, Rodriguez-Martinez X, Gomez A, Reparaz JS, Laromaine A, Roig A. Campoy-Quiles M. Farming thermoelectric paper. Energy Environ Sci 2019;12:716–26.
[265] Jia Y, Jiang Q, Sun H, Liu P, Hu D, Pei Y, Liu W, Crispin X, Fabiano S, Ma Y, Cao Y. Wearable Thermoelectric Materials and Devices for Self-Powered Electronic Systems. Adv Mater 2021;33:2102990.
[266] Vining CB. An inconvenient truth about thermoelectrics. Nat Mater 2009;8:83–5.
[267] Sirringhaus H. Reliability of Organic Field-Effect Transistors. Adv Mater 2009;21:3859–73.
[268] Bobbert PA, Sharma A, Mathijssen SGJ, Kemerink M, de Leeuw DM. Operational Stability of Organic Field-Effect Transistors. Adv Mater 2012;24:1146–58.
[269] Nava D, Shin Y, Massetti M, Jiao X, Biskup T, Jagadeesh MS, Calloni A, Duò L, Lanzani G, McNeill CR, Sommer M, Caironi M. Drastic Improvement of Air Stability in an n-Type Doped Naphthalene-Diimide Polymer by Thionation. ACS Appl Energy Mater 2018;1:4626–34.
[270] Han J, Fan H, Zhang Q, Hu Q, Russell TP, Katz HE. Dichlorinated Dithienylethene-Based Copolymers for Air-Stable n-Type Conductivity and Thermoelectricity. Adv Funct Mater 2021;31 2005901.